UNESCO Chair on Coastal Geo-Hazard Analysis
Research Institute for Earth Sciences
Geological Survey of Iran
unesco Chair

Abstract

The Persian Gulf, south of Iran, has been a key maritime theater for Persian Empires and Arab Caliphates, yet its Holocene coastal dynamics remain poorly understood. This thesis investigates how relative sea-level (RSL) changes, salt tectonics, and climate shifts affected ancient harbors and navigation in the northern Gulf. Using a multidisciplinary approach—including geomorphology, archaeology, sedimentology, and remote sensing—the study aims to assess natural and anthropogenic risks to waterfront archaeological sites. Results show RSL is controlled by regional sea-level change and local salt tectonics, with two post-mid-Holocene lowstands recorded. The first lowstand (250–450 AD) deepened the Shatt-al-Arab, shifting Sassanian harbors from Rishar to Apologus. The second lowstand (from 650 AD), combined with summer Shamal winds, made Apologus too shallow for large vessels, favoring Siraf as an alternative. A later lowstand and +3.7 m coastal uplift at Bataneh (Najirum), due to salt injection, increased RSL oscillation intervals. RSL rise and winter Shamal winds degraded Siraf's harbor between 950–1100 AD, leading to economic decline and a trade shift to Kish Island by 1000 AD. Shoreline analysis (1973–2006) along 244 transects reveals 70% erosion, driven by drought, coastal development, and watershed changes, damaging Siraf's waterfront. Modern petrochemical expansion has destroyed 90% of Bataneh's ancient site in the last 20 years. Urgent geoarchaeological studies are needed, as Persian Gulf waterfront sites face rapid destruction from development, ongoing RSL rise, and coastal erosion.

ISBN : 978-622-8423-74-6

2025

UNESCO Chair on Coastal Geo-Hazard Analysis
Research Institute for Earth Sciences
Geological Survey of Iran
unesco Chair

Geoarchaeology of Some Persian Gulf Ancient Harbours

UCCGHA 036

2025

Geoarchaeology of Some Persian Gulf Ancient Harbours

سرشناسه : پور کرمان، مجید--

عنوان و نام پدیدآور : Geoarchaeology of some Persian Gulf ancient harbours [Book]/ author Majid Pourkerman...[et al.].; Research Institute for Earth Sciences.; with cooperation UNESCO Chair on Coastal Geo-Hazard Analysis.

مشخصات نشر : تهران: خزه، ۱۴۰۴= ۲۰۲۵م.

مشخصات ظاهری : h، ۱۸۸ص.: مصور.

شابک : ۹۷۸-۶۲۲-۸۴۲۳-۷۴-۶

وضعیت فهرست نویسی : فیپا

یادداشت : زبان: انگلیسی.

یادداشت : authors Majid Pourkerman, Nick Marriner, Christophe Morhange, Morteza Djamali.

یادداشت : عنوان به فارسی: زمین‌باستان‌شناسی تعدادی از بنادر باستانی خلیج فارس

آوانویسی عنوان : جئوآرکئولاجی...

موضوع : زمین باستان‌شناسی -- ایران -- خلیج فارس

موضوع : Archaeological geology -- Iran -- Persian Gulf

موضوع : بندرها -- ایران

موضوع : Harbors -- Iran

شناسه افزوده : پورکرمان، مجید، ۱۳۶۴-

شناسه افزوده : Pourkerman, Majid, ۱۹۸۵-

شناسه افزوده : یونسکو. کرسی مخاطرات زمین شناختی ساحلی

شناسه افزوده : UNESCO Chair on Coastal Geo-Hazard Analysis

رده بندی کنگره : ۷/CC۷۵

رده بندی دیویی : ۱/۹۳۰

شماره کتابشناسی ملی : ۱۰۴۵۴۷۸۳

Geoarchaeology of Some Persian Gulf Ancient Harbours

Author:

Majid Pourkerman

Nick Marriner, Christophe Morhange, Morteza Djamali

نشر خزه

اطلاعات گزارش

عنوان: زمین‌باستان‌شناسی تعدادی از بنادر باستانی خلیج فارس

مجری: پژوهشکده علوم زمین، دانشگاه اکس- مارسی

زبان مرجع: انگلیسی

خروجی: تحلیل و مقاله

نویسندگان: مجید پورکرمان، نیک مارینر، کریستوف موقانژ، مرتضی جمالی

رئیس کرسی یونسکو در مخاطرات زمین شناختی ساحلی: حمید نظری

مسئول شورای اجرایی: راضیه لک

ناشر: نشر خزه

با همکاری کرسی یونسکو در مخاطرات زمین شناختی ساحلی

چاپ اول: ۱۴۰۴

شمارگان: ۵۰ نسخه

صفحات: ۱۸۸

شابک: ۹۷۸-۶۲۲-۸۴۲۳-۷۴-۶

khazepub@gmail.com

Report Information

Title: Geoarchaeology of some Persian Gulf Ancient Harbours

Employer: Research Institute for Earth Sciences, Universite D'aix-marseille Ecole Doctorale 355 – Espaces, Cultures, Societes, Geological Survey of Iran

Original language: English

Output: Report, Scientific paper

Authors: Majid Pourkerman, Nick Marriner, Christophe Morhange, Morteza Djamali

Chairholder in the UNESCO Chair on Coastal Geo-Hazard Analysis: Hamid Nazari

Head of the Executive Council: Razyeh Lak

Publisher: Khazeh Publication

with cooperation UNESCO Chair on Coastal Geo-Hazard Analysis

First Edition: 2025

Edition number: 50

Page: 188

Shabak: 978-622-8423-74-6

khazepub@gmail.com

Scientific Council	
Name	**Affiliation**
Behrouz Abtahi	Shahid Beheshti University (SBU)
Philippe Agard	University of Sorbonne
Justin Ahanhanzo	Intergovernmental Oceanographic Commission of UNESCO (IOC-UNESCO)
Hamid Alizadeh Lahijani	Iranian National Institute for Oceanography and Atmospheric Science
Ryo Anma	Tokushima University
Franck A. Audemard	Department of Geology, Central University of Venezuela
Alice Aurelie	UNESCO Water Sciences Division
Ara Avagyan	IGS: Institute Geological Sciences
Yeong Bae Seong	Korea University
Rick J Bailey	IOC-UNESCO Indian Ocean Tsunami Warning and Mitigation System/ UNESCO
Abbas Banj Shafiei	Urmia University
Eric Barrier	University of Sorbonne
Yahya Djamour	Shahid Beheshti University (SBU)
Issa El-Hussain	Sultan Qaboos University
Aram Fathian Baneh	University of Calgary
Hassan Fazeli Nashli	University of Tehran
Magdi Guirguis	Institut français d'archéologie orientale du Caire
Martin Hanz	German under water archaeology association

Ekkehard Holzbecher	German University of Technology in Oman
Egor Krasinskiy	Underwater research center Russian Geographical Society
Razyeh Lak	Research Institute for Earth Sciences
John Lambert	Deltares, UNESCO
Mohammad Mokhtari	International Institute of Earthquake Engineering and Seismology
Hamid Nazari	Research Institute for Earth Sciences
Jafar Omrani	Geological Survey of Iran
Klaus Reicherter	Aachen University
Jean-François Ritz	University of Montpellier
Stefano Salvi	National Institute of Geophysics and Volcanology (INGV)
Morteza Talebian	Research Institute for Earth Sciences
Mohammad Tatar	International Institute of Earthquake Engineering and Seismology
Judith Thomalsky	German Archaeological Institute Tehran Branch
Richard Walker	University of Oxford
Wenjiao Xiao	Chinese Academy of Sciences
Alireza Zarasvandi	Iranian Research Organization for Science & Technology (IROST) – Ministry of Science, Research & Technology
Mahdi Zare	International Institute of Earthquake Engineering and Seismology

Executive Committee	
Name	**Affiliation**
Nasir Ahmadi	Environmental Protection Organization of Mazandaran Province
Arash Amini	Golestan University
Alireza Amrikazemi	Scientific Coordinator, Qeshm Island UNESCO Global Geopark
Parviz Armani	Imam Khomeini International University
Ataollah Dadashpour	Geological Survey of Iran, Sari branch
Asghar Dolati	Kharazmi University
Hasan Fazelinashli	**University of Tehran**
Fahimeh Foroghi	Iranian National Institute for Oceanography and Atmospheric Science
Abdolazaim Ghanghormeh	Golestan University
Habibolah Ghasemi	Shahrood University of Technology
Mohammad reza Ghasemi	Research Institute for Earth Sciences
Manouchehr Ghorashi	Research Institute for Earth Sciences
Ahmed Hadidi	German University of Technology in Oman (GUTECH)
Jafar Hassanpour	**University of Tehran**
Ataollah Kavian	Environmental Protection Organization of Mazandaran Province
Razyeh Lak	Head of RIES and Executive Manager
Mahmoudreza Majidifard	Research Institute for Earth Sciences

Majid Moghadam	Iranian Research Organization for Science & Technology (IROST)
Ali Akbar Momeni	Shahrood University of Technology
Babak Moradi	Iranian National Institute for Oceanography and Atmospheric Science
Seyed Mohsen Mortazavi	**Hormozgan University**
Hasan Nasrollah Zadeh	Caspian Sea Ecological Research Center
Ehsan Pegah	Kharazmi University
Abdolwahed Pehpouri	Qeshm Island UNESCO Global Geopark
Ahmadreza Rabani	University of Science and Technology of Mazandaran
Mahdi Rahmanian	Shargh Daily newspaper
Ahmad Rashidi	**International Institute of Earthquake Engineering and Seismology**
Masoud Sadri Nasab	**University of Tehran**
Mohammad Tatar	**International Institute of Earthquake Engineering and Seismology**
Alireza Vaezi	*Research Institute for Earth Sciences*
Mojtaba Yamani	**University of Tehran**
Secretariat	
Name	**Affiliation**
Elnaz Aghaali	Research Institute for Earth Sciences
Keivan Ajdari	Research Institute for Earth Sciences
Hourieh AliBeygi	Research Institute for Earth Sciences
Bahman Bahrami	Memaran Asr Ertebat Company

Hanieh Bakhshaei	Geological Survey of Iran
Reza Behbahani	Geological Survey of Iran
Javad Darvishi khatooni	Geological Survey of Iran
Mohammadreza Ensani	Geological Survey of Iran
Marziyeh Estrabi Ashtiyani	Geological Survey of Iran
Sedigheh Ghanipour	Research Institute for Earth Sciences
Elaheh Ghayoumi	Memaran Asr Ertebat Company
Gholamreza Hoseinyar	Geological Survey of Iran
Mojtaba Kavianpour Sangno	Geological Survey of Iran
Zeinab Kazeminia	Research Institute for Earth Sciences
Hamoon Memarian	Research Institute for Earth Sciences
Mehrnoosh Pour Saeid	Graphic Designer
Shirin Safavi	Research Institute for Earth Sciences
Aazam Takhtchin	Research Institute for Earth Sciences

Contents

Table of Figures

Table of Table

CHAPTER ONE: General Background

General introduction

The Persian Gulf basin is situated at junction of the Arabian Platform and Iranian continental block. The tectonic history of the Persian Gulf is subdivided into four important phases (Baniasad et al., 2017; Bordenave and Hegre, 2006; Hosseiny et al., 2016; Konyuhov and Maleki, 2006; Smith et al., 1994:

1- Late Permian opening of Neo-Tethys: the Arabian-Nubian continental block was amalgamated with Gondwana that this stage named "Hidjaz tectonic". During Paleozoic, the Persian Gulf was located at rear part of the passive Gondwana margin of the ancient Paleo-Tethys Ocean (Ziegler, 2001).

2- Late Permian to middle Triassic phase of extension: concurrent Tethys I opening Iranian plate was separated from Gondwana. By the time the Persian Gulf was a passive margin of Neo-Tethys I (Ziegler, 2001).

3- Late Triassic to Early Jurassic: rifting occurred at the northern end of the Arabian Platform. It led to creat a new northern passive margin with Neo-Tethys II. By the Early to late Middle Jurassic, the Gotnia Basin created across the northern parts of the Persian Gulf

4- Late Middle Eocene and Early Miocene: Arabian Plate started impact to southern Asia, and the initiation of the Zagros Orogeny. The maximum compression between Arabian continent and southern Asia happened in

Miocene to Pliocene which is coincident with the Late Alpine Orogeny in Europe (Ziegler, 2001).

Zagros Fold-Thrust Belt is a part of the Alpine–Himalayan orogenic belt. Zagros is located at the northeastern margin of the Arabian plate. It resulted from the opening and closing of the Neo-Tethys oceanic realm (Takin, 1972, Stöcklin, 1974, Berberian and King, 1981, Agard et al., 2005, Frizon de Lamotte et al., 2011, Mouthereau et al., 2012). The Zagros is one of the most active collisional belts in the world.

The main axis of the asymmetric Persian Gulf follows the Zagros folding system. The axis has generated two main synclines in the western and central northern half of the Gulf, named the western and central basins (Purser and Seibold, 1973, Seibold and Vollbrecht, 1969). The basins are connected through transverse shoal between two synclinal areas reflected to uplift along the northward prolongation of the Qatar Arc. In the central basin, the axis is situated close to the Iranian coast. This section of the Gulf is generally steeper and deeper than the western basin and contains huge folds with steeply-dipping flanks in the hinterland (Kassler, 1973).

The central basin is well known for several salt domes and diapiric folds along its coast (Kalat, Bostaneh, Mughu, Moallem, Homiran and Darang) and offshore islands (Great and small Tunb, Farur, Abu Musa) in Iran, the United Arab Emirates (Sir Abu Nuayer, Arzanah, Sir

Bani Yas) and Qatar (Halul and Sharao). (Beydoun, 1991; Thomas et al., 2015). The source of salt structures originates from two main evaporation layers, namely the Neoproterozoic-Cambrian Hormuz Salt and the Oligocene-Miocene Fars Salt deposits. The salt extrusion of the Hormuz formation occurred during Oman-Zagros contraction events during the Cretaceous to Cenozoic and predates Fars salt deposition. In the early Miocene, during the onset of the Zagros continental collision, the Hormuz salt extrusion was reactivated. Consequently, Fars salt diapirism is triggered by gravitational loading produced by an overriding allochthonous Hormuz Salt sheet. This process pushed the Fars salt outwards (Snidero et la., 2020). The salt diapir close to the present coast of the Persian Gulf emerged following the reactivation of salt domes by the final Zagros folding phase (Fars salt diapirism through the narrow zone of fold-thrust belt) (Talbot and Alavi, 1996; Edgell, 1996; Motiei, 2001, Jahani et al., 2007).

The Persian Gulf coastal morphology is influenced by plate and salt tectonic regimes Three morphological zones are detectible along the Persian Gulf coastal zones: (i) Zone I: gently sloping marshland coasts with permanent rivers Such as Shat-al-Arab, Zohre, Hilla and Mand, and several ephemeral rivers with high sediment supply to the shallow coastal zone; (ii) Zone II diapiric uplifting coasts with salt domes; and (iii) Zone III rocky coasts with steep coastal slopes.

During the early Holocene global sea level rise continued following the lowstand during the last glacial maximum at 18th millennium BC (Clark et al., 2009). Most areas of the exposed Persian Gulf were covered by siliciclastic sand dunes (Sarnthein, 1972). By 8th millennium BC, relative sea level was 30 m below present and the main part of the Persian Gulf was submerged (Lambeck, 1996). The present sedimentary regime was initiated shortly after 8th millennium BC and coincided with the transition to a more humid climate, which contrasts with the arid climate of the late Holocene. The Persian Gulf transgression exceeded present sea level by 5150 - 5030 BC and it reached a highstand shortly after at 3340 – 2620 BC (Lokier et al., 2015). At this time, the lowland coastal zones in the south and north of the Persian Gulf and Mesopotamia were inundated (Aqrawi, 2001; Heyvaert and Baeteman, 2007). Hyper-arid climate conditions were initiated in the south of the Persian Gulf since 2150 BC concurrent with dune reactivation (Parker and Goudie, 2008). Relative sea level recorded a lowstand at 510 – 780 AD and it is reached present levels around 950 ADS (Lokier et al., 2015; Paul and Lokier, 2017).

The main weather phenomenon in the Persian Gulf is a strong northwesterly Shamal wind that occurs during summer and winter (Perrone, 1979). The summer Shamal winds result from interaction between summer monsoon low-pressure systems over NW India, that extend to the W and SE areas of the Gulf, and stationary

high-pressure systems over the Mediterranean with a ridge extending SE towards the NW of the Persian Gulf (Bartlett, 2004). Winter Shamal wind over the north of the Persian Gulf is affected by cold air carried into the region by quasi-stationary Siberian high pressure in the east (Crook, 2009). It is usually interrupted by frontal systems that are created in the Eastern Mediterranean Sea and moves southeast following the polar front jet. The frontal system moves towards the Persian Gulf where the polar front jet and sub-tropical jet converge to strengthen the system by generating strong winds at the front. The strong NW wind passes over the northern Persian Gulf and it attains five times the initial speed close to the surface (15-20 m/s) in the center of the Gulf (Thoppil and Hogan, 2010). The intensity of the Shamal wind is enhanced by the funnel-like structure of the Zagros Mountain along the Iranian coast (Giannakopoulou and Toumi, 2012). The other weather system that affects the summer-time Shamal wind is the Indian Ocean Dipole (IOD). A positive IOD leads to decreased summer precipitation in the Persian Gulf and increasing duration and intensity of the summer Shamal wind (Senafi and Anis, 2012). The winter Shamal brings cold and dry air that leads to falling temperatures and evaporation (Thoppil and Hogan, 2010). The winter-time Shamal wind, that blows during January and February, creates the highest waves in the middle part (central basin) of the Persian Gulf, whereas, the summer-time Shamal (June and July) influences the northwestern

part of the Persian Gulf, especially at Shatt-al-Arab and Ras-e-Motaf. The intensity of the Shamal wind is attenuated following the summertime Shamal and it reaches its minimum during September and October (Kamranzad, 2018).

The Persian Gulf has an arid and semi-arid climate with low local fluviatile run-off. Numerous streams draining the Zagros Mountain area in the Iranian coastal characterized by frequent flash flooding. Different pattern of precipitation and humidity transportation are existed over Persian Gulf and southern Zagros Mountains. Study on 17 years winter precipitation over the Persian Gulf reveal that special patterns of heavy precipitations during La Niña and neutral El Niño-Southern Oscillation (ENSO) years in the northern coast. Meanwhile, during warm ENSO precipitations were taken place over entire of the Persian Gulf. The source of humidity in the Persian Gulf are generally from Red and Arabian Seas (Sandeep and Ajayamohan, 2018).

Evaporation and freshwater inputs create differences in water densities between the northern and southern parts of the Persian Gulf. This feature leads to the inflow marine water via the Straits of Hormuz be close to Iranian coast, It subsequently splits into two branches: (i) one branch continues on a NW path and the second, veers offshore and joins the returning southeastern flow. The Shamal wind intensifies the outflowing branch. The

highest wave energy occurs in the Ras-e-Motaf during storm condition. This part of the Persian Gulf is known as Iran's "Bermuda triangle" (Reynolds, 1993; Thoppil and Hogan, 2010).

The Persian Gulf has semi-diurnal and diurnal tides with an oscillation period between 21.6 and 27 hours (Defant, 1961). The tidal currents are mediated by Persian Gulf water circulation and bathymetry. In the Bandar-e Abbas (Straits of Hormuz), because of water exchanges between the Persian Gulf and the Oman Sea, tidal currents are faster and Mean Higher High Water (MHHW) is higher (3.4 m) than the other parts of the Gulf. Tidal currents are also strong in shallow waters (Pous et al., 2012) and MHHW in the Shatt-al-Arab estuary is +3 m.

For the Persian Gulf coast of Iran, much of our understanding of waterfront archaeological heritage and maritime trade activities can be attributed to the works of Stiffe (1895, 1896,1897a, 1897b, 1899, 1900), Goitein (1954), Ricks (1970), Whitehouse (1968, 1969, 1970 and 1971), Caspers (1971), Whitehouse and Williamson (1973), Whitcomb, (1984), Gyselen, (1989), Rougeulle et al., (1999) Priestman and Kennet (2002), Daryaee, (2003), Khosrowzadeh et al., (2006), Priestman (2003, 2005, 2013, 2020), Daryaee, (2009), Potter (2009), Whitehouse et al., (2009), Esmaeili Jelodar (2011), Khakzad (2012), Averbuch (2013), Azarian (2013), Carter et al., (2013), Khakzad and Trakadas (2014), Pashazanous et al. (2014),

Khakzad et al., (2015), Howard-Johnston (2017), Swan et al., (2017), Ghasemi and Gyselen (2018), Tomber et al., (2020). The mentioned works are focused on archaeological excavation, historical literature reviews, filed surveys and analysis on ceramic morphology, origin, distribution patterns, mineralogy and geochemistry analysis.

The first evidence of maritime trade dates back to the 3rd millennium BC, along the Arabian coast of the Persian Gulf. The archaeological remains attest to trade connections between both Mesopotamian and Indus civilizations (Caspers, 1971). By the 247 BC- 224 AD Parthians Empire ruled in both northern and southern Persia Gulf under the local kingdoms in order to benefited Silk Road trade via sea trading route (Daryaee, 2009). Maritime trade continued under the Sassanid empires. The Sassanian empires sought to gain control of the Persian Gulf for both political and economic aspirations. Daryaee (2009) believes that the Sasanians saw the Persian Gulf as their mare nostrum and part of Iranshahr, or the "Domain of the Iranians." A flourishing maritime trade between the Persians and the Romans reduced the amount of traffic on the Silk Road (Potter, 2009). The first acceleration in maritime trade in the Persian Gulf was happened during late Antiquity when the connection between Fars and East Asia leads to creating conflicts between Persian and Roman (Daryaee, 2003).

According to historical texts such as Tabari, al-Istakhri, Ibn Hawqal, al-Mas'udi (Tabari, 1987, al-Istakhri 1870, Ibn Hawqal 1965, Al-Mas'udi, 1962) maritime trade flourished again during the 9th and 10th centuries AD Siraf (chief port) and Najirum (subsidiary) played key roles in facilitating maritime navigation for oceangoing vessels. For the first time in history, regular trade between merchants from Persian Gulf with India, Southern Asia, South Arabia and East Africa merchants had been started. In fact, Siraf was a redistribution center network linking to Basra (Abbasid caliphate capital). By the time, Siraf became the wealthiest city in the world (Priestman, 2007). The prosperity of Siraf during Sassanian and early Islamic (highest prosperity of the Port) is confirmed by archaeozoological studies by Driesch and Dockner (2002). Their results suggested the variety of animal's species decreased from133 during flourishing stages to 72 when the Siraf lost importance. By the 13 to 16 AD it reached just to 39 species that it suggested gradually abandonment of Siraf. The decline of Siraf was concurrent with dramatic economic decline in southern Iraq and northwest of the Persian Gulf (Adams, 1965; Wilkinson, 2003).

Although, the historical and archaeological studies shed light on the maritime history of the Persian Gulf but none of them could not explain impacts of environmental impacts on maritime trade and important harbours shifts in the Persian Gulf. Any understanding of

ancient maritime trade in the Persian Gulf must be based on a proper contextualization of the physical factors involved in shipping goods from one place to another (Caspers, 1971). Without consideration of the main physical parameters - involving maritime navigation and port facilities, such as wind and surface current regimes, relative sea level history, climate changes and tectonic settings – it is not possible to fully grasp maritime trade and ancient harbours. There are still several unanswered questions regarding maritime trade in the Persian Gulf and its waterfront archaeological remains. Until now, there we no data on the reasons for a spatial shift in important harbours from the northwest to the central part of the Gulf during the Abbasid dynasty (9th to 10th centuries A.D.). According to the existing hypothesis, political issues are the most important factors for this change. But key questions remain:

- Despite a central government located in Basra during the Abbasid dynasty, why did maritime and trade activities suddenly shift from Apologus (located at Shatt-al-Arab) to Siraf, around 450 km along the coast?

- Although several Sassanid harbours existed close to Shatt-al-Arab, such as Rishahr (Rev Ardashir) in the northwest Persian Gulf, why were key harbours relocated to the central basin?

- What were the impacts of natural processes such as climate change, relative sea-level changes, coastal erosion

and coastal uplift on the harbour facilities and navigation in the Persian Gulf?

It is impossible to answer these archaeological questions without considering palaeo-environmental changes. Unfortunately, despite the Persian Gulf's rich history and the presence of several waterfront heritage sites, our knowledge is limited to just a handful of field surveys and ancient geographers' texts. Our understanding of the Persian Gulf's mediaeval history is sparse.

It is impossible to answer these archaeological questions without considering palaeo-environmental changes. Unfortunately, despite the Persian Gulf's rich history and the presence of several waterfront heritage sites, our knowledge is limited to just a handful of field surveys and ancient geographers' texts. Our understanding of the Persian Gulf's mediaeval history is sparse.

Alarmingly, during the last two decades, we have been witnessing serious damage to coastal heritage sites, by oil-gas companies and urbanization. Some archaeological sites have been completely destroyed. Furthermore, coastal erosion is another important risk for waterfront heritage sites. Until now, there have been no damage assessment reports with regards to natural and anthropogenic impacts on heritage remains.

In sum, much of the Persian Gulf's history is still unknown and it is at risk of being lost forever. Multidisciplinary geoarchaeological studies are required to shed light on the data gaps and to produce both natural and anthropogenic risk assessments. The present thesis is the first geoarchaeological study on waterfront archaeological records on the northern coast of the Persian Gulf. In this study, we selected Siraf and Najirum as important Sassanid-Islamic ancient harbours after visiting 13 Sassanid Islamic waterfront ancient remains from Mahroban that located at northwest end of the Persian Gulf to Kalat opposite of Kish Island (Fig 1). Siraf and Najirum are located at different coastal zones (Zone III and II respectively) with a close distance.

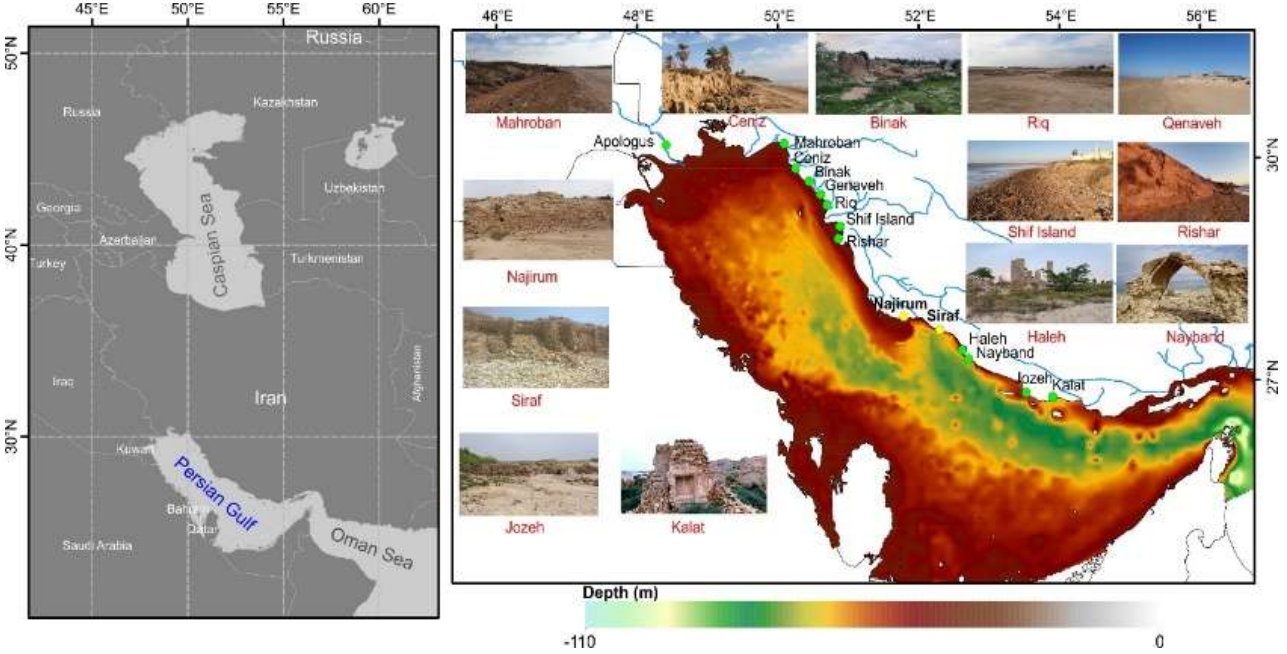

Figure 1: Location of visited Sassanid-Islamic waterfront ancient remains and studied sites

Multidisciplinary proxies such as Remote Sensing (RS), Geographic Information Systems (GIS), geomorphology, sedimentology, stratigraphy, biostratigraphy, magnetic susceptibility, physical oceanography and tectonics are considered in order to:

1-Investigate the impacts of Relative Sea level oscillations, environmental changes and crustal mobility on ancient navigation in the Persian Gulf, displacement of important harbours from the northwest to the central part of the Gulf and harbours history of Siraf and Najirum as two important ancient harbours during Sassanid and Islamic Periods.

2- Evaluate risk of coastal erosion and human impacts on waterfront heritage remains by remote sensing and geography information system.

The thesis is contained three chapters. The first chapter is addressed to impact of crustal mobility on Relative Sea Level (RSL) changes in the northern part of the Persian Gulf and harbour history of Bataneh (Najirum). Second chapter is deal with impacts of RSL changes and Summer Shamal wind on the ancient navigation risk through the Persian Gulf and shifting important harbours from northwest (Apologus) to central (Siraf) part of the Persian Gulf. Also, in this chapter an attempt has been made evaluate environmental impacts on

flourishing and falling of Siraf. Finally in chapter 3 looks at impacts of coastal erosion on the Siraf waterfront heritage remains with remote sensing and geography information system.

Reference

Adams, R. M. (1965). Land behind Baghdad: a history of settlement on the Diyala Plains. University of Chicago Press.

Agard, P., Omrani, J., Jolivet, L., & Mouthereau, F. (2005). Convergence history across Zagros (Iran): constraints from collisional and earlier deformation. International journal of earth sciences, 94(3), 401-419.

Al Senafi, F., & Anis, A. (2015). Shamals and climate variability in the Northern Arabian/Persian Gulf from 1973 to 2012. International Journal of Climatology, 35(15), 4509-4528.

Al-Istakhri, (1870), M. J. de Goeje (trans. & ed.), Kitab Al-Masalik wa-al-Mamalik. Leiden.

al-Mas‘udi, A. L. H. (1962). Les prairies d’or. Trans. C. Barbier de Meynard, Pavet de Courteille, and Charles Pellat. Paris: Société asiatique.

Aqrawi, A. A. (2001). Stratigraphic signatures of climatic change during the Holocene evolution of the Tigris–Euphrates delta, lower Mesopotamia. Global and Planetary Change, 28(1-4), 267-283.

Averbuch, B. D. (2013). From Siraf to Sumatra: Seafaring and Spices in the Islamicate Indo-Pacific, Ninth-Eleventh Centuries CE. Harvard University.

Azarian, M. (2013). Bataneh ancient site systematically survey in order to identification location of Najirum ancient harbour [master’s thesis]. Tarbiat Modares University, Tehran, Iran. [Farsi]

Baniasad, A., Rabbani, A. R., Moallemi, S. A., Soleimany, B., & Rashidi, M. (2017). Petroleum system analysis of the northwestern part of the Persian Gulf, Iranian sector. Organic Geochemistry, 107, 69-85.

Bartlett KS. (2004). Dust Storm Forecasting for Al Udeid Ab, Qatar: An Empirical Analysis. Master's thesis, Air University, Islamabad.

Berberian, M., & King, G. C. P. (1981). Towards a paleogeography and tectonic evolution of Iran. Canadian journal of earth sciences, 18(2), 210-265.

Beydoun, Z. R. (1991). Arabian plate hydrocarbon geology and potential.

Bordenave, M. L., & Hegre, J. A. (2005). The influence of tectonics on the entrapment of oil in the Dezful Embayment, Zagros Foldbelt, Iran. Journal of petroleum Geology, 28(4), 339-368.

Carter, R. A., Challis, K., Priestman, S. M., & Tofighian, H. (2006). The Bushehr Hinterland Results of the First Season of the Iranian-British Archaeological Survey of Bushehr Province, November-December 2004. Iran, 44(1), 63-103.

Caspers, E. C. D. (1971). New archaeological evidence for maritime trade in the Persian Gulf during the Late Protoliterate period. East and West, 21(1/2), 21-44.

Clark, P. U., Dyke, A. S., Shakun, J. D., Carlson, A. E., Clark, J., Wohlfarth, B., ... & McCabe, A. M. (2009). The last glacial maximum. science, 325(5941), 710-714.

Crook, J. (2009). Climate analysis and long-range forecasting of dust storms in Iraq. Naval Postgraduate School Monterey CA.

Daryaee, T. (2009). The Persian Gulf in late antiquity: the Sasanian era (200–700 CE). In The Persian Gulf in History (pp. 57-70). Palgrave Macmillan, New York.

Defant, A. (1961). Physical oceanography (Vol. 1). Pergamon.

Driesch, A., & Dockner, A. (2002). Animal exploitation in medieval Siraf. Iran, based on the faunal remains from the excavations at the Great Mosque (seasons 1966-1973). Bonner zoologische beitrage, 50(3), 227-248.

Edgell, H. S. (1996). Salt tectonism in the Persian Gulf basin. Geological Society, London, Special Publications, 100(1), 129-151.

Esmaeili Jelodar, M. (2011). A propose for Identification of Najirum ancient harbour according to the early-Islamic texts and archaeological survey. Journal of the Persian Gulf research paper, 3, 129-159. [Farsi]

Frizon de Lamotte, D., Raulin, C., Mouchot, N., Wrobel-Daveau, J. C., Blanpied, C., & Ringenbach, J. C. (2011). The southernmost margin of the Tethys realm during the Mesozoic and Cenozoic: Initial geometry and timing of the inversion processes. Tectonics, 30(3).

Ghasemi, P., & Gyselen, R. (2018). 'Bulles administratives sassanides trouvées à Tole Qaleh Seyfabad (Fārs)'. in L'Orient est son Jardin. Hommage à Rémi Boucharlat. GONDET S. et HAERINCK E. (Eds). Acta Iranica 58. Peeters, Leuven, Paris Bristol.

Giannakopoulou, E. M., & Toumi, R. (2012). The Persian Gulf summertime low-level jet over sloping terrain. Quarterly Journal of the Royal Meteorological Society, 138(662), 145-157.

Goitein, S. D. (1954). Two Eyewitness Reports on an Expedition of the King of Kīsh (Qais) against Aden. Bulletin of the School of Oriental and African Studies, 16(2), 247-257.

Gyselen, R. (1989). 'La géographie administrative de l'Empire sassanide'. Les témoignages sigillographiques, (Res Orientales I), Paris.

Heyvaert, V. M. A., & Baeteman, C. (2007). Holocene sedimentary evolution and palaeocoastlines of the Lower Khuzestan plain (southwest Iran). Marine Geology, 242(1-3), 83-108.

Hosseiny, E., Rabbani, A. R., & Moallemi, S. A. (2016). Source rock characterization of the Cretaceous Sarvak Formation in the eastern part of the Iranian sector of Persian Gulf. Organic Geochemistry, 99, 53-66.

Howard-Johnston J. (2017). The India Trade in Late Antiquity (Chapter 13) - Sasanian Persia. Edinburgh University Press, 284-304.

Ibn Hawqal, (1965). J. H. Kramers (trans. & ed.), Kitab Surat al-Ard. Bibliotheca Georaphorum Arabicorum, Leiden.

Jahani, S., Callot, J. P., de Lamotte, D. F., Letouzey, J., & Leturmy, P. (2007). The salt diapirs of the eastern Fars Province (Zagros, Iran): A brief outline of their past and present. In Thrust Belts and Foreland Basins. Springer, Berlin, Heidelberg.

Kamranzad, B. (2018). Persian Gulf zone classification based on the wind and wave climate variability. Ocean Engineering, 169, 604-635.

Kassler, P. (1973). The structural and geomorphic evolution of the Persian Gulf. In The Persian Gulf (pp. 11-32). Springer, Berlin, Heidelberg.

Khakzad, S. (2012). Siraf archaeological report. Sasanika Archaeology, 10.

Khakzad, S. and Trakadas, A. (2014). The world in a grain of sand: Siraf, in S. Sindbæk and A. Trakadas (eds), The World in the Viking Age, 108–110. Roskilde.

Khakzad, S., Trakadas, A., Harpster, M., & Wittig, N. (2015). Maritime Aspects of Medieval S iraf, I ran: a pilot project for the investigation of coastal and underwater archaeological remains. International Journal of Nautical Archaeology, 44(2), 258-276.

Khosrowzadeh, A., Aali, A., Kennet, D., Priestman, S. 1385 (2006). Kahur Langar Chini: a Parthian port on the coast of Persian Gulf. Iranian Centre for Archaeological Research, Archaeological Reports 5: 55-70. [Farsi].

Konyuhov, A. I., & Maleki, B. (2006). The Persian Gulf Basin: Geological history, sedimentary formations, and petroleum potential. Lithology and Mineral Resources, 41(4), 344-361.

Lambeck, K. (1996). Shoreline reconstructions for the Persian Gulf since the last glacial maximum. Earth and Planetary Science Letters, 142(1-2), 43-57.

Lokier, S. W., Bateman, M. D., Larkin, N. R., Rye, P., & Stewart, J. R. (2015). Late Quaternary sea-level changes of the Persian Gulf. Quaternary Research, 84(1), 69-81.

Motiei, H. (2001). Simplified table of rock units in southwest Iran. Keyhan Exploration and Production Services, Tehran.

Mouthereau, F., Lacombe, O., & Vergés, J. (2012). Building the Zagros collisional orogen: timing, strain distribution and the

dynamics of Arabia/Eurasia plate convergence. Tectonophysics, 532, 27-60.

Parker, A. G., & Goudie, A. S. (2008). Geomorphological and palaeoenvironmental investigations in the southeastern Arabian Gulf region and the implication for the archaeology of the region. Geomorphology, 101(3), 458-470.

Pashazanous, H. R., Montazer Zohouri, M., & Ahmadi, T. (2014). Sea trade between Iran and China in the Persian Gulf based on the excavations of Sīrāf city. Indian Journal of Economics and Development, 2, 6-13.

Paul, A., & Lokier, S. W. (2017). Holocene marine hardground formation in the Arabian Gulf: Shoreline stabilisation, sea level and early diagenesis in the coastal sabkha of Abu Dhabi. Sedimentary Geology, 352, 1-13.

Perrone, T.J., 1979. Winter shamal in the Persian Gulf, Naval Env. Prediction Res. Facility, Technical Report, 79-06, Monterey.

Peters, J. M., Filbrandt, J. B., Grotzinger, J. P., Newall, M. J., Shuster, M. W., & Al-Siyabi, H. A. (2003). Surface-piercing salt domes of interior North Oman, and their significance for the Ara carbonate 'stringer'hydrocarbon play. GeoArabia, 8(2), 231-270.

Potter, L. (2009). The Persian Gulf in History. Springer.

Pous, S., Carton, X. J., & Lazure, P. (2012). A process study of the tidal circulation in the Persian Gulf.

Priestman S. (2007). The British museum Siraf project. The British institute of Persian studies, Newsletter no 32, 5-6.

Priestman, S. (2003). The Williamson Collection Project: Sasanian and Islamic survey ceramics from southern Iran, current research. Iran, 41(1), 345-348.

Priestman, S. (2005). Settlement & ceramics in Southern Iran: An analysis of the Sasanian & Islamic periods in the Williamson collection (Doctoral dissertation, Durham University).

Priestman, S. (2013). A quantitative archaeological analysis of ceramic exchange in the Persian Gulf and Western Indian Ocean, AD c. 400-1275 (Doctoral dissertation, University of Southampton).

Priestman, S. (2020). Late Islamic ceramic distribution networks in the Gulf: new evidence from Jazīrat al-Ḥamrāʾ in Ras al-Khaimah. In Proceedings of the Seminar for Arabian Studies (Vol. 50, pp. 293-306).

Priestman, S., & Kennet, D. (2002). The Williamson collection project: Sasanian and Islamic pottery from southern Iran. Iran, 40(1), 265-267.

Purser, B. H., & Seibold, E. (1973). The principal environmental factors influencing Holocene sedimentation and diagenesis in the Persian Gulf. In The Persian Gulf (pp. 1-9). Springer, Berlin, Heidelberg.

Reynolds, R. M. (1993). Physical oceanography of the Gulf, Strait of Hormuz, and the Gulf of Oman—Results from the Mt Mitchell expedition. Marine Pollution Bulletin, 27, 35-59.

Ricks, T. M. (1970). Persian Gulf seafaring and East Africa: ninth-twelfth centuries. African Historical Studies, 339-357.

Rougeulle, A., Parabha Ray, H., Salles, J., (1999). : Medieval Trade Networks in the Western Indian Ocean (8th-14th centuries):

Some Reflections from the Distribution Patterns of Chinese Imports in the Islamic World. Manohar, 80-159.

Sandeep, S., & Ajayamohan, R. S. (2018). Modulation of winter precipitation dynamics over the Arabian Gulf by ENSO. Journal of Geophysical Research: Atmospheres, 123(1), 198-210.

Sarnthein, M. (1972). Sediments and history of the postglacial transgression in the Persian Gulf and northwest Gulf of Oman. Marine Geology, 12(4), 245-266.

Seibold, E., Vollbrecht, K. (1969). Die Bodengestalt des Persischen Golfs. "METEOR" Forsch. Ergebnisse, Reihe C, No. 2, 29-56

Smith, A. G., Smith, D. G., & Funnell, B. M. (2004). Atlas of Mesozoic and Cenozoic coastlines. Cambridge University Press.

Snidero, M., Carrera, N., Mencos, J., Butillé, M., Granado, P., Tavani, S., ... & Muñoz, J. A. (2020). Diapir kinematics in a multi-layer salt system from the eastern Persian Gulf. Marine and Petroleum Geology, 104402.

Stiffe, A. W. (1895). Ancient Trading Centres of the Persian Gulf: I. Siráf. Geographical Journal, 166-173.

Stiffe, A. W. (1896). Ancient Trading Centres of the Persian Gulf. II. Kais, or Al-Kais. The Geographical Journal, 7(6), 644-649.

Stiffe, A. W. (1897a). Ancient Trading Centers of the Persian Gulf, III: Pre-Mohammedan Settlements. Geographical Journal, 9(3), 309-314.

Stiffe, A. W. (1897b). Ancient Trading Centres of the Persian Gulf: IV Maskat. The Geographical Journal, 10(6), 608-618.

Stiffe, A. W. (1899). Former Trading Centres of the Persian Gulf. V. Kung. The Geographical Journal, 13(3), 294-297.

Stiffe, A. W. (1900). Ancient Trading Centres of the Persian Gulf: VI Bandar'Abbas. The Geographical Journal, 16(2), 211-215.

Stöcklin, J. (1974). Possible ancient continental margins in Iran. In The geology of continental margins (pp. 873-887). Springer, Berlin, Heidelberg.

Stoecklin, J. (1968). Structural history and tectonics of Iran: a review. AAPG bulletin, 52(7), 1229-1258.

Swan, C. M., Rehren, T., Lankton, J., Gratuze, B., & Brill, R. H. (2017). Compositional observations for Islamic glass from Sīrāf, Iran, in the Corning Museum of Glass collection. Journal of Archaeological Science: Reports, 16, 102-116.

Tabari, 1987, The History of al-Tabari vol.1. State University of New York, Albany.

Takin, M. (1972). Iranian geology and continental drift in the Middle East. Nature, 235(5334), 147-150.

Talbot, C. J., & Alavi, M. (1996). The past of a future syntaxis across the Zagros. Geological Society, London, Special Publications, 100(1), 89-109.

Thomas, R. J., Ellison, R. A., Goodenough, K. M., Roberts, N. M., & Allen, P. A. (2015). Salt domes of the UAE and Oman: probing eastern Arabia. Precambrian Research, 256, 1-16.

Thoppil, P. G., & Hogan, P. J. (2010). Persian Gulf response to a wintertime shamal wind event. Deep Sea Research Part I: Oceanographic Research Papers, 57(8), 946-955.

Tomber, R., Spataro, M., & Priestman, S. (2020). Early Islamic Torpedo Jars from Siraf: Scientific Analyses of the Clay Fabric and Source of Indian Ocean Transport Containers. Iran, 1-24.

Uchupi, E., Swift, S. A., & Ross, D. A. (1996). Gas venting and late Quaternary sedimentation in the Persian (Arabian) Gulf. Marine Geology, 129(3-4), 237-269.

Whitcomb, D., (1984). 'Qasr e Abu Nasr and the Gulf'. in Arabie Orientale, Mésopotamie at Iran Méridional de l'âge du Fer an début de la Période Islamique. Paris: Editions Recherche sur les Civilisations, pp.331-37.

Whitehouse, D., & Williamson, A. (1973). Sasanian maritime trade. Iran, 11(1), 29-49.

Whitehouse, D., (1968), Excavations at Siraf: First Interim Report. Iran 6, 1–22.

Whitehouse, D., 1969, Excavations at Siraf: Second Interim Report. Iran 7, 39–62.

Whitehouse, D., 1970, Excavations at Siraf: Third Interim Report. Iran 8, 1–18.

Whitehouse, D., 1971, Excavations at Siraf: Fourth Interim Report. Iran 9, 1–17.

Whitehouse, D., Whitcomb, D. S., & Wilkinson, T. J. (2009). Siraf: history, topography and environment. Oxbow Books.

Wilkinson, T. J. (2003). Archaeological landscapes of the Near East. University of Arizona Press.

Ziegler, M. A. (2001). Late Permian to Holocene paleofacies evolution of the Arabian plate and its hydrocarbon implications: GeoArabia, v. 6.

CHAPTER TWO:
Late Holocene Relative Sea-Level fluctuations and Crust Mobility in Bataneh (Najirum) Archaeological Site, Persian Gulf, Iran

Abstract

The impacts of relative sea-level (RSL) variations, crust mobility on the development of ancient harbours in the northern Persian Gulf is poorly understood. Many unanswered questions remain with regards to the main reasons of shifting the most important ancient harbours location along the norther part of the Persian Gulf coastal during last 2 kyr B.P. Furthermore, some important early Islamic harbours, such as Siraf, have ancient city quarters that are today below present sea-level. The aim of this study is evaluation probably relationship between halokinesis and RSL changes via sea-level modeling and multidisciplinary geoarchaeological methods on Sassanid –Islamic Bataneh ancient site, presently known as Najirum ancient harbour, located at foothill of active Darang salt diapir. The result of this study reveals that after the mid-Holocene highstand, regressive phase of RSL was not continuously and studied facies were logged three RSL oscillations. The oscillation time intervals are changed correlated with eustatic sea level position. By the first lowstand, important Sassanid harbours had changed from Rishar to Apologus. Second lowstand with together summer Shamal wind led to transition maritime trade from Apologus to Siraf in the Abbasid dynasty. Coastal uplift at Bataneh coastal zone exposed the city at risks from flooding and fluvial debris flows. With a modification of

the local watershed, runoff water originating from the salt anticlinal was controlled and used for the extraction of gypsum in evaporation ponds. The economic expansion of Siraf, led to Bataneh being abandoned with a shift in trade to Kish Island.

Keywords: Relative sea-level, Geoarchaology, Najirum, ancient harbour, Crust mobility, Persian Gulf

1. Introduction

The Persian Gulf is located between the Zagros Mountains to the northwest and the Arabian Platform to the southeast. Collison of the Arabian and Eurasian continents played out during the Tertiary. In the end of Oligocene, opening of the Red Sea divided Arabia from Africa that it has produced the uplift of the Arabian Shield and exposed Precambrian crystalline basement. The main fault systems with N-S trend are from Qatar Arc and SE boundary of the Shield. During Zagros orogenic system evolution, the Arabian Plate was flexed and Mesopotamia foreland basin and the Persian Gulf in the front of the Zagros Mountain have formed (Konert et al., 2001). The asymmetry of the Persian Gulf has been accentuated due to the tilting of the Arabian Peninsula, associated with an opening of the Red Sea in the Neogene. Zagros is one of the most active collisional belts in the world and much of the deformation and seismicity of the Zagros Mountains and high-relief topography on the northeastern margin of the Persian Gulf are related to its active tectonics. On the southern margin of the Gulf, the aseismic low-relief is consistent with a tectonically static region (U. S. Geological Survey, 2011).

Zagros tectonic setting and halokinesis are controlled the Persian Gulf basin and coastal morphology. According to Pourkerman et al., (2020) classification, the

Persian Gulf coastal is subdivided in three morphological zones with different tide level: (i) gently sloping marshland coasts with permanent rivers (Zone 1); (ii) diapiric uplifting coast salt domes (Zone II) and rocky coast with steep coastal slope (Zone III) (Fig 1, table 1).

Several studies have done in the Persian Gulf in order to reconstruct Holocene RSL changes (Kassler, 1973; McClure and Vita-Finzi, 1982 Lambeck, 1996; Aqrawi, 2001; Williams and Walkden, 2002; Lokier et al., 2015; Paul and Lokier 2017). Uchupi et al., (1999) suggested that Holocene marine transgression was accelerated basin subsidence at axial zone and local uplifts were happened especially in the northeast of the Persian Gulf. The coastal uplift in United Arab Emirates was happened under the influences of Holocene RSL rise and halokinesis (Wood et al., 2012). By the contrast, Steven et al., (2014) believes that RSL in southeast of Persian Gulf is controlled by eustatic sea level changes and halokinesis and neo-tectonic had no impacts on RSL and coastal elevation changes.

In order to understand past coastal changes, especially RSL fluctuations, multidisciplinary geoarchaeological studies of ancient harbours and maritime structures are widely used (e.g., Morhange et al., 2001; Marriner and Morhange, 2007, Marriner et al., 2010, Marriner et al., 2017; Benjamin et al., 2017; Vacchi et al., 2020, Pourkerman et al., 2020). The most important

ancient harbours in the Persian Gulf were located in the Iranian sector until the twentieth century A.D. (Potter, 2009). Coastal cabotage and the location of ancient harbours in the Persian Gulf were partly controlled by RSL changes, coastal morphology, the meteo-marine context (e.g. Shamal winds) and sea surface currents (Pourkerman et al., 2020).

The Sassanian Empires were interested in gaining control of the Persian Gulf, for both political and economic aspirations. Flourishing maritime trade between Persians and Romans reduced the amount of land-based traffic on the Silk Road (Potter, 2009). The foundation of Najirum dates back to the Sassanid Empire (Al-Istakhri, 1870). It is classified as a sector of Siraf in the Ardeshir Khooreh ("Khooreh" means "province" in Persian). The Ardeshir Khooreh was one of the largest provinces between the five main united provinces of Fars (Al-Istakhri, 1870). The southern part of the province was demarcated by the Persian Gulf coast. Because it was adjacent to the central Sassanid Empire, and due to the importance of maritime trade activities at this time, Ardeshir Khooreh became one of the most important provinces.

After the demise of the Sassanid Empire, an important eastward shift in harbours took place in the early Abbasid period, from Ubulla (Apologus) to Siraf in the central basin when Basra was the caliphate capital

(Potter, 2009). Najirum and Siraf became important sites for maritime trade during the Abbasid dynasty, as attested by the writings of ancient geographers such as Al-Istakhri (1870), Ibn Hawqal (1965) and Ibn Balkhi (1984). After 150 years, Siraf lost its importance and it was replaced by Kish Island.

In this study, we employ geoarchaeology to investigate the evolution of Bataneh (Najirum) ancient site. The site was selected because of its location at the foothill of a salt diapiric fold in order to reconstruct RSL changes and the role of halokinesis in driving coastal changes.

2. Salt tectonic

One of the most important features of the Zagros belt is presence several salt diapir of Late Precambrian-Early Cambrian Hormuz salt that existed in the eastern part of Zagros fault thrust belt and the Persian Gulf. Halokinesis was started shortly after the deposition of the Hormuz salt in the early Paleozoic and it is continued up to present (Jahani et al., 2007). The salt domes are generally existed along near N-S and NE-SW fault system (Jahani et al, 2017).

The central basin of the Persian Gulf is well known for several salt domes and diapiric folds along its coast (Kalat, Bostaneh, Mughu, Moallem, Homiran and

Darang) and offshore islands (Great and small Tunb, Farur, Abu Musa) in Iran, the United Arab Emirates (Sir Abu Nuayer, Arzanah, Sir Bani Yas) and Qatar (Halul and Sharao). (Beydoun, 1991; Thomas et al., 2015). In the eastern of the central basin salt tectonic is linked to salt bearing system form Hormuz salt formation and late Oligocene-Early Miocene Fars salt (Fig 2) (Hassanpour et al., 2020). In the early Miocene, after the beginning of the Zagros continental collision, the Hormuz salt extrusion started again. Consequently, Fars salt diapirism is triggered by gravitational loading produced by an overriding of the allochthonous Hormuz salt sheet. This process pushed the Fars salt outwards (Snidero et la., 2020). The salt diapir close to the present coast of the Persian Gulf emerged following the reactivation of salt domes during the final Zagros folding phase (Jahani et al., 2007). The impacts of halokinesis on the coastal elevation of the United Arab Emirates has been discussed by Wood et al. (2012) and Lidour et al. (2020). But its effects on RSL and coastal dynamics in the northern Persian Gulf is still unknown.

The ancient site of Bataneh is located in the foothills of the Darang Anticline (diapiric fold, Zone II) (Fig 2B). The Darang salt pillow is located along the southern end of Dashti Fault system with N-S orientation (Fig 2) and it is core of Darang anticlinal. The Darang salt pillow have started to grow since Paleozoic and it continuous through geological time (Jahani et al., 2017).

The diapiric fold has exposed lithological units with evaporation minerals such as gypsum and gypsum marl. The concentration of deep rill erosion features in the upland areas shows their high sensitivity to water erosion (Fig 2C). Bataneh has an open coastal morphology and NW-SE longshore current responsible for coastal erosion and moving sandbars along the coast (Pourkerman et al., 2019).

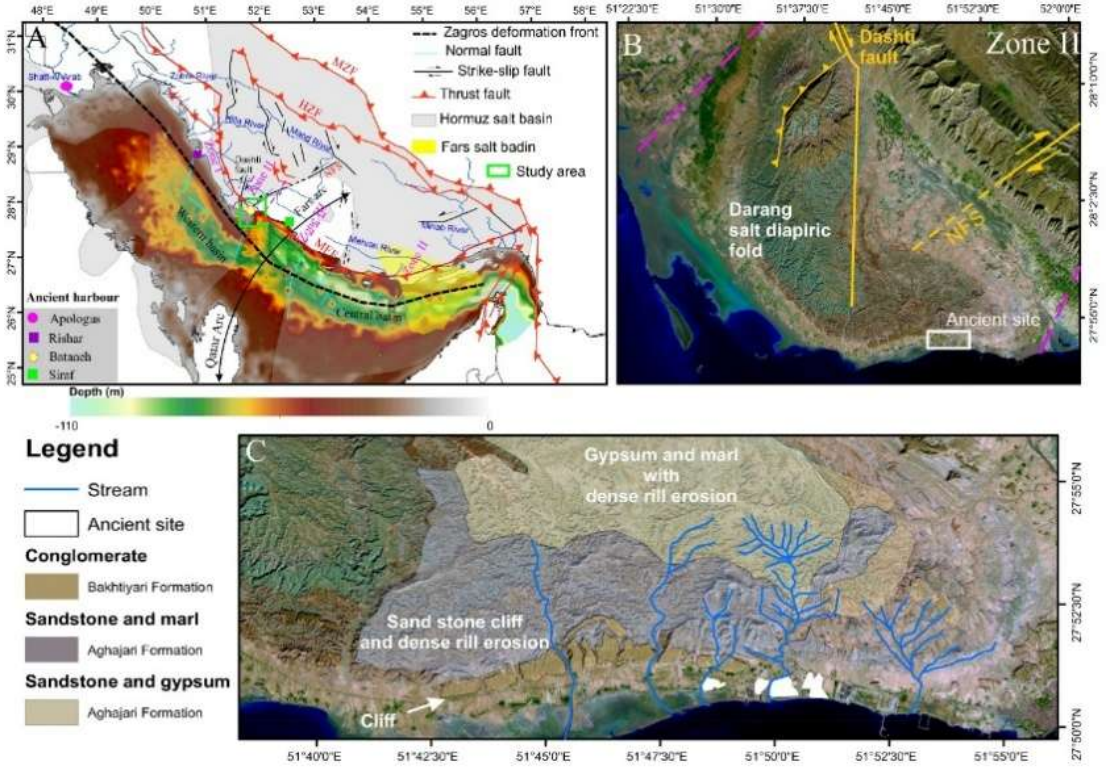
A
Zagros deformation front
Normal fault
Strike-slip fault
Thrust fault
Hormuz salt basin
Fars salt badin
Study area
MZF
HZF
Ancient harbour
Apologus
Rishar
Bataoch
Sirraf
Depth (m)
-110
0
B
Zone II
Dashti fault
Darang salt diapiric fold
NFS
Ancient site
Legend
Stream
Ancient site
Conglomerate
Bakhtiyari Formation
Sandstone and marl
Aghajari Formation
Sandstone and gypsum
Aghajari Formation
C
Gypsum and marl with dense rill erosion
Sand stone cliff and dense rill erosion
Cliff

Figure 2: A) The Persian Gulf bathymetry, coastal geomorphological classification and major structural elements of Zagros fold-and-thrust belt (modified after Berberian, 1995, Jiménez-Munt et al., 2012; Jahani et al., 2017, Hassanpour et al., 2020 and Pourkerman et al., 2020). MZF = Main Zagros Fault; HZF = High Zagros Fault; MFF = Mountain Front Flexure; NFS = Nezamabad Fault system. B) Position of the ancient site at the Darang salt diapiric fold on the Landsat 8 (RGB= 753), position of N-S Dashti and NE-SW Nezamabad fault systems. C) Lithological units.

Table 1: Geomorphological zonation and tidal levels at sites from the Strait of Hormuz to Shatt-al-Arab

Place	Ancient site	Lat N	Long E	Height in meters above datum				Class
				MHHW	MLHW	MHLW	MLLW	
Bandar-e Abbas	unknown	29° 22'	56° 17'	3.4	2.6	1.4	0.7	Zone II
Asaluyeh	Siraf	27° 28'	52° 37'	1.6	1.5	0.7	0.3	Zone III
Dayyer	Bataneh (Najirum)	27° 50'	51° 56'	2.0	1.6	0.8	0.5	Zone II
Bandar-e Bushehr	Rishar	28° 54'	50° 45'	1.9	1.3	1.1	0.5	Zone I
Bandar-e Ganaveh	Jannaba	29° 34'	50° 31'	2.2	1.5	1.3	0.6	Zone I
Imam Hassan	Ceniz	29° 50'	50° 15'	2.4	1.7	1.3	0.6	Zone I
Shatt-al-Arab	Apologus	29°50'	48°43'	3.0	2.4	1.3	0.4	Zone I

3. Geomorphological features and archaeological context

According to field observations, the ancient site of Bataneh comprises four sectors separated by natural geomorphological features such as rocks, bays and flood plains. All of the ancient sites lie on high ground, 7 to 11 m above present sea level. Several streams and ephemeral rivers are sourced in the evaporation unit; the largest one passes north of site B. Alluvial fans, floodplains and wadis are the most important geomorphological features, with a high potential risk of flooding and debris flows for archaeological remains (Fig 3).

Our knowledge about the historic sites is limited to just two surveys conducted by Esmaeili Jelodar (2011) and Azarian (2013). Esmaeili Jelodar (2011) introduced three (A, B, C) ancient zones. He dated the sites to the late Sassanid – early Islamic period on the basis of a ceramics chrono-typology. His study focused on zone B because of the presence of features mentioned in historic texts, such as ancient mosques with stair cases carved into the rock (Talle Ashrafi), to the north and an estuary to the west (Fig 4). A variety of ceramics and Chinese porcelains attest to a thriving city. The archaeological remains and spatial location of the ancient site (distance from Siraf) harbour have led archaeologists to identify the ancient site as the missing port town of Najirum.

The site is elevated 8 to 10 m above present sea level to the north. To the south, the elevation decreases with a gentle slope. An ephemeral river channel passes between zones B and C. Five alluvial fans are located 200 m north of the ancient site, along two ephemeral rivers (Fig 3).

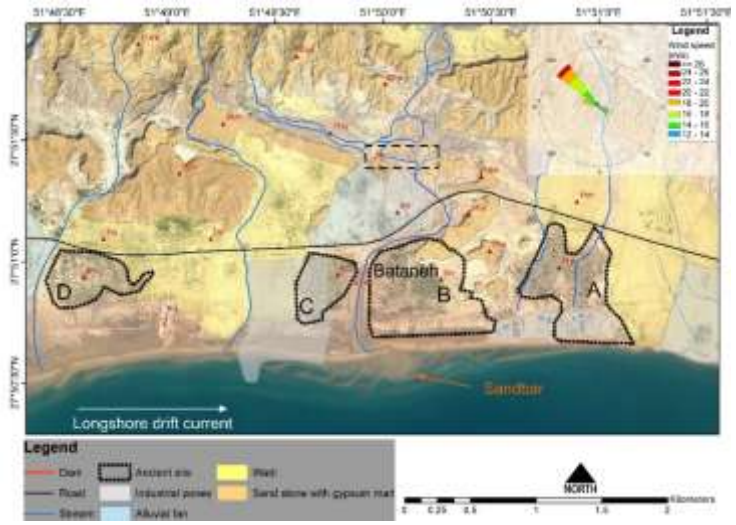

Figure 3: General geomorphological map of Bataneh and its ancient sites located on a Google Earth image (2011). Zones A, B and C are reported by Esmaeili Jelodar (2011) and D is introduced in this study. The black dashed-line denotes the location of a manmade dike and artificial watercourse for redirecting runoff water. The recent industrial constructions at site C have been updated using a Landsat 8 panchromatic band (2020).

Although zone B has been damaged by recent industrial constructions, zones A and C contain three important types of artefacts. (i) Urban fabric containing several ancient walls and decorative gypsum objects. The building walls are made of rubble and baked gypsum. On the interior side, the walls are covered with plaster motifs. (ii) An artisanal area with remains of furnaces and (iii) an

area of rectangular embankments (ponds) connected via an ancient canal (Fig 4).

To the west of the city, two ancient embankments have been erected along either bank of the stream, for channel stability. A trace of dikes is observed at the end of the walls in order to prevent water runoff to the sea. The eastern embankment is distinct, with the ancient canal that stretched along the ponds (Fig 4).

Figure 4: A) General geomorphological features of zone B and sectors of the ancient city of Bataneh. The green point indicates the coring site. B) Remnants of the ancient city wall, comprising rubble and baked gypsum. C) Remains of an ancient furnace in the old industrial area (purple zone). D) Several samples showing the use of baked gypsum for decorative elements and E) plaster motifs.

4. Methodology

In this study we integrated high-resolution Corona, Google Earth and moderate resolution Landsat OLI images (overpass frequencies of 16 days) in order to map the ancient site and its geomorphological features (Beck et al., 2007, Myers, 2010, Saleem et al., 2018), in addition to updating the most recent anthropogenic constructions over the historical site. The satellite images were georeferenced using 1:100,000 topographic maps from the National Cartographic Center (NCC) with a Root Mean Square Error (RMSE) of between 0.01and 0.05 pixels.

A 3-m borehole was extracted from sector (iii) zone B, an area in which human disturbance was negligible. The core was leveled using a theodolite (+4.5 meter) in relation to present Mean Sea Level (MSL). After core collection, nondestructive magnetic susceptibility (MS) was measured using a Bartington MS2c 100-mm diameter loop sensor with an MS2 meter at 2 cm resolution (Delile et al., 2014). Subsamples were obtained using the high-resolution sampling procedure described by Marriner and Morhange (2007). Subsamples were oven-dried at 50°C for 12h. Each sample was separated into three fractions for biostratigraphy, granulometry, Organic Matter (OM) and carbonate content. Wet sieving was performed using mesh sizes of 2 mm and 63 microns. After processing and oven-drying, the ostracods were

picked from 10 g of the >125 µm size fraction and placed on microslides in order to count and identify the species (Marriner et al., 2005). Simultaneously, microscopic sedimentary properties and general minerals were noted. Macrofossils (>2mm) were identified using the Persian Gulf dataset described by Sahafi et al. (2000).

Laser granulometry was performed using a Horiba La950E after treatment of sediments by peroxide hydrogen and HCL 0.1 in order to remove the effects of biological production on the sedimentary textures. The sediments were classified according to Folk (1954) ternary diagrams and statistical parameters calculated by the method of moments (Folk and Ward, 1957). Organic matter (OM) and carbonate properties were calculated using loss-on-ignition (LOI) at 550°C and 950°C (Heiri et al., 2001).

According to the main facies changes and anthropogenic horizons, 14C dates were performed at Poznan Radiocarbon Laboratory, mainly on charcoal and juvenile bivalve shells due to the absence of organic matter. The data were calibrated using CALIB 8.1, with a marine delta reservoir specific to the Persian Gulf (Southon et al., 2002) (Table 2).

The Glacial Isostatic Adjustment (GIA) simulations performed in this work are based on model ICE-6G (VM5a) of Peltier (2012) and Peltier et al. (2015). The Late-Pleistocene-ice-sheets chronology of model

ICE-6G (VM5a) was been implemented in the program SELEN4 (Spada and Melini, 2019). SELEN4 solves the Sea-Level Equation by taking into account the horizontal migration of shorelines, for the transition from grounded to floating ice and for the effects of rotational feedback on sea level. The Sea-Level Equation was solved using a pseudo-spectral approach with a spatial resolution corresponding to the maximum harmonic degree lmax=256, on a grid with a spacing of ~40 km.

Table 2: Calibrated radiocarbon ages for three important facies.

ID	Dating material	Depth cm	Radiocarbon age	Calibration			
				1 sigma	Significant	2 sigma	Significant
Naj1-1	Charcoal	78	1175 ± 30	823-892 AD	0.78	774-899 AD	0.82
Naj2-1	Shell	145	2035 ± 30	482-535 AD	1.0	380-725 AD	1.0
Naj3-1	Shell	268	2400 ± 30	50-247 AD	1.0	50 BC- 354 AD	1.0

5. Results

5.1. Geomorphological and archaeological contexts

5.1.1 Local watershed management

The alluvial geomorphological features such as wadis, alluvial fans and flood plains underscore the high potential risk of flooding and debris flow by flash flooding events during winter and autumn, on this specific lowland coast. One of the most important factors mediating runoff

power discharge to downstream areas is soil permeability (Sampson, 2016). The upstream lithological units are made of low permeability gypsum marls with sandstone interlayers. The gypsum marl unit contains soluble evaporation minerals and fine-grained sediment (silt and clay). This leads to a decrease in permeability and soil strength against erosion (Heshmati et al., 2013). As a result, a huge amount of sediment was reworked to downstream areas through the stream channels, leading to coastal progradation at base level. Decreases in slope angles and sudden changes in watershed bedrock types from marl (soft bedrock) to sandstone (hard bedrock) means that the runoff cannot be evacuated. Abrupt stream channel disruption has led to the formation of alluvial fans north of the ancient site at base level (Fig 5B).

In order to protect the city from flash floods, a cemented dike was erected at the end of the stream, with an aim to reduce runoff energy. The water was channeled in an artificial watercourse that was excavated into the bedrock (Fig 3, Fig 5C and D). The watercourse directed runoff water to the city via a channel which passed north of the city. During flooding events, muddy sediment passed through the artificial channel (Fig 5E). The runoff water, containing high amounts of dissolved salts, was channeled to the city for industrial purposes.

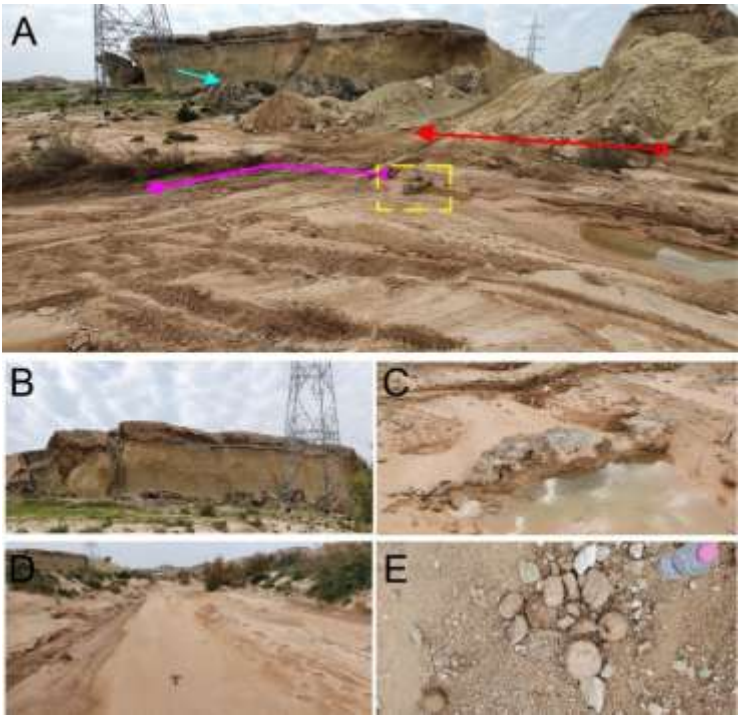

Figure 5: A) The red arrow represents an old ephemeral river direction that has led to erosion of the marl section of the rock. The cyan arrow and C) show eroded sandstone rock from the outcrop. The yellow dashed line and B) shows the manmade dike used to reduce floodwater velocity and sluice water along a narrow artificial channel shown in purple. D and E) artificial channel over sandstone bedrock. Mud balls are formed due to the reworking of mud pieces over the hard bedrock.

5.1.2. Analysis of the urban area

We could not find any preserved ancient buildings to analyses the urban fabric, due to extensive erosion and destruction by industrial activities and also

the absence of archaeological excavations. Based on the remains of building walls it is possible to infer the widespread use of rubble and cooked gypsum for construction (Fig 4).

South of the zone, we identified 15 almost rectangular embankments, probably used as ponds (Fig 4). The ponds were fed by an ancient canal. The canal lies on a gentle west-to-east slope and it has distribution canals between the ponds. The runoff water was stopped behind the dike to prevent outflow to the sea. The trapped water entered the canals and moved through them under gravity. Different elevations between each row of ponds (from north to south) facilitated this flow. So, saturated water collected in the wet seasons and gypsum precipitated due to evaporation processes during warm and arid seasons. The resulting gypsum crystals were collected for baking in the furnaces of the artisanal area.

5.1.3 Evaluation of site damage

In terms of archaeological erosion, the study site has been significantly damaged by anthropogenic processes during last 20 years. Satellite images and field observations demonstrated that anthropogenic activities have destroyed much of the ancient urban and artisanal areas. According to Esmaeili Jelodar's (2011) report, the destruction of the ancient site predates recent industrial developments. Unfortunately, we can presently see the

same trend in the other ancient zones A and C. But a newly discovered site (site D) is almost virgin (Fig 6).

Figure 6: A) View of part of the bulldozed ancient site of Bataneh (zone B); B) industrial construction in ancient zone C. C) and D) newly discovered ancient zone D containing late Sassanid-early Islamic ceramics.

5.2. Litho- and biostratigraphy

The core station is +4.5 meter above current seal-level. In the coastal stratigraphy, two main marine (A) and brackish (B) environments have been identified. The facies were differentiated according to the lithology, sediment properties (mineralogy and grain morphology), ostracods assemblages and grain size. The core was divided into four facies (Fig 7).

5.2.1. Unit A: marine facies and RSL fluctuations

The first marine facies is observed at 267-280 cm where yellowish brown silty sand changes to the dark brown sandy silt with negatively skewed, poorly sorted

sediment and high organic matter (OM) content. The ostracod species Cytherella sericea, Chrysocythere corralloides, Keijella karwarens, Asymmetricythere indoiranica together with Hemicytheridea paiki and Keijella neaki are consistent with a marine sub-tidal environment. The sandy portions have two different sources: (i) the first is bar-like shaped quartz with rounded edges, linked to an inter-basin source and (ii) the second comprises fine to very fine sub-rounded quartz, biotite sheets, imported by aeolian processes. The inter-basin portions are generally aggregated by evaporitic minerals with rounded edges. The absence of euryhaline species and sudden changes in facies without a transitional facies shows a marine transgression over a disconformity surface. This transition from playa (1-A) to marine (2-C) conditions was concurrent with increasing MS concurrent with imported iron (biotite) into the environment by wind and emerging Venericythere darwinii, Hemicytheridea paiki and Keijella neaki species. The finest sediment grain size, with the highest amounts of MS and OM in the marine environment, is observed at 278 cm.

An assemblage of euryhaline ostracods C. torosa and the marine lagoonal Cytherella sericea, Venericythere papuensis species may indicate a minor oscillation of the RSL and the extension of shallow marine conditions (2-B). A marked increase in sediment grain size due to an increasing sand fraction (13.3 to 71.75%), decreasing sorting, OM and MS suggest a higher energy environment

at 250-267 cm during 50 BC – 354 AD. An upward increase in sediment grain size continues to 235-250 cm where the mean size is 2.2 phi with near symmetrical skewness. Improved sorting in the yellowish-brown sand is consistent with stable environmental energy. A significant decrease in C. torosa and the high abundance of Cytherella sericea, Cerallicythere adenensis, Cistacythereis sp, Alocopocythere reticulata, indoaustralica species, in addition to abundant joined juvenile bivalves, is consistent with a marine environment (2-C). At 225-235 cm, a decrease in mean grain size and a sandy texture was accompanied by improved sorting and positive skewness concomitant with a high-energy setting. These data testify to the onset of permanent longshore drift currents leading to the creation of sandbars. The abundance of C. torosa shows relative instability in the coastal environment. Nevertheless, other species such as Cytherella sericea (marine lagoonal), Asymmetricythere whatleyi, Lankacythere elaborara, Corallicythere adenensis, Moosella striata, Chrysocythere keiji (coastal) and Keijella karwarens (subtidal) indicate the extension of the marine (2-C) setting. Also, high MS values indicate inputs of iron-rich minerals such as biotite to the environment through wind processes. This transgressive facies represents a lower shoreface facies with shoreface ridges. The ridges, comprising fine to coarse sands, are attributed to longshore transportation of tidal inlets are mainly active for cross shore mobility

during marine transgression (McBride and Moslow, 1991).

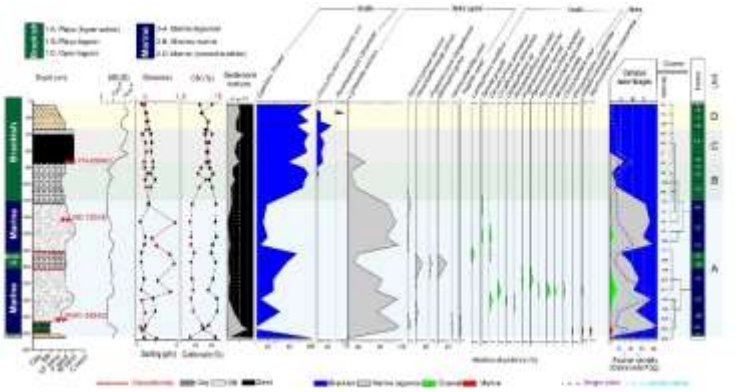

Figure 7: Sediment stratigraphy, biostratigraphy, chronology and sedimentology of the studied core. Six main palaeoenvironments are defined.

OM enrichment in the silty sand sediment, as well as a decline in sorting indices, positive skewness values and a significant reduction in single ostracod valves confirms a gradually decreasing energy setting. Marine lagoonal ostracod species (Cytherella sericea and Venericythere papuensis) together with C. torosa and coastal species (Paijenborchellina venosa, Paranesidea handel) indicate a shifting environment from 2-C to 2-A (212-225 cm). These data translate a backshore facies with oscillations in marine inundation and vegetation growth. A return to muddy deposition is identified within the sandy sediment of shore ridges or cheniers.

The first brackish facies is between marine lagoonal facies (2-A) (192-202 (1-B) and 181-192 (1-C). The ostracod assemblages and sediment textures in the two yellowish brown sands are different from the other brackish facies. The main difference is the presence of a tiny crust of syn-sedimentary marine cement fractions (beachrock) in these facies. Mean sorting and skewness indices imply increasing environmental energy (increasing sediment grain size with increasing sorting index from base to top). C. torosa is the main species in both facies but its abundance increases from base to top (57.17% to 73.17%). The beachrock fractions generally contain fine to very fine sand portions resulting from wind influxes during cementation. The cementation occurred during increases in seawater injection within the sediments via increasing wave and tidal energy (increase wind events). Storm waves could be responsible for developing coarser sediment over marine lagoonal facies and creating Chenier structures.

At 181-192 cm when hypersaline species abundances were high due to the RSL expansion, C. torosa is observed with marine lagoonal and coastal (2-C) species such as Cytherella sericea, Venericytherepap uensis, Propontocypris bengalensis and Bishopina guhai. There is a mixture of rounded and angular sands with angular to sub-rounded beachrock fractions consistent with RSL expansion and increasing sediment transport with coastal processes.

Marine lagoonal species (Cytherella sericea and Venericcythere darwinii) and low abundances of C. torosa appear again at 171-181 cm (facies 2-A). An increase in sediment grain size, sorting index and skewness evokes a RSL expansion and developing backshore facies (2-C) at 144-162 cm. A variety of ostracod species are observed in these facies, including brackish (C. torosa), marine lagoonal (Cytherella sericea and Venericcythere darwinii) and marine (Tanella gracilis, Cerallicythere adenensis) taxa.

The RSL started to fall during 380-725 AD and a marine lagoonal environment (2-A) with Cytherella sericea and Venericcythere darwinii species was created at 123-144 cm. Decreasing sediment grain size together with increasing sorting index and positive skewness values shows that deposition occurred in a confined environment without biotite sheets. The absence of biotite suggests a shift in wind directions and probably the onset of NW Shamal winds. RSL reduction led to the deposition of the second brackish facies at 123 cm. By this time accessibility to the northwest ports had been restricted via Ras-e-Motaf and the unique morphological shape of Shatt-al-Arab palaeo-delta (Pourkerman et al., 2020). Navigation through Ras-e-Motaf became dangerous following the onset of summer time NW Shamal wind ca 650 AD. The highest wave energy, with an anti-clockwise whirlpool under storm conditions, occurred in the Ras-e-Motaf. This part of the Persian Gulf is known as Iran's «

Bermuda triangle » and it has been an area of numerous shipping accidents (Kamranzad et al., 2013).

5.2.2. Unit B: open lagoon with freshwater flux

The second brackish facies at 103 to 123 cm is characterized by a dramatic decrease in the marine lagoonal species Cytherella sericea (15.63%) and an increase in the hypersaline species C. torosa which represents 84% of total valves. Plant remains are also observed and constitute the first evidence of fresh water flux in the open lagoon facies (1-C). The sediment changes to dark brown silty sand with light gray sandy silt lenses at 94-103 cm. The lenses contain charcoal and plant remains. The presence of the macrofossil Neogastropoda olividae points to the extension of an open lagoon (1-C) setting.

Increasing mean sediment grain size, negative skewness, decreasing MS, increasing sorting index and the appearance of aggregated fine sand at 87-94 cm are consistent with changes in the environmental setting. C. torosa attains relative abundances of 94% and the percentage of single valves versus joined valves is 30.4 to 69.5%, respectively. This facies represents a hypersaline playa environment (1-A) with aeolian influxes. Dark brown silty sand with a rounded sand fraction, nearly symmetrical skewness and extremely poor sorting (4.3 phi) is observed at 80-87 cm. The presence of the marine lagoonal species Cytherella sericea (14.06%), together

with C. torosa (85.9%) and gravels, suggests the onset of limited access to the sea. Cytherella sericea attains relative abundances of up to 20% with Urocythereis margaritifera and C. torosa at 75-80 cm suggesting an open lagoon environment (1-C). This facies represents the last evidence of marine species following isolation from the sea due to coastal uplift.

5.2.3. Unit C: anthropogenic zone

An anthropogenic facies is observed at 40-75 cm, where brownish black sediment contains ceramics, charcoal and gypsum (crystals with charcoal inclusions, baked and amorphous) (Fig 8). Radiocarbon dating reveals that the first human trace occurred between 774 - 899 AD. MS recorded maximum magnetic contents (3.8 and 4.48×10^{-4}SI) and is positively correlated with OM. The anthropogenic facies begins with poorly sorted silty sand with positive skewness. It gradually changes to very poorly sorted sandy silt with near symmetric skewness. The grain size fines upwards, with a decreasing sorting index. MS and OM values continue to increase up to 40 cm where the euryhaline species C. torosa attains 94.87%. A thin layer of amorphous white gypsum is deposited at the top of the unit and constitutes a marker for the termination of the anthropogenic facies.

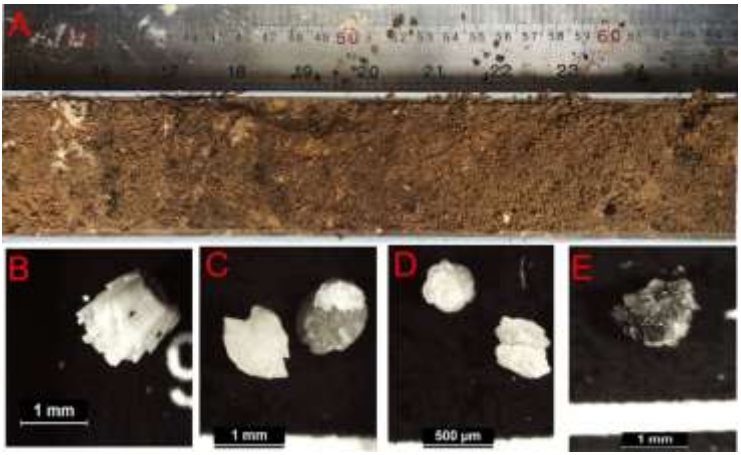

Figure 8: A) anthropogenic section of the studied core with evaporation minerals of different crystal morphologies. This section ends with gypsum crystals at 38-40 cm. B) Needle aragonite C, D, E) different crystal shapes of gypsum with black organic matter inclusions.

5.2.4. Unit D: lagoon

The anthropogenic horizon is covered by aeolian sediments that contain yellowish brown rounded to sub-rounded silty sand, gypsum crystals, plant remains, charcoal and small fraction of ceramics with rounded edges (consistent with reworking by wind action from the exposed archaeological site). Sorting ranges between very poor to poor (3.46-1.24 phi). The sediment sorting improves from base to top. The sedimentology suggests environmental oscillation changes between playa (1-A) and playa-lagoon (1-B) in the manmade evaporation ponds. Lagoonal species such as Urocythereis

margaritifera and Penthesilenula olivencae, together with C. torosa, are consistent with variable salinities, typical of playa-lagoon environments (1-B). The abundance of ostracod shells decreases from the base to the top. A maximum shell abundance is observed at 5-7 cm (1-A) where C. torosa is the single species. At 35-37 cm and 15-17 cm (1-B) the percentage of C. torosa decreases and Urocythereis margaritifera comprises a quarter of the shells. MS varies between 3.32 and 4.66×10^{-4}SI, with a maximum value logged at 15-17 cm where carbonate content and mean sediment size decreases.

6.Discussion

RSL changes in the Persian Gulf is controlled by eustatic seal level rise, basin subsidence and local uplifts. During the Holocene the axial zone of the Persian Gulf experienced twofold subsidence following to a rapid sea level rise especially in the central basin (Uchupi et al., 1999). The central basin is contained plenty of active salt diapirs along N-S deep-seated extensional faults and tear fault systems with origin of Hormuz salt formation (Jahani et al., 2007; Jahani et al., 2017). Correlation between Darang salt pillow growth and RSL fall suggested probably impacts of halokinesis on the RSL oscillations. During the Persian Gulf highstand (3340 BC – 2620 BC) the lower Khuzestan plain experienced several RSL oscillations with small periods (Heyvaert and

Baeteman, 2007). The oscillations were continued with RSL retrogradation. By a contrast a rapid RSL fall occurred in Abu Dhabi during a short period after a highstand (Lokier et al., 2015) and reached below current sea level by 510 – 780 AD. Therefore, variety RSL changes in north and south part of the Persian Gulf could be result of difference tectonic setting and fault systems.

Halokinesis have direct effect on RSL oscillations via the Persian Gulf axial zone subsidence and local uplifts at basin and coastal through the fault systems. As result, our reconstructed RSL was not correlated with ICE—6G (VM5a) model for the studied sites. Although the model shows a continuous fall, but, the studied facies were logged three RSL oscillations. Duration between each oscillation was correlated with modeled sea-level position. Increase water column in central basin floor leads to increasing crust mobility at basin and coastal zones. Meanwhile, time interval between lowstand with next highstand were decreased. Darang salt anticlinal foothill was recorded cal. +3.7 m uplift by the second lowstand.

RSL in the Persian Gulf is an important factor for ancient harbour location. Rishar (Rev Ardeshir) and Apologus were two important Sassanid harbours in the northwest of the Persian Gulf (Strange 1905; Whitehouse and Williamson; 1973). Apologus was a riverine harbour located at Shatt-al-Arab and Rishar is situated on the

Bushehr coastal peninsula. The archaeological evidence shows that the port of Bushehr was connected to Kazirun and Shiraz via a road used for the export of commodities to other regions. It was the nearest port to Fars and it made Rishar an important port (Boucharlat and Salles, 1981). The first sea water column reduction had negative impacts on the Rishar harbour operation because of its coastal morphology (Fig 2). The same trend is observed in other zone I ancient harbours (Mahroyan, Ceniz, Jenaba). This problem of harbour accessibility provided an opportunity for Apologus to replace them. Apologus maintained its importance in maritime trade until the early Abbasid Caliphate (750 – 1260 AD), which coincided with the second RSL reduction. After then, in the first century of Islam, the main harbours shifted from Apologus (Ubulla) to Siraf (Wilson, 2011).

The first sea water column reduction was also concurrent with the foundation of a defensive outpost with a port at Siraf (Whitehouse and Williamson; 1973) but maritime trade flourished at Apologus. It could be related to maintaining sea level due to the Karun-Tigris-Euphrates delta subsidence and local uplift (Uchupi et al., 1999). Seawater intrusion to the river channel during high-tide increased the water depth for ocean-going navigation. It was favorable to Apologus's maritime trade until the late Sassanid Empire (ca. 450 to 650 AD). During the Sassanid to early Islamic periods, the settlement

density reached its maximum in Mesopotamia (Lawrence et al., 2016).

Present an unconformity over subtidal facies and emerging coastal environment at studied facies would be result of rapid sea water oscillation. The water column reduction is correlated with the first evidence of anthropogenic trace at Siraf. RSL rise and developing coastal facies was concurrent with progradation of marine facies over the first Sassanid anthropogenic horizon at Siraf (50 BC – 550 AD) (Fig 9).

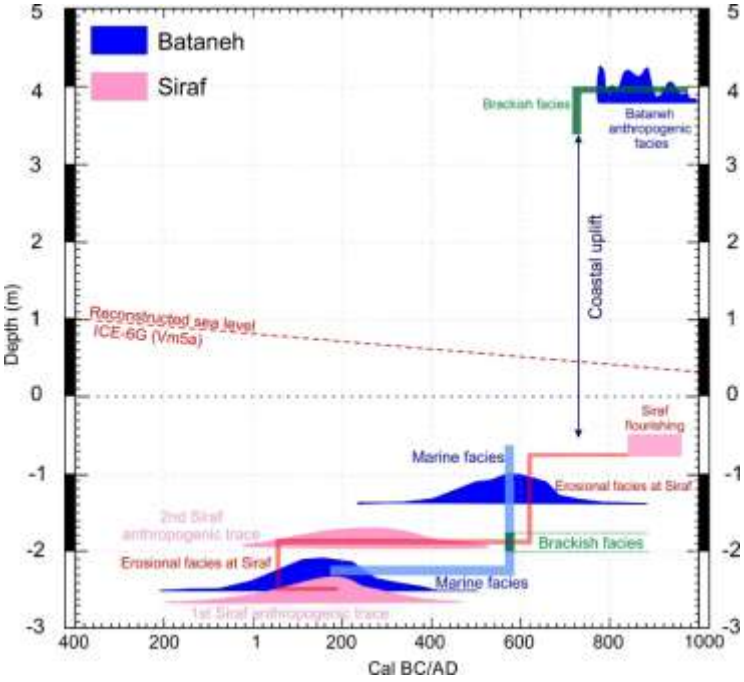

Figure 9: Geoarchaeology-age depth model of the Bataneh facies changes, Siraf anthropogenic trace (Pourkerman et al., 2020) and ICE-6G (VM5a) model. This figure suggested impacts of RSL changes and coastal uplift on Siraf ancient harbour and Bataneh.

The second sea water column reduction was coincided with changes in sediment origin following to an increase in summer northwest winds around 650 AD and flourishing of Siraf (Pourkerman et al., 2020) (Fig 9). This period was concurrent with dune reactivation and a peak in aeolian deposition in the southeast of the Persian Gulf (Stokes et al., 2003; Parker et al., 2011)

During the Umayyad to early Abbasid dynasties (650-750 AD), there was a decrease in maritime trade in the Gulf (Potter, 2009). It could be related to sudden changes in both RSL reduction and economic/political changes. A decreasing river water column at Shatt-al-Arab following RSL fall and decreases in precipitation led to accessibility problems at Apologus for oceangoing vessels (Al-Istakhri, 1870). By contrast, risk of navigation in the western part of the Persian Gulf was accelerated during summer by the interaction of Persian Gulf water circulation and summer Shamal winds at Ras-e-Motaf (Pourkerman et al., 2020). The Shamal wind generates the highest wave energy with an anti-clockwise whirlpool (under storm conditions) at Ras-e-Motaf. This area is famous as being Iran's « Bermuda triangle » and has been an area of numerous shipping accidents (Kamranzad et al., 2013).

Bataneh is located in zone II where halokinesis have had direct effects on the coastal zone and its hinterland. Darang salt diapiric fold and the geomorphological changes in the hinterland was concurrent with a second RSL fall. The rapid transition from open lagoon to brackish facies translates a rapid uplift of ca. +3.7 m in the coastal zone due to the Darang salt pillow growth. The uplift changing local watershed geomorphology and fluvial directions. These changes caused the abrupt cessation of the stream channel and extending alluvial fans. The stream sourced in the sensitive gypsum marl unit was a great risk for the ancient city. The city was protected by embankment walls and a dam with artificial canal over hard bedrock that it redirects flooding water to the city through a safe path.

One of the reasons that Bataneh port failed was probably due to coastal uplift. The expansion of Siraf brought rapid urbanization of the city and local towns. This rapid expansion necessitated new building materials. At this time, cooked gypsum was widely used as cement, plaster motifs and decorative objects. Therefore, gypsum very soon became a noteworthy commercial good. Several ancient gypsum mines existed around Siraf. Traditional mining necessitated time and labor for the extraction and transfer of raw gypsum. As a result, gypsum became expensive. New gypsum extraction methods via evaporation pools at Bataneh led to cheaper gypsum. The method took advantage of Bataneh's

geomorphological traits and gypsum units present in the local geology.

7.Conclusions

Two RSL fall have been recorded. The first event (250 – 400 AD) had negative impacts on harbours in the western basin such as Rishar. There were only minor impacts on Apologus due to the crustal mobility balance at Shatt-al-Arab delta. The second RSL fall event at 770 – 900 AD and onset summer Shamal wind since 650 AD was coincident with important harbours shifted to the central part of the Persian Gulf. Both Bataneh and Siraf were suitable locations. Siraf was surpassed by Bataneh because of its stable rocky coast. Uplift at Bataneh led to changing geomorphological features in the hinterland and the city was exposed to flooding risk. The runoff water that originated from marl gypsum units was harnessed by a dam and artificial canal and sluiced to the city through safe channels. The runoff water was collected in evaporation ponds and left to precipitate as gypsum during the warm and arid summers. The gypsum trade brought prosperity to the city. Coastal uplift was a key factor in reducing port accessibility and therefore activity at Bataneh. The location of Najirum's harbour is still unclear.

Recent oil and gas infrastructure has destroyed large parts of the ancient sites. These structures are also at

risk from natural hazards such as coastal uplift and flooding. South Pars offshore oil and gas field has led to the expansion of several petrochemical companies along the coastal. They have had direct and indirect impacts on the destruction of ancient sites. Further geoarchaeological studies are required at waterfront sites of the Persian Gulf because many sites are being destroyed by modern developments, present RSL rise and coastal erosion (Pourkerman et al., 2018).

Acknowledgements

This work was supported by the Center of International Scientific Studies and Collaborations (CISSC), Iran National Science Foundation (INSF grant number 94-44915), the French Embassy in Iran, Campus France (PHC GUNDISHAPUR 2016–2017, project number 35630QH) and Labex OT-Med (ANR-11-LABX-0061). Radiocarbon datings were funded through the project “LIA HAOMA” supported by Centre National de Recherche Scientifique (CNRS, France). It also Partial supported by Iran national elite’s foundation and National science foundation grant 94-44915. GS is funded by an FFABR (Finanziamento delle At- tivita` Base di Ricerca) grant of the MIUR (Ministero dell’Istruzione, dell’Universita` e della Ricerca) and by a DiSPeA (Dipartimento di Scienze Puree Applicate of the Urbino University) research grant

References

Al-Istakhri, (1870). M. J. de Goeje (trans. & ed.), Kitab Al-Masalik wa-al-Mamalik. Leiden.

Azarian, M. (2013). Bataneh ancient site systematically survey in order to identification location of Najirum ancient harbour [master's thesis]. Tarbiat Modares University, Tehran, Iran. [Farsi]

Balkhi, Ibn. "Fārsnāmeh." Guy le Strange &R. A Nicholson. Tehrān: Donyā-ye Ketāb (1984).

Beck, A., Philip, G., Abdulkarim, M., & Donoghue, D. (2007). Evaluation of Corona and Ikonos high resolution satellite imagery for archaeological prospection in western Syria. antiquity, 81(311), 161-175.

Benjamin, J., Rovere, A., Fontana, A., Furlani, S., Vacchi, M., Inglis, R. H., ... & Mourtzas, N. (2017). Late Quaternary sea-level changes and early human societies in the central and eastern Mediterranean Basin: An interdisciplinary review. Quaternary International, 449, 29-57.

Beydoun, Z. R. (1991). Arabian plate hydrocarbon geology and potential.

Boucharlat, R., & Salles, J. F. (1981, January). The history and archaeology of the Gulf from the fifth century BC to the seventh century AD: a review of the evidence. In Proceedings of the Seminar for Arabian Studies. Seminar for Arabian Studies.

Arhan, D., Pavlopoulos, K., Fouache, E. (2020). Holocene relative sea-level variations and archeological

implications, Abu Dhabi western region, United Arab Emirates. Arabian Journal of Geosciences, 13(6), 1-16.
Delile, H., Mazzini, I., Blichert-Toft, J., Goiran, J.P., Arnaud-Godet, F., Salomon, F., Albarède, F., 2014. Geochemical investigation of a sediment core from the Trajan basin at Portus, the harbour of ancient Rome. Quat. Sci. Rev. 87, 34–45.

Esmaeili Jelodar, M. (2011). A propose for Identification of Najirum ancient harbour according to the early-Islamic texts and archaeological survey. Journal of the Persian Gulf research paper, 3, 129-159. [Farsi]

Folk, R. L., & Ward, W. C. (1957). Brazos River bar [Texas]; a study in the significance of grain size parameters. Journal of Sedimentary Research, 27(1), 3-26.

Folk, R.L., (1954). The distinction between grain size and mineral composition in sedimentary rock nomenclature. Journal of Geology 62 (4), 344–359.

Hansman, John (1968), "The Problems of Qūmis", Journal of the Royal Asiatic Society, 100 (2): 111–139

Heiri, O., Lotter, A. F., & Lemcke, G. (2001). Loss on ignition as a method for estimating organic and carbonate content in sediments: reproducibility and comparability of results. Journal of paleolimnology, 25(1), 101-110.

Heshmati, M., Majid, N. M., Jusop, S., Gheitury, M., & Abdu, A. (2013). Effects of soil and rock mineralogy on soil erosion features in the Merek watershed, Iran.

Ibn Hawqal, (1965). J. H. Kramers (trans. & ed.), Kitab Surat al-Ard. Bibliotheca Georaphorum Arabicorum, Leiden.

Jahani, S., Callot, J. P., de Lamotte, D. F., Letouzey, J., & Leturmy, P. (2007). The salt diapirs of the eastern Fars Province (Zagros, Iran): A brief outline of their past and present. In Thrust Belts and Foreland Basins. Springer, Berlin, Heidelberg.

Kamranzad, B., Etemad-Shahidi, A., & Chegini, V. (2013). Assessment of wave energy variation in the Persian Gulf. Ocean Engineering, 70, 72-80.

Khadivi, S., Mouthereau, F., Barbarand, J., Adatte, T., & Lacombe, O. (2012). Constraints on palaeodrainage evolution induced by uplift and exhumation on the southern flank of the Zagros–Iranian Plateau. Journal of the Geological Society, 169(1), 83-97.

Lawrence, D., Philip, G., Hunt, H., Snape-Kennedy, L., & Wilkinson, T. J. (2016). Long term population, city size and climate trends in the Fertile Crescent: A first approximation. PloS one, 11(3).

Le Strange, G. (1905). The lands of the Eastern caliphate: Mesopotamia, Persia, and central Asia, from the Moslem conquest to the time of Timur. University Press.

Lidour, K., Béarez, P., Charpentier, V., & Méry, S. (2020). The prehistoric fisheries of Akab Island (United Arab Emirates): New insights into coastal subsistence during Neolithic in eastern Arabia. The Journal of Island and Coastal Archaeology, 15(1), 80-103.

Lokier, S. W., Bateman, M. D., Larkin, N. R., Rye, P., & Stewart, J. R. (2015). Late Quaternary sea-level changes of the Persian Gulf. Quaternary research, 84(1), 69-81.

Marriner, N., & Morhange, C. (2007). Geoscience of ancient Mediterranean harbours. Earth-Science Reviews, 80(3-4), 137-194.

Marriner, N., Kaniewski, D., Morhange, C., Flaux, C., Giaime, M., Vacchi, M., & Goff, J. (2017). Tsunamis in the geological record: Making waves with a cautionary tale from the Mediterranean. Science advances, 3(10), e1700485.

Marriner, N., Morhange, C., & Goiran, J. P. (2010). Coastal and ancient harbour geoarchaeology. Geology Today, 26(1), 21-27.

Marriner, N., Morhange, C., Boudagher-Fadel, M., Bourcier, M., & Carbonel, P. (2005). Geoarchaeology of Tyre's ancient northern harbour, Phoenicia. Journal of Archaeological Science, 32(9), 1302-1327.

Marriner, N., Morhange, C., Flaux, C., & Carayon, N. (2017). Harbours and ports. Encyclopedia of geoarchaeology, 382-403.

McBride, R. A., & Moslow, T. F. (1991). Origin, evolution, and distribution of shoreface sand ridges, Atlantic inner shelf, USA. Marine Geology, 97(1-2), 57-85.

Morhange, C., Laborel, J., & Hesnard, A. (2001). Changes of relative sea level during the past 5000 years in the ancient harbor of Marseilles, Southern France. Palaeogeography, palaeoclimatology, palaeoecology, 166(3-4), 319-329.

Mouthereau, F., Lacombe, O., & Vergés, J. (2012). Building the Zagros collisional orogen: timing, strain distribution and the dynamics of Arabia/Eurasia plate convergence. Tectonophysics, 532, 27-60.

Myers, A. (2010). Field work in the age of digital reproduction: a review of the potentials and limitations of Google Earth for archaeologists. SAA archaeological record, 10(4), 7-11.

Parker, A. G., & Goudie, A. S. (2008). Geomorphological and palaeoenvironmental investigations in the southeastern Arabian Gulf region and the implication for the archaeology of the region. Geomorphology, 101(3), 458-470.

Paul, A., & Lokier, S. W. (2017). Holocene marine hardground formation in the Arabian Gulf: Shoreline stabilisation, sea level and early diagenesis in the coastal sabkha of Abu Dhabi. Sedimentary geology, 352, 1-13.

Peltier, W. R., Argus, D. F., & Drummond, R. (2015). Space geodesy constrains ice age terminal deglaciation: The global ICE-6G_C (VM5a) model. Journal of Geophysical Research: Solid Earth, 120(1), 450-487.

Peltier, W. R., Argus, D., Drummond, R., & Moore, A. W. (2012). Postglacial rebound and current ice loss estimates from space geodesy: the new ICE-6G (VM5a) global model. In AGU Fall Meeting Abstracts.

Potter, L. (2009). The Persian Gulf in History. Springer.

Pourkerman, M., Marriner, N., Morhange, C., Djamali, M., Alizadeh, H., Tofighian, H. (2019). Tracking shoreline erosion of “at risk” coastal archaeology (Persian Gulf: Sassanid-Islamic heritage relics in southestern Bataneh, Iran). Final conference- what kind of environmental transition for the Mediterranean region, Marseille, France. http://www.otmed.fr/final-conference-what-kind-environmental-transition-mediterranean-region-october-14-16-2019

Pourkerman, M., Marriner, N., Morhange, C., Djamali, M., Amjadi, S., Lahijani, H., Naderi Beni, A., Vacchi, M., Tofighian, H., Shah-Hoesseini, M. (2018). Tracking shoreline erosion of “at risk” coastal archaeology: the example of ancient Siraf (Iran, Persian Gulf). Applied geography, 101, 45-55.

Pourkerman, M., Marriner, N., Morhange, C., Djamali, M., Spada, G., Amjadi, H., Vacchi, S., Lahijani, Esmaeil Jelodar, E., M.,Tofighian, M. Naderi Beni, A. (2020). Geoarchaeology as a tool to understand ancient navigation in the northern Persian Gulf and the harbour history of Siraf. Accepted manuscript.

Saleem, A., Corner, R., & Awange, J. (2018). On the possibility of using CORONA and Landsat data for evaluating and mapping long-term LULC: Case study of Iraqi Kurdistan. Applied geography, 90, 145-154.

Sampson, S. E. (2016). The Correlation between soil permeability and flooding in the northeast sector of the Dog River watershed. Department of Earth Sciences, University of South Alabama, Alabama http://www. southalabama.

Snidero, M., Carrera, N., Mencos, J., Butillé, M., Granado, P., Tavani, S., ... & Muñoz, J. A. (2020). Diapir kinematics in a multi-layer salt system from the eastern Persian Gulf. Marine and Petroleum Geology, 104402.

Southon, J., Kashgarian, M., Fontugne, M., Metivier, B., & Yim, W. W. (2002). Marine reservoir corrections for the Indian Ocean and Southeast Asia. Radiocarbon, 44(1), 167-180.

Spada, G., & Melini, D. (2019). SELEN4 (SELEN version 4.0): a Fortran program for solving the gravitationally and

topographically self-consistent Sea Level Equation in Glacial Isostatic Adjustment modeling. Geoscientific Model Development, 12(12), 5055-5075.

Stokes, S., Goudie, A. S., Colls, A. E. L., & Al-Farraj, A. (2003). Optical dating as a tool for studying dune reactivation, accretion rates and desertification over decadal, centennial and millennial timescales. Desertification in the Third Millenium. Balkema, Rotterdam, 57166.

Thomas, R. J., Ellison, R. A., Goodenough, K. M., Roberts, N. M., & Allen, P. A. (2015). Salt domes of the UAE and Oman: probing eastern Arabia. Precambrian Research, 256, 1-16.

U. S. Geological Survey, (2011). World Seismicity Maps, Middle East 1990–2006. http:// earthquake.usgs.gov/earthquakes/world/seismicity/m_east.php 2011last accessed September 2011.

Vacchi, M., Ermolli, E.R., Morhange, C., Ruello, M.R., Di Donato, V., Di Vito, M.A., Giampaola, D., Carsana, V., Liuzza, V., Cinque, A. and Boetto, G. (2020). Millennial variability of rates of sea-level rise in the ancient harbour of Naples (Italy, western Mediterranean Sea). Quaternary Research, 93(1), 284-298.

Warrak, M. (2019). Sedimentary environment and diapirism of the Pleistocene–Holocene deposits of the Zirku salt plug, southern Arabian Gulf. Arabian Journal of Geosciences, 12(13), 397.

Whitehouse, D., & Williamson, A. (1973). Sasanian maritime trade. Iran, 11(1), 29-49.

Wilson, A. (2011). The Persian Gulf (Vol. 10). Routledge.

Wood, W. W., Bailey, R. M., Hampton, B. A., Kraemer, T. F., Lu, Z., Clark, D. W. James, R.H. and Al Ramadan, K. (2012). Rapid late Pleistocene/Holocene uplift and coastal evolution of the southern Arabian (Persian) Gulf. Quaternary Research, 77(2), 215-220.

CHAPTER THREE:Geoarchaeology as a tool to understand ancient navigation in the northern Persian Gulf and the harbour history of Siraf

Abstract

Historical texts and archaeological studies attest to the maritime and trade importance of the Persian Gulf since the Sassanid Empires. Nonetheless, there is a paucity of data regarding ancient navigation and the reasons for a shift in maritime trade from the western (e.g. Shatt-al-Arab) to eastern (Siraf) Persian Gulf by the Abbasid dynasty. For some scholars, Siraf was occupied between 360 and 977 CE, after which time an earthquake entrained the demise of the city. However, it is unclear when Siraf was founded and how natural navigation conditions changed for ocean-going vessels in harbours of the NW Persian Gulf. To address this knowledge gap, we here present new geoarchaeological data from Siraf. Two anthropogenic facies were detected in drilled cores. They suggest that Siraf dates back to 2 BC-317 CE. After a hiatus, a second occupation phase began during the reign of Shapur II. Relative Sea-Level (RSL) fluctuations, climate change and Persian Gulf bathymetry all affected the possible nautical accessibility of this ancient Persian harbour. A fall in RSL, leading to a shortening of navigable water columns and amplified summer-time Shamal wind from 550 CE onwards possibly led to a loss in the importance of Shatt-al-Arab and other ports in the western Persian Gulf. It appears to have made Siraf the

best alternative for seafarers. According to the wind regimes, the best time for arrival and departure from Siraf was August and October, respectively. RSL rise and increasing coastal erosion during the winter-time Shamal winds led to the degradation of harbour potentialities and was possibly at the origin of economic decline and poorly adapted harbour works at Siraf during a 150-year period between 850 and 1000 CE.

Keywords: Siraf, Gerchaeology Persian Gulf, Shamal winds Coastal geomorphology, Relative sea level

1. Introduction

Although the history of maritime trade in the Persian Gulf dates back to the 3rd century BC (Caspers, 1971), maritime trade did not thrive until the 8th century AD onwards. During the 9th to 10th centuries AD, historians such as Tabari, al-Istakhri, Ibn Hawqal, al-Mas'udi (Tabari, 1987, al-Istakhri 1870, Ibn Hawqal 1965, Al-Mas'udi, 1962) describe Siraf as the most important port of the Persian Gulf. Much of our understanding of Siraf's archaeological record is attributed to the work of Stiffe (1985) Whitehouse (1968, 1969, 1970 and 1971) and Whitehouse and Williamson (1973). Since these studies, however, just a handful of investigations and excavations have taken place in Siraf (Khakzad and Trakadas, 2014; Pashazanous et al., 2014; Khakzad et al., 2015). Numerous knowledge gaps remain regarding the rise and fall of Siraf as a key port settlement.

Geoarchaeological studies based upon geoscience tools have the potential to answer key archaeological questions about ancient sites (Marriner and Morhange, 2007, Marriner et al., 2010, Marriner et al., 2017). Geoarchaeological studies in coastal areas can shed light on human-environment interactions using a multidisciplinary framework that marries archaeology, geomorphology, palaeoclimatology, relative sea-level changes, biology and geochemistry (Marriner and

Morhange, 2007; Ferrario, et al., 2015). However, very few geoarchaeological studies have been undertaken on medieval Mediterranean harbours (Marriner et al., 2006; Morhange and Marriner, 2010; Goiran et al., 2014, Vacchi et al., 2020). In a similar vein, no comprehensive geoarchaeological studies have been conducted on ancient harbours of the Persian Gulf from this period (Pourkerman et al., 2018).

Apologus, formerly known as Ubulla, was the most important port in the northwest Persian Gulf during Sassanid to Abbasid periods (Le Strange, 1905). The port was located at the mouth of the Shatt-al-Arab River. Basra (Abbasid capital) was supported by Ubulla port. The trade seasons in Basra were mediated by the rhythm of the Indian monsoon. The ships and goods arrived in July and vessels had to depart before the onset of Indian Ocean winds in October (Potter, 2009). By the early centuries of Islam, maritime trade in Ubulla declined. There was a successful transition of the most important harbours from Ubulla (northwest) to Siraf (center) (Sheriff, 1987).

The aim of this paper is to investigate the impacts of RSL and climate changes on ancient navigation in the Persian Gulf, including the displacement of important harbours from the northwest to the central part of the Gulf. In this study, we also analyze Siraf's infrastructure and its coastal morphology in order to shed light on its evolution during mediaeval times.

2. Geological and geomorphological settings

The present morphological features of the Persian Gulf are the result of Paleozoic to Quaternary orogeny (Kashfi, 1976; Alavi, 1994, 2004; Sharland et al., 2001). The main axis of the asymmetric Persian Gulf follows the Zagros folding system (Fig 10). The axis has generated two main synclines in the western and central northern half of the Gulf, named the western and central basins (Seibold & Vollbrecht 1969) (Fig 10). The basins are connected through transverse shoal between two synclinal areas reflected to uplift along the northward prolongation of the Qatar Arc (Ras-e-Motaf). In the central basin, the axis is situated close to the Iranian coast, in the Kangan area. This section of the Gulf is generally steeper and deeper than the western basin and contains huge folds with steeply-dipping flanks in the hinterland. These features have created narrow coastal plains associated with numerous ephemeral streams, estuaries and a steep coastal bathymetry close to the shoreline (Fig. 10) (Purser and Seibold, 1973).

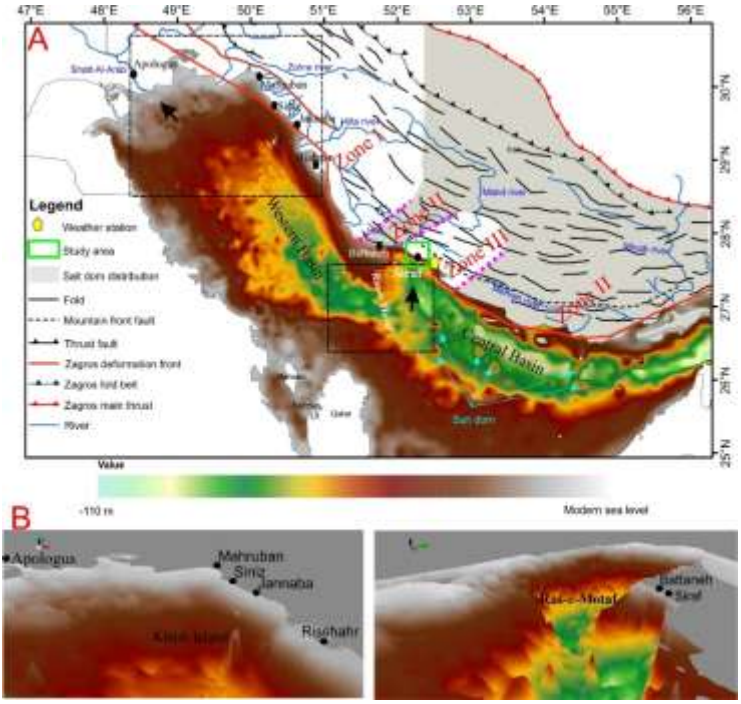

Figure 10: A) General morphology of the Persian Gulf with the location of some of its ancient harbours and distribution of the salt domes in southern Iran (Arian and Noroozpour; 2015) (B) 3D coastal morphology of the harbours. The black arrows denote the positions of the Shatt-al-Arab delta and the Siraf coastline. The bathymetry values are also valid for B.

Marl (Kazhdomi, Mishan), sandstone with gypsum and marl (Aghajari) and conglomerates with calcareous sandstone (Bakhtiyari) are the main Cretaceous-Pliocene formations that folded in the last Zagros orogenic movement during Miocene/Pliocene times. Erosion has generated a scarp-and-valley landscape

(Fig 11). Siraf is flanked by calcareous sandstone with interlayers of conglomerate rock to the north, into which several wells and graves have been cut (Wilkinson, 1974).

The Persian Gulf coastal morphology is influenced by plate and salt tectonic regimes. Three morphological zones are recognizable: (i) Zone I: gently sloping marshland coasts with permanent rivers (Shat-al-Arab, Zohre, Hilla and Mand) and several ephemeral rivers with high sediment supply to the shallow coastal zone; (ii) Zone II diapiric uplifting coasts with salt domes; and (iii) Zone III rocky coasts with steep coastal slopes (Fig 10). The ancient city of Siraf is located in zone III, in the central basin. It is characterized by a narrow coastal plain and numerous short fluvial systems, including three ephemeral rivers (Figs 11 and 12) (Whitehouse, 1968).

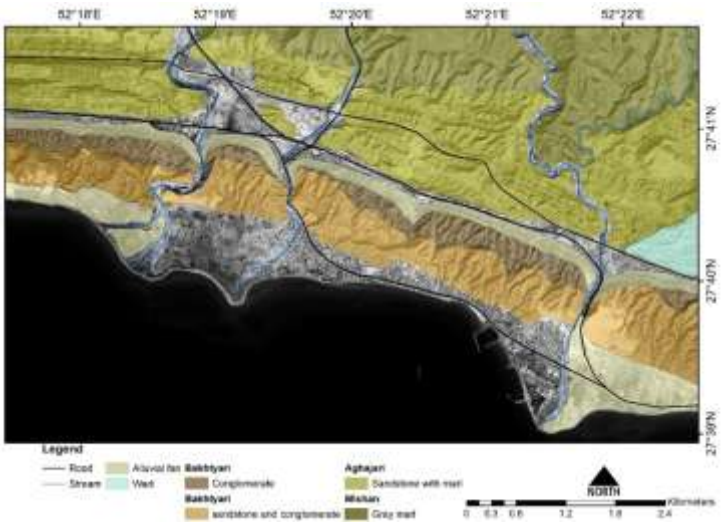

Figure 11:Geological and geomorphological map of the Siraf watershed. The background image derives from Google Earth Pro and shows the ancient urban fabric in July 2018. Most of the historic sectors have been destroyed with the exception of some coastal quarters at risk from coastal erosion.

3. Palaeoenvironments and salt tectonics

During the early Holocene inundation of the Persian Gulf (8550 – 7550 BC) (Lambeck, 1996), the mean latitudinal position of the summer ITCZ advanced rapidly northwards. A RSL highstand of +2 m occurred around 5150 to 4940 BC (Lambeck, 1996; Lokier et al., 2015). At this time, monsoon rains migrated further north than at present, over the Persian Gulf and Iran (Fleitmann et al., 2003; Djamali et al., 2010. Enhanced precipitation over northern Oman and the central part of the Persian

Gulf, resulted from the more northerly monsoon position (Fleitmann and Matter, 2009). It would have been conducive to heightened erosion of continental zones and increased sediment supply/progradation to/of coastal areas. A comparable situation has been observed along the coastline of the Nile Delta, which, after a phase of deltaic growth and progradation has become more vulnerable to coastal erosion during the past 4000 years, due to falling sediment supply (Mariner et al., 2013). For instance, in the Bay of Abukir, on the western flank of the delta, the ancient cities of Eastern Canopus and Herakleion today lie 5 to 7 meters below current mean sea level (Flaux et al., 2017).

Furthermore, it is possible that inundation of the Persian Gulf led to increased vertical stress of the basin floor that could have reactivated regional salt domes. The salt domes lie in the Hormuz formation and were active before the Zagros folding. The domes were reactivated by subsidence resulting from Zagros tectonic events (Jahani et al., 2007). The distribution of the salt domes is depicted in Figure 10. Deformation of a narrow zone along the Persian Gulf littoral has led to a concentration of domes along the present coast that are classified as active salt domes (zone II) (Jahani et al., 2007). These coastal salt domes could have been reactivated following the displacement of salt to the edge of the area due to basin subsidence resulting from increased vertical stress (Wood et al., 2012).

4. Meteorological and physical oceanography

The main weather phenomenon in the Persian Gulf is a strong northwesterly Shamal wind that occurs during summer and winter (Perrone, 1979). The summer Shamal winds result from interaction between summer monsoon low-pressure systems over NW India, that extend to the W to SE parts of the Gulf, and stationary high-pressure systems over the Mediterranean with a ridge extending SE towards the NW of the Persian Gulf (Bartlett, 2004). Winter Shamal wind over the north of the Persian Gulf is affected by cold air carried into the region by quasi-stationary Siberian high pressure in the east (Crook, 2009). It is usually interrupted by a frontal system that is created in the east of the Mediterranean Sea and tracks to the southeast following the polar front jet. The frontal system moves toward the Persian Gulf with the polar front jet behind and sub-tropical jet ahead of the frontal system converge, strengthening the system and generating strong wind at the front. The NW wind is strong during its passage over the northern Persian Gulf and it reaches five times its initial surface speed (15-20 m/s) in the central part of the Gulf (Thoppil and Hogan, 2010). The intensity of the Shamal wind is enhanced by the funnel-like structure of the Zagros Mountain along the Iranian coast (Giannakopoulou and Toumi, 2012). The other weather system that affects the summer-time Shamal wind is the Indian Ocean Dipole (IOD). A positive IOD leads to decreased summer precipitation in the Persian Gulf and increasing duration and intensity of the summer Shamal wind (Al Senafi and Anis, 2012). The

winter Shamal brings cold and dry air that leads to falling temperatures and evaporation (Thoppil and Hogan, 2010). The winter-time Shamal wind, that blows during January and February, creates the highest waves in the middle part (central basin) of the Persian Gulf, whereas, the summer-time Shamal (June and July) influences the northwestern part of the Persian Gulf, especially at Shatt-al-Arab and Ras-e-Motaf. The intensity of the Shamal wind is attenuated following the summertime Shamal and it reaches its minimum during September and October (Kamranzad, 2018).

Evaporation and freshwater inputs create differences in water densities between the northern and southern parts of the Persian Gulf. This feature leads to marine water inflow via the Straits of Hormuz, before flowing in a NW direction along the Iranian coast (Reynolds, 1993). It subsequently splits into two branches: (i) one branch continues on a NW path, while (ii) the second veers offshore and joins the returning southeastern flow. The Shamal wind intensifies the outflowing branch (Thoppil and Hogan; 2010). Water circulation and the distribution of basin wave power is represented in Figure 14. The highest wave energy, with an anti-clockwise whirlpool under storm conditions, occurs in the Ras-e-Motaf. This part of the Persian Gulf is known as Iran's "Bermuda triangle" and it has been an area of numerous shipping accidents (Kamranzad et al., 2013).

The Persian Gulf has semi-diurnal and diurnal tides with an oscillation period between 21.6 and 27 hours (Defant, 1961). The tidal currents are mediated by Persian Gulf water circulation and bathymetry. In the Bandar-e Abbas (Straits of Hormuz), because of water exchanges between the Persian Gulf and the Oman Sea, tidal currents are faster and Mean Higher High Water (MHHW) is higher than elsewhere in the Gulf (Table 3). Tidal currents are also strong in shallow waters (Pous et al., 2012). MHHW in the Shatt-al-Arab estuary is +3 m and MLLW is 0.4 m.

Table 3 : Geomorphological zonation and tidal levels at different sites from the Strait of Hormuz to Shatt-al-Arab.

Place	Lat N	Long E	Height in meters above datum				Class
			MHHW	MLHW	MHLW	MLLW	
Bandar-e Abbas	29° 22'	56° 17'	3.4	2.6	1.4	0.7	Zone II
Asaluyeh*	27° 28'	52° 37'	1.6	1.5	0.7	0.3	Zone III
Bandar-e Bushehr	28° 54'	50° 45'	1.9	1.3	1.1	0.5	Zone I
Bandar-e Ganaveh	29° 34'	50° 31'	2.2	1.5	1.3	0.6	Zone I
Imam Hassan	29° 50'	50° 15'	2.4	1.7	1.3	0.6	Zone I
Shatt-al-Arab	29°50'	48°43'	3.0	2.4	1.3	0.4	Zone I

5. The ancient urban fabric of Siraf

The port of Siraf was a point of connection between the Persian Gulf and the Far East. Merchants imported spices, silk and other luxury goods, and exported pearls, Arabian-produced frankincense and other precious resins (Whitehouse and Williamson, 1973). Our knowledge of the ancient urban fabric of Siraf is limited because of sparse excavations and the loss of ancient remains due to natural and anthropogenic activities. In this study, we focus on the work of Whitehouse (1968, 1969,

1970, 1971), who performed a comprehensive investigation of medieval Siraf, producing valuable data and maps. The buildings generally manifest a NE-SW orientation except the great mosque (for religious reasons) and benefit from shallow wells (Fig. 12).

The archaeological excavation by Whitehouse (1968) in the northwest area of the great mosque (section B) (Fig 12) elucidated three important occupation layers. The earliest occupation (Period 1) contained undisturbed beach sand, located 1 m above current sea level. It lies beneath mixed sand and clay with a horizon showing abundant Sassanid-Islamic pottery (before cal. 825 AD). Period 2 contains four generations of buildings that are covered by rubble from the collapse of large buildings. The approximate age of period 2 is between 825 ± 25 to 977 ± 78 AD. Finally, period 3, dating to the late 11th century AD onwards, comprises a poor agricultural soil.

Figure 12: Map of Medieval Siraf, with the location and orientation of its buildings (Whitehouse, 1968). The rose diagram shows that the ancient buildings trend towards the north. The most important waterfront remains are A) the Potter's Quarter, B) the great mosque and C) the Bazaar. The different colours represent different orientations. D) Rock cut grave at Shilau valley and E) water front remains that exposed severe coastal erosion (Pourkerman et al., 2018)

Construction materials were selected as a function of accessibility to natural resources. Bakhtiray conglomerate was exploited as a source of rubble and the Aghajari formation was quarried for gypsum. These materials were broadly used for building constructions and city protection structures. Cooked gypsum was employed as cement and for interior-exterior facing. The cooked gypsum absorbs humidity from the air and would have helped to decrease inside temperatures during warm and humid seasons. The use of rubble stone materials with

gypsum mortar, in addition to gypsum as an interior decorative material, was very common under Sassanian rule (Huff, 2005).

6. Methods and data acquisition

The main parts of the coastal zone in the medieval sector of Siraf are covered by gravel. The gravel accumulations result from the destruction of archaeological remains by coastal erosion (Pourkerman et al., 2018). A continuous series of 3-m cores was drilled using a vibracore in the SE part of the medieval Bazaar at 17 cm above current Mean Sea Level (MSL) (Fig 12). The core tubes were immediately transported to the laboratory for nondestructive magnetic susceptibility analysis (MS). The coring site was levelled using a theodolite and benchmarked relative to current sea level. All depths are relative to present mean sea level. A 2.4 m outcrop section was logged at a site called the "Potter's Quarter" (Fig 12) where a whole sedimentary sequence was observed beneath an ancient building.

Before subsampling, magnetic susceptibility was measured using a Bartington MS2C 100-mm diameter loop sensor with an MS2 meter. Magnetic susceptibility was measured every 2 cm (Delile et al., 2014), in order to probe human impacts on the sedimentary properties.

High-resolution sampling was undertaken on each of the cores (44 sub-samples over 3 m). Each sample

was split into two subsamples for grain-size, organic matter and carbonate-content analyses. Wet sieving was employed to separate the >2mm and <63 micron fractions. Dry sieving was performed for the sand granulometry and a laser grain-size analyzer (Horiba La 950 E) was used for the silt/clay fractions. The sediments were classified and plotted on a ternary diagram using the methodology outlined by Folk (1954, 1980). Organic Matter (OM) and carbonate content were measured using Loss-On-Ignition (LOI) at 550 °C and 950 °C (Heiri et al., 2001). The mean grain size was calculated using Folk and Ward (1957). The chronological data are based on the correlation of core facies with archaeological excavation data from Siraf. Juvenile marine shells contained in the anthropogenic facies were used for radiocarbon dating. The ^{14}C data were calibrated using Calib version 7.1.0 online version (http://calib.org) and a standard Persian Gulf marine reservoir age (Southon et al., 2002) (Table 4). Historic wind directions and durations were obtained from the database of the Iranian Meteorological Office (http://irimo.ir). Bathymetric maps and 3D models of the seafloor were created based on hydrological maps of the Iranian National Cartographic Center and international chart series published by the United Kingdom hydrographic office in scales 1:100000 for the Persian Gulf and 1:20000 for the Shatt-al-Arab pro-delta area.

Table 4: Calibrated radiocarbon ages for two anthropogenic facies.

ID	Depth	Radiocarbon Age	Calibration			
			1 sigma	Significant	2 sigma	Significant
Siraf 1	177 cm	2305±67	cal AD 223- 404	68.3	cal AD 113-478	95.4
Siraf 2	235 cm	2385±101	cal AD 91- 342	68.3	cal BC 44-AD 459	95.4

The RSL curve was obtained by a Glacial Isostatic Adjustment (GIA) simulation in which we adopted model ICE-6G (VM5a) of Peltier (2012) and Peltier et al. (2015). The simulation used the ICE-6G (VM5a) model through the program SELEN4 (Spada and Melini, 2019). SELEN4 solves the Sea-Level Equation by taking into account the horizontal migration of shorelines, for the transition from grounded to floating ice and for the effects of rotational feedbacks on sea level. The Sea-Level Equation was solved using a pseudo-spectral approach with a spatial resolution corresponding to the maximum harmonic degree lmax=256, on a grid with a spacing of ~40 km.

7. Results

7.1. Present-day wind and wave regimes

The winter and summer-time Shamal winds have a WNW direction. The wind speed in wet seasons (Oct-Mar) is stronger than in dry seasons, although wind duration in the dry seasons (Apr-Sep) is longer (Table 5, Fig. 13). Secondary wind directions in the dry and wet seasons blow from the S and NW respectively. The NW

wind direction is less frequent and blows in April, October and November, for around 83 days with an average speed of 14 m/s. It is as strong as the WNW Shamal wind. The S wind is weaker than the dominant wind direction and it blows from July to September for 118 days with an average speed of 9.75 m/s. The S wind is the dominant wind in August.

Table 5: 17-year wind speed (m/s) and duration averages, categorized by month and by wet and dry seasons.

	Month												season	
	Jan	Feb	Mar	Apr	May	Jun	Jul	Aug	Sep	Oct	Dec	Nov	Wet	Dry
Speed m/s	10.8	13.5	13.4	12.8	14.5	12.6	11	10.5	9.25	9.5	11.8	10.8	12.5	11.3
Days (number)	76	117	57	59	174	56	88	16	63	76	86	120	331.7	473

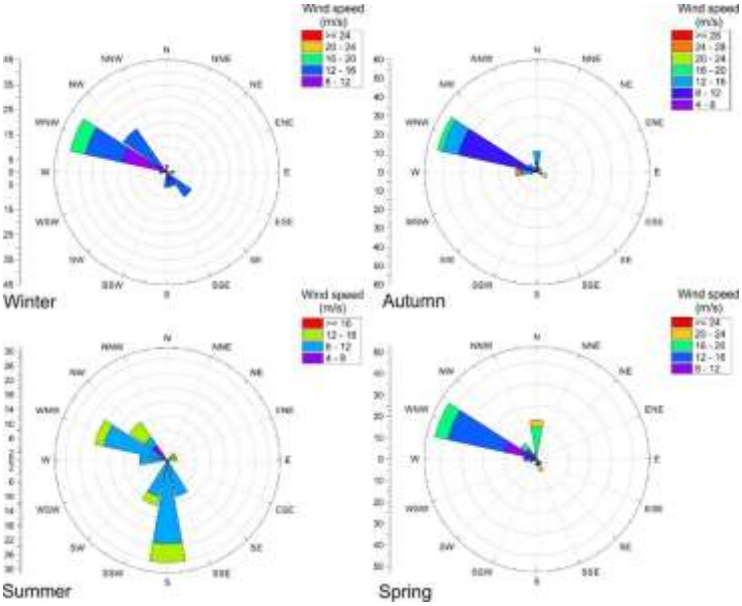

Figure 13: Central Persian Gulf wind directions and speed (m/s) for the period 2001-2018. The data were obtained from the Iranian Meteorological Office (http://irimo.ir).

7.2. Fresh-water management system

According to field observations, the city is located in a coastal desert with average precipitation of 13.2 mm/yr. Flash flooding takes place during winter and autumn; at the time of writing, the most recent example dated to the 23rd March 2020. The city's fresh water was supplied by harnessing and storing rainfall via numerous wells and cisterns on the hills overlooking Siraf, and stocked in alluvial sediments overlooking the ancient settlement (Fig 12). The wells, excavated into the hills, are protected from sediment influx by manmade rocky stairs,

plastered mortared rubble and a 5-10 cm protuberance. Further features of the wells are shallow rills to direct water to the well mouth. Pronounced water erosion in the upstream Shilau valley, with several outlet tunnels, was observed on the downside of the wells. Shallow wells (upper present sea-level) and cisterns are reported for medieval Siraf, for both cultivation and domestic purposes (Whitehouse, 1968, 1969, 1971) (Fig 14).

Figure 14: A and B) plastered mortar rubble to restrict downstream debris flows and sediment influx into the excavated wells. C) Surface water channels into the wells. D) Well associated with a tank, drain and cistern (850 AD) from Whitehouse (1971).

7.3. Paleoenvironmental analysis

7.3.1. Upper shore facies

The stratigraphic units were bounded between two upper shore facies (US1 and US3 at the base and top,

respectively). Another upper shore facies were also logged at 72-82 cm (US2). The US1 transitioned between slightly gravelly sand ((g) S) with bivalve shells and juvenile shells of Veneridae to gravelly sand (g S) with abundant shell debris. An increase in OM is observed between 284-267 cm; OM decreases with rising carbonate and sediment grain size. MS in the US1 is also represented decrease trend from base to top (1.4×10^{-4} SI to 4.06×10^{-5} SI). The facies changes in US1 represent rising energy conditions due to the transition in sedimentary environments from lower shoreface to upper shoreface following a sea-water regression. US2 is made of gravelly sand with fine shell debris and sand. US2 sediments comprise medium to fine sands. Gravel decreases dramatically from base to top concurrent with increasing fine sand ((g) S). An inverse trend is observed for MS (2.5×10^{-5} SI to 5.06×10^{-5} SI) (Fig 15). The increase of carbonate content in these facies is related to increasing shell debris. The positive correlation between MS and carbonate content results from the impact of winnowing on magnet mineral residuals and bioclast debris reworking. US3 transitions from gravelly sand to slightly gravelly sand. The mean sediment grain size decreases upwards. The main difference between the facies US2 and US3 is the absence of bivalve shells at US2. It is suggested that US2 is more under the influence of wind processes than coastal action.

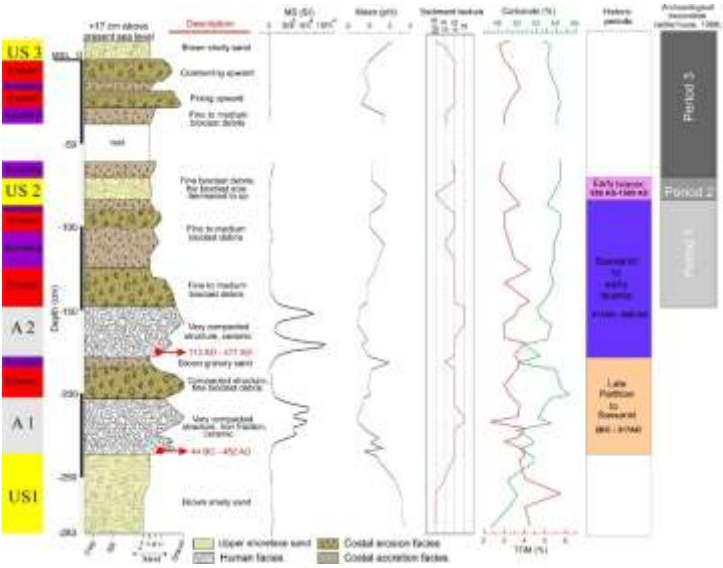

Figure 15: Stratigraphic log of the study core with MS values, mean grain size, sediment texture, OM, carbonate content and archaeological periods (Whitehouse, 1968).

The sediment outcrop exposed in the Potter's Quarter shows a shoreface facies between 95 and 200 cm above present-day sea level. It contains light brown shelly sand with ceramics at the top, with alluvial facies at the base. The alluvial facies comprise fine sand and silt with interlayers of cobbles in a sandy silt matrix. This facies attests to flooding events during heavy precipitation and debris flows resulting from flashflood events. A narrow coastal plain void of any significant vegetation cover increased the risk of flooding at Siraf. The thickness of the

outcrop facies decreases from west to east of the Potter's Quarter section (Fig 12 E).

7.3.2. Unit B (anthropogenic facies)

7.3.2.1. Anthropogenic facies

Two important anthropogenic facies (A1 and A2) are recorded at 203-240 and 149-178 cm. According to radiocarbon analysis, A1 is dated to 44 cal. BC – 425 cal. AD; it comprises a very compacted facies, with iron and ceramic fragments. A1 is located above US1 and the facies comprises 30 to 89 % gravel and the mean grain size is between 1 to -1.1 phi. The MS data manifests three peaks in this unit, with a maximum of 1.03×10^{-3} (SI) and an average of 7×10^{-4} (SI). Meanwhile, we did not observe upper shore facies above A1 and beneath A2, suggesting the resumption of anthropogenic activities shortly after the RSL fall (Fig 16). A2 contained coarser sediments (-0.6 to -1.11 phi) with 65-90% of the sediments comprising gravels. A sample from this second anthropogenic facies yielded a calibrated radiocarbon age of 113 – 477 cal. AD. Two MS peaks of 1.53×10^{-3} and 1.21×10^{-3} are logged in this unit, with an average MS of 6.6×10^{-4} SI (Fig 15).

7.3.2.2. Erosion and accretion facies

The marine facies above A1 is generally made-up of sandy gravel sediments. The gravel abundance changed from 70% to 46%, from base to top. Furthermore, MS decreased from base to top (6.78×10^{-4} SI to $4.63\times10^{-}$

^{5} SI) consistent with a decreasing gravel fraction. Sediment texture changed to gravelly sand with significant decline in carbonate that overlies the accretion facies. Fining upward in the accretion zone is consistent with a fall in energy dynamics. The same trend is observed for A2, the main difference being that the erosion and accretion facies above it are thicker than A1. It could suggest that RSL oscillations in the central part of the Persian Gulf happened over longer periods (Fig 16). In other words, RSL oscillations in the Persian Gulf were controlled by hydrostatic pressure changes over the central basin floor resulting from global sea-level fluctuations (Pourkerman et al., 2020). The thickness of erosion-accretion facies decreases upwards and end at US2. The facies are recognized by changes in sedimentary structures and manifest reworked manmade material in the stratigraphic column. The sediment grain size in the erosional facies is upward fining. 46-75% of the sediment properties are created by >2 mm portions and the sediment texture is sandy gravel. Upwardly decreasing magnetic susceptibility values (1.2×10^{-4} SI and 1.6×10^{-4} SI) over the anthropogenic facies represents a rapid rise in RSL and increasing marine-sediment deposition. US2 is covered by accretion facies after a rising in RSL (950-1230 AD).

Gravel accumulations at 0-13 cm and 16-27 cm resulted from a decrease in the rate of sand deposition and an

increase of cumulative bed-load transport during storm events (Lisle, 1989). Therefore, the gravel portions were mixed with fine to very fine sand. These erosional facies were influenced by storm action rather than RSL oscillations.

8. Discussion

8.1. Impact of RSL and Shamal winds on the geography of important harbour locations

RSL in the central basin is controlled by global sea-level rise and salt tectonics (Pourkerman et al., 2020). The modeled relative sea level (RSL) curve for Siraf suggests that RSL was higher than present during the late Parthian and early Sassanid (Fig 16) periods. Meanwhile, a rapid RSL fall started at ~50 cal. BC and with a lowstand between 50 and 150 AD. The chronological data suggest that the first anthropogenic activity in the coastal area of Siraf is recorded during the late Parthian to the first Sassanid empires (44 BC- 452 AD). After a short time, marine facies overly A1 following a RSL rise. Seafaring in the Persian Gulf was vital to Persia's commercial and maritime activities during the Sassanian period. Rising RSL created opportunities to extend maritime trade along the northwest coast. As a result, several ports were founded between 226 and 241 AD (Vosougi and Sefatgo, 2016).

Flourishing seafaring and maritime trade in the Persian Gulf during the Sassanid Empire prompted

Shapur II to build coastal defenses along the Siraf coastline to counter the threat of Arab raids (Whitehouse, Williamson, 1973). Subsequently, the most important harbours during the Sassanian dynasty were built in the northwest part of the Persian Gulf because of their vicinity to the capital, Istakhr. Apologus, located on the river Shatt-al-Arab, became the main port for Sassanian trade (Le Strange, 1905).

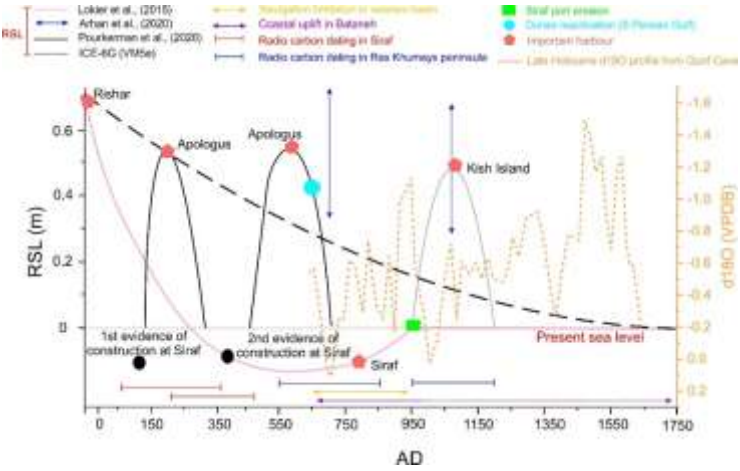

Figure 16: The black line RSL curve in the northern part of the central basin (Pourkerman et al., 2020). The pink line denotes the reconstructed RSL for the United Arab Emirates (UAE) (Lokier et al., 2015). The blue arrow shows the RSL recorded at Ras Khumays peninsula in the UAE (Arhan et al., 2020). The dashed line indicates RSL changes evaluated by ICE-6G (VM5a) at Siraf. The dashed brown line shows late Holocene oxygen isotope records from the Arabian Peninsula (Fleitmann et al., 2013).

The radiocarbon chronology confirms that the facies A2 elucidated in our studied core can be attributed

to the early Sassanian period (113 AD- 477 AD), when Siraf was erected as a military base in order to protect the maritime trade activites. The unit A2 was concurrent with a second RSL fall. The thicker marine facies over A2 represents slower RSL changes between 450 and 750 cal. AD. RSL in the Persian Gulf experienced another lowstand with the onset of summer Shamal winds during the late Umayyad to mid Abbasid dynasties, around 700 to 950 cal. AD. It led to an increase in navigation risk, such as sinking in shallow water, for ocean-going ships from Janaba (Ganaveh) to Basra (Shatt-al-Arab) (Fig 10). From an environmental perspective, the last RSL fall coincided with the development of Siraf harbour from 850 to 1000 AD (Fig 16).

The demise of the Umayyad dynasty and the rise of the Abbasid dynasty in 750 AD was associated with the introduction of Islamic maritime trade. By that time, RSL was at a lowstand and the Shatt-al-Arab river channel had prograded into the sea over its palaeo-delta. The delta was prograding by fluvial and tidal processes. It had negligible impacts on the pro-delta that was below low-tide level. A small and shallow tidal channel developed at the delta front. As a result, the navigable water column became too shallow during low-tide in the Shatt-al-Arab estuary. This acted as an obstacle for ocean-going vessels to enter and navigate the Shatt-al-Arab river channel. As a result, ocean-going vessels were no longer able to use the

harbours at Shatt-al-Arab and in zone I (Fig 17 and Fig 10).

> "In this deadly sea (Persian Gulf) several dangerous routes exist and the toughest one is Jannaba (Bandar-e Ganaveh) to Basra, the so-called Hor-e Jannaba, which is a terrible place during storms. Also, there is a place called Kheshbat at 6 meel (distance unit) from Abadan on the sea, along the Tigris River. In some cases the water is so shallow that big ships cannot enter, even at high tide. Several towers have been erected in order to guide the ships to the Tigris estuary using fire light at night. Those ships that deviate from the path run aground in shallow water" (Ibn Hawqal, 1965)

These environmental changes led to a shift in the location of the most important harbours from the west (zone I) to the central basin (zone III) of the Persian Gulf (Apologus to Siraf). During the latter half of the ninth century, the harbours of Apologus and Basra went into decline at the same time as Siraf grew in importance (Ricks, 1970). Siraf became a key maritime port due to the location of the site (close to Ras-e-Motaf), relative coastal stability with low vertical movements and a steep coastal morphology (Fig 17).

Southward migration of the monsoon between 750 BC to 650 AD led to an interruption of precipitation in northern Oman (Fleitmann and Matter, 2009) and decreasing summer Shamal wind intensity. Northwest harbours were more accessible for merchants through Ras-e-Motaf. The monsoon resumed after 650 AD, coincident with an intensification of summer Shamal winds (Fig 16). Around this time, there is evidence of dune reactivation in the south of the Persian Gulf (Stokes et al., 2003; Parker et al., 2011).

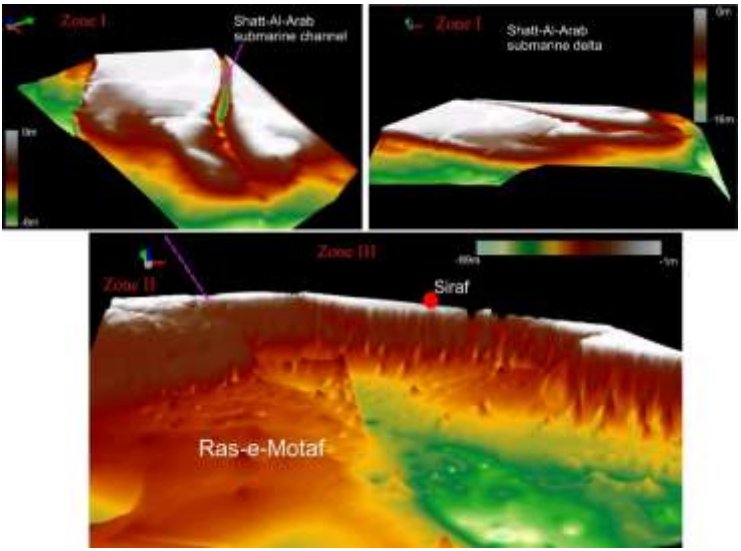

Figure 17: 3D model of Shatt-al-Arab submarine river delta and Siraf coastal morphology.

Navigation risks in the western part of the Persian Gulf increased during summer months by the

interaction of Persian Gulf water circulation and summer Shamal winds at Ras-e-Motaf. The most significant impact of the summer Shamal wind was on Ras-e-Motaf. Ras-e-Motaf lies on the border between the central and the western basins (zone III). Due to its unique morphology, the highest wave energy in the Persian Gulf is created in this area during storm conditions (Kamranzad et al., 2013). Therefore, navigating through the Ras-e-Motaf was dangerous for sea-going vessels, and damage/sinking was not uncommon (Fig 18).

A RSL rise after 950 AD, and increasing monsoon activities, led to significant erosion of the Siraf structures in the coastal zone and maritime trade shifted to Kish Island (Fig 16). The most important barrier to rekindling prosperity in western ports such as Siraf was seafaring conditions. Ocean-going vessels accessed the Persian Gulf via the Strait of Hormuz when the counter wind and swell was minimum.

During the dry season, particularly in August, the impacts of the summer-time Shamal wind on the central basin was minimum. Furthermore, the S winds and the NNE to NE surface current directions were favorable to seafaring in the central basin.

Inaccessibility of the western basin's ports eventually led to them being superseded by ports in the central basin. Furthermore, the winter-time Shamal wind began in October with minimum intensity. WNW winds,

with southeastward surface currents, allowed vessels to travel from the Persian Gulf into the Indian Ocean. As a result, Siraf provided the best alternative roadstead for Persian and Arabian harbours in the western basin.

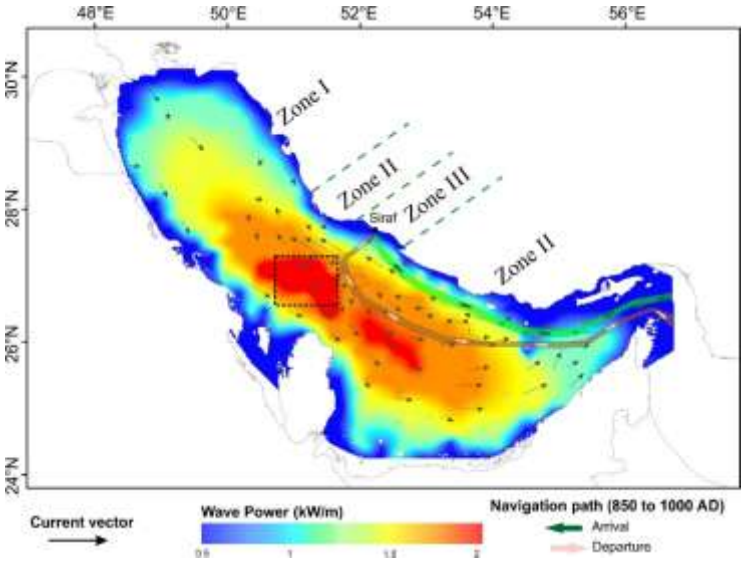

Figure 18: Persian Gulf wave-power distribution (Kamranzad et al., 2013) and current directions (Thoppil and Hogan; 2010). The black dashed line shows the location of the Gulf's "Bermuda triangle" and probable ancient navigation route in the central basin.

8.2. Advantages of Siraf as an important harbour

The falling RSL provided Siraf with suitable conditions for seafarers to access both the hinterland and the sea. The advantage of Siraf was: (i) its unique coastal morphology; (ii) its location in the Gulf (the nearest possible place to Ras-e-Motaf); and (iii) its close ties with the hinterland. The harbour of Siraf is located in zone III.

Its connection to the deep water was possible via its steep coastal morphology (Fig. 17). The close proximity of Siraf to Firuzabad made Siraf's port facilities particularly attractive to seafarers and merchants. The city's initial military vocation (Lowick, 1985) was gradually superseded by a commercial raison d'être and Siraf became one of the main trade cities of the Persian Gulf. Concurrent with the decline of the port of Apologus around 750 AD, the first evidence of trade with China is observed at Siraf (Whitehouse, 2009; Pashazanous et al., 2014). Underwater surveys have demonstrated that the city extended at least 300 m from the present shoreline (Khakzad et al., 2015). This suggests that falling RSL and positive coastal sediment budgets allowed the medieval city to extend seawards.

According to the stratigraphic section and Whitehouse (1968) the city is erected atop coastal sandy sediments with shell fractions. The facies constituted a permeable basement for the transfer of fresh water. A modified Qanat system was designed for collecting and transferring freshwater to the city. The technique was adapted to Siraf's geomorphological context, characterized by saline seawater levels to the south and the hills to the north. The Qanat system comprised a series of wells dug into alluvial sediments beneath the groundwater level in foothills and water flow by gravity via a network of gently sloping tunnels that transported water to lower elevations (Beaumont, 1971). At Siraf, the

wells were dug into the sandstone with interlayers of conglomerates on the steeper hillside slopes. The wells were interconnected via underground tunnels and/or permeable layers.

The exposed coastal section of medieval Siraf, shows interlayers of fine sand with pebbles that translate flooding (Fig 19). To alleviate flood damage but harness water for consumption during the wet seasons, the local watershed was extensively modified. Several variously-sized dams, sandstone carving and plastered rubble were used to alleviate water energy and trap water on the hillside. Water was collected in numerous wells behind the dams. Nonetheless, these hillside wells were not sufficient in meeting the needs of all domestic and agricultural activities. Whitehouse (1968) has suggested that other wells and cisterns were used to tap underground water resources.

Collected water was discharged downstream and transported to the irrigation system or stored underground in wells and cisterns. The different densities between the saline sea water and fresh water created a mixing zone (Back et al., 1986) that ensured that fresh water did not flow into the sea. Furthermore, the unique geomorphology of Siraf, with a small and flat tidal area, reduced the mixing zone (Pourkerman et al., 2018). Therefore, the city possessed a sustainable fresh-water

resource, in the form of shallow wells (above sea level), for domestic and agriculture purposes (Fig 19).

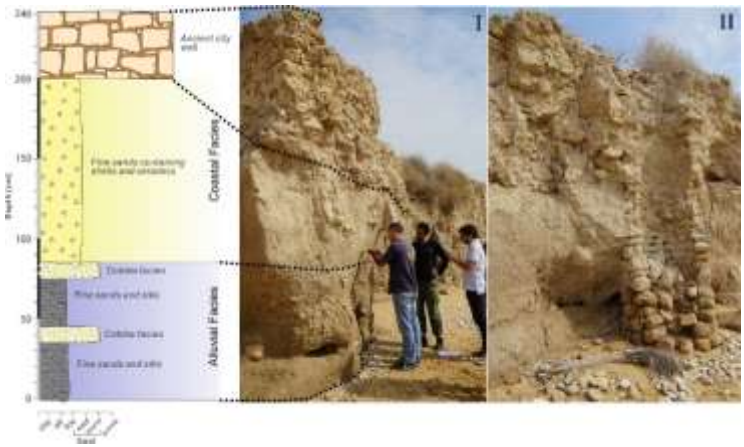

Figure 19: Stratigraphic section of the ancient wall in the Potter's Quarter, I) A: natural deposits and B: Ancient wall II) Cross section of the well.

8.3. The decline of Siraf

In the eleventh century, the great port of Siraf went into decline and Kish Island replaced it for maritime trade (Whitehouse, 1983). Al-Muqaddasi reported that the 977 AD earthquake significantly damaged Siraf. According to archaeological excavations and the voyage descriptions of Ya¯qu¯t, medieval Siraf was used until the 13th century AD (al-Muqaddasi, 1906, Whitehouse and Williamson, 1973; Ya¯qu¯ t, 1955, Whitehouse, 2009; Pashazanous et al., 2014). Environmental factors such as RSL and climate changes probably contributed to the gradual demise of Siraf.

In Abu Dhabi, RSL reached the present level after 780 AD (Lokier et al., 2015). A highstand is recorded between 950 to 1230 AD (Arhan et al., 2020) that it is correlated with the US2 marine facies. Rising RSL and increasing summer Shamal wind intensity (Fig 16) accentuated erosion of Siraf's port. The coastal stratigraphy shows two erosional facies over the anthropogenic horizons that clearly underline the impacts of marine currents on anthropogenic facies.

The Shamal winds, which played an important role in developing maritime trade at Siraf, turned into a hazard during the ensuing phase of RSL rise. The foundations of medieval Siraf were sensitive to erosion. Erosion removed the lower compact sediments leading to the collapse of overlying infrastructure. Due to the absence of robust construction materials, coastal processes easily eroded gypsum between the plastered rubble. Therefore, the structures were easily degraded and the sediment fractions reworked by coastal processes and longshore currents. This could explain why there are no reports of preserved underwater structures in Siraf. Furthermore, RSL rise significantly compromised the city's water resources. RSL rise, led to salt-water intrusion into wells. Access to fresh water in the city therefore became limited. In light of the environmental impacts on civil and trade infrastructure, Siraf's population gradually migrated away from the city.

Due to changing coastal processes, erosion took place with the reworking of finer sediment stocks. Erosional facies between the accretion layers suggest a fall in sediment supply during RSL rise or an increase in environmental energy resulting from storm events during an intensification of monsoon events between 1600-1500 AD (Fig 16). In both cases, coarse sediment derives from the erosion of waterfront anthropogenic remains. Erosion of the coastal archaeology is clearly attested along the present shoreline (Pourkerman et al., 2018).

9. Conclusion

Maritime trade in the Persian Gulf was very important for Sassanian and Islamic dynasties, who prioritized the best locations for commercial ports. Several archeological studies have been undertaken on medieval Siraf and other ports of the Persian Gulf. However, numerous questions remain unanswered. In conclusion, we would like to insist on the following factors to explain the evolution of medieval Siraf.

- Early evidence of human settlement in Siraf dates back to early Sassanid and possibly late Parthian periods.

Siraf became important for Persian Gulf maritime trade because other important ports (e.g. Apologus, Bushehr, Mahruban) located in the western basin could not be used by ocean-going vessels. Climate

change, RSL fall, coastal morphology and the Shamal winds were keys factors in the rise in importance of Siraf for maritime trade. The ports located in Shatt-al-Arab and the western Persian Gulf lost their significance when RSL in the Gulf reached a lowstand after 550 AD and a more vigorous summer-time Shamal disconnected the western and central basins of the Persian Gulf.

The fresh water-management system of Siraf was unique and cleverly adapted to the local geomorphology. Its design was based on the local environment, and its lithological and sedimentological properties. It was a modified version of the Qanat system, adapted to the coastal environment. In addition to meeting the fresh-water demands of the city, it also alleviated the impact of flooding events from the northern hills.

The decline of medieval Siraf partially resulted from RSL rise and winter-time Shamal winds that eroded waterfront infrastructure and degraded harbour amenities.

Seafarers exploited the Shamal winds for sailing in the Persian Gulf. August and October were the best times for the arrival and departure of ocean-going vessels in the central basin, respectively.

The RSL results show that sea level rose from its lowstand position to present levels between 850 to 950 AD.

During the last two last decades, concurrent with oil-gas industry developments in the coastal zone, several archaeological sites have been destroyed due to industrial constructions and urbanization. A number of heritage remains have already been lost and others are at risk. This study has revealed the importance of geoarchaeological studies in understanding the environmental evolution of ancient maritime sites of the Persian Gulf.

Acknowledgements

This work was supported by the Center of International Scientific Studies and Collaborations (CISSC), Iran National Science Foundation (INSF grant number 94-44915), the French Embassy in Iran, Campus France (PHC GUNDISHAPUR 2016–2017, project number 35630QH) and Labex OT-Med (ANR-11-LABX-0061). Radiocarbon datings were funded through the project "LIA HAOMA" supported by the Centre National de Recherche Scientifique (CNRS, France). The study was also supported by Iran's National Elite Foundation.

Reference

Al Senafi, F., & Anis, A. (2015). Shamals and climate variability in the Northern Arabian/Persian Gulf from 1973 to 2012. International Journal of Climatology, 35(15), 4509-4528.

Alavi, M. (1994). Tectonics of the Zagros orogenic belt of Iran: new data and interpretations. Tectonophysics, 229(3-4), 211-238.

Alavi, M. (2004). Regional stratigraphy of the Zagros fold-thrust belt of Iran and its proforeland evolution. American journal of science, 304(1), 1-20.

Al-Istakhri, (1870), M. J. de Goeje (trans. & ed.), Kitab Al-Masalik wa-al-Mamalik. Leiden.

al-Mas'udi, A. L. H. (1962). Les prairies d'or. Trans. C. Barbier de Meynard, Pavet de Courteille, and Charles Pellat. Paris: Société asiatique.

Al-Muqaddasi, (1906), M. J. de Goeje (trans. & ed.), Ahsan al-Taqasim fi Ma'rifat al-Aqalim. Bibliotheca Georaphorum Arabicorum, Leiden.

Arhan, D., Pavlopoulos, K., Fouache, E. (2020). Holocene relative sea-level variations and archeological implications, Abu Dhabi western region, United Arab Emirates. Arabian Journal of Geosciences, 13(6), 1-16.

Arian, M., & Noroozpour, H. (2015). Tectonic geomorphology of Iran's salt structures. Open Journal of Geology, 5(02), 61.

Back, W., Hanshaw, B. B., Herman, J. S., & Van Driel, J. N. (1986). Differential dissolution of a Pleistocene reef in the ground-water mixing zone of coastal Yucatan, Mexico. Geology, 14(2), 137-140.

Bartlett KS. (2004). Dust Storm Forecasting For Al Udeid Ab, Qatar: An Empirical Analysis. Master's thesis, Air University, Islamabad.

Beaumont, P. (1971). Qanat systems in Iran. Hydrological Sciences Journal, 16(1), 39-50.

Belgrave, J. H. (1952). A brief survey of the history of the Bahrain Islands. Journal of the Royal Central Asian Society, 39(1), 57-68.

Caspers, E. C. D. (1971). New archaeological evidence for maritime trade in the Persian Gulf during the Late Protoliterate period. East and West, 21(1/2), 21-44.

Crook, J. (2009). Climate analysis and long range forecasting of dust storms in Iraq. Naval Postgraduate School Monterey CA.

Defant, A. (1961). Physical oceanography (Vol. 1). Pergamon.

Delile, H., Mazzini, I., Blichert-Toft, J., Goiran, J.P., Arnaud-Godet, F., Salomon, F., Albarède, F., (2014). Geochemical investigation of a sediment core from the Trajan basin at Portus, the harbour of ancient Rome. Quat. Sci. Rev. 87, 34–45.

Djamali, M., Akhani, H., Andrieu-Ponel, V., Braconnot, P., Brewer, S., de Beaulieu, J.-L., Fleitmann, D., Fleury, J., Gasse, F., Guibal, F., Jackson, S. T., Lézine, A.-M. Médail, F. Ponel, P., Roberts, N., Stevens, L. (2010). Indian Summer Monsoon variations could have affected the early-Holocene woodland expansion in the Near East. The Holocene, 20, 813-820.

Ferrario, M. F., Brunamonte, F., Caccia, A., Livio, F., Martinelli, E., Mazzola, E., Michetti, A.M. & Terrana, S. (2015). Buried landscapes: geoarchaeology of the roman harbour of Como (N Italy). Alp. Mediterr. Quat, 28(2).

Flaux, C., Marriner, N., el-Assal, M., Kaniewski, D., Morhange, C. (2017). Late Holocene erosion of the Canopic promontory (Nile Delta, Egypt). Marine Geology, 385, 56-67.

Fleitmann, D., and Matter, A. (2009). The speleothem record of climate variability in Southern Arabia. Comptes Rendus Geoscience, 341(8-9), 633-642.

Fleitmann, D., Burns, S. J., Mudelsee, M., Neff, U., Kramers, J., Mangini, A., Matter, A. (2003). Holocene Forcing of the Indian Monsoon Recorded in a Stalagmite from Southern Oman. Science, 5626, 1737-1739.

Folk, R. L. (1980). Petrology of sedimentary rocks. Hemphill publishing company.

Folk, R. L., and Ward, W. C. (1957). Brazos River bar [Texas]; a study in the significance of grain size parameters. Journal of Sedimentary Research, 27(1), 3-26.

Folk, R.L., (1954). The distinction between grain size and mineral composition in sedimentary rock nomenclature. Journal of Geology 62 (4), 344–359.

Giannakopoulou, E. M., & Toumi, R. (2012). The Persian Gulf summertime low-level jet over sloping terrain. Quarterly Journal of the Royal Meteorological Society, 138(662), 145-157.

Goiran, J. P., Salomon, F., Mazzini, I., Bravard, J. P., Pleuger, E., Vittori, C., Boetto, G., Christiansen, J., Arnaud, P., Pellegrino, A. & Pepe, C. (2014). Geoarchaeology confirms location of the ancient harbour basin of Ostia (Italy). Journal of Archaeological Science, 41, 389-398.

Heiri, O., Lotter, A.F., Lemcke, G., (2001). Loss on ignition as a method for estimating organic and carbonate content in sediments: reproducibility and comparability of results. J. Paleolimnol. 25, 101–110. http://dx.doi.org/10.1023/A:1008119611481.

Huff, D., (1986). Architecture: III: Sasanian period. Encyclopedia Iranica 2, 329–334.

Ibn Hawqal, (1965), J. H. Kramers (trans. & ed.), Kitab Surat al-Ard. Bibliotheca Georaphorum Arabicorum, Leiden.

Jahani, S., Callot, J. P., de Lamotte, D. F., Letouzey, J., & Leturmy, P. (2007). The salt diapirs of the eastern Fars Province (Zagros, Iran): A brief outline of their past and present. In Thrust Belts and Foreland Basins (pp. 289-308). Springer, Berlin, Heidelberg.

Kamranzad, B. (2018). Persian Gulf zone classification based on the wind and wave climate variability. Ocean Engineering, 169, 604-635.

Kamranzad, B., Etemad-Shahidi, A., & Chegini, V. (2013). Assessment of wave energy variation in the Persian Gulf. Ocean Engineering, 70, 72-80.

Kashfi, M. S. (1976). Plate tectonics and structural evolution of the Zagros geosyncline, southwestern Iran. Geological Society of America Bulletin, 87(10), 1486-1490.

Khakzad, S. and Trakadas, A. 2014, The world in a grain of sand: Siraf, in S. Sindbæk and A. Trakadas (eds), The World in the Viking Age, 108–110. Roskilde.

Lambeck, K. (1996). Shoreline reconstructions for the Persian Gulf since the last glacial maximum. Earth and Planetary Science Letters, 142(1-2), 43-57.

Le Strange, G. (1905). The lands of the Eastern caliphate: Mesopotamia, Persia, and central Asia, from the Moslem conquest to the time of Timur (Vol. 4). CUP Archive.

Lisle, T. E. (1989). Sediment transport and resulting deposition in spawning gravels, north coastal California. Water resources research, 25(6), 1303-1319.

Lokier, S. W., Bateman, M. D., Larkin, N. R., Rye, P., & Stewart, J. R. (2015). Late Quaternary sea-level changes of the Persian Gulf. Quaternary Research, 84(1), 69-81.

Lowick, N. M., (1985). The Coins and Monumental Inscriptions, Siraf XV. London: British Institute of Persian Studies, 11–16.

Marriner, N., & Morhange, C. (2007). Geoscience of ancient Mediterranean harbours. Earth-Science Reviews, 80(3-4), 137-194.

Marriner, N., Flaux, C., Morhange, C., Stanley, J.-D. (2013). Tracking Nile Delta vulnerability to Holocene change. PLoS One, 8, 7, e69195.

Marriner, N., Morhange, C., & Doumet-Serhal, C. (2006). Geoarchaeology of Sidon's ancient harbours, Phoenicia. Journal of Archaeological Science, 33(11), 1514-1535.

Marriner, N., Morhange, C., & Goiran, J. P. (2010). Coastal and ancient harbour geoarchaeology. Geology Today, 26(1), 21-27.

Marriner, N., Morhange, C., Boudagher-Fadel, M., Bourcier, M., Carbonel, P., 2005. Geoarchaeology of Tyre's ancient northern harbour, Phoenicia. Journal of Archaeological Science 32, 1302– 1327.

Marriner, N., Morhange, C., Flaux, C., & Carayon, N. (2017). Harbours and ports. Encyclopedia of geoarchaeology, 382-403.

Morhange, C., & Marriner, N. (2010). Mind the (stratigraphic) gap: Roman dredging in ancient Mediterranean harbours. Bollettino di Archeologia on line, 23-32.

Pashazanous, H. R., Montazer Zohouri, M., & Ahmadi, T. (2014). Sea trade between Iran and China in the Persian Gulf based on the excavations of Sīrāf city. Indian Journal of Economics and Development, 2, 6-13.

Peltier, W. R., Argus, D. F., & Drummond, R. (2015). Space geodesy constrains ice age terminal deglaciation: The global ICE-6G_C (VM5a) model. Journal of Geophysical Research: Solid Earth, 120(1), 450-487.

Peltier, W. R., Argus, D., Drummond, R., & Moore, A. W. (2012). Postglacial rebound and current ice loss estimates from space geodesy: the new ICE-6G (VM5a) global model. In AGU Fall Meeting Abstracts.

Perrone, T.J., 1979. Winter shamal in the Persian Gulf, Naval Env. Prediction Res. Facility, Technical Report, 79-06, Monterey, 180pp.

Potter, L. (2009). The Persian Gulf in History. Springer.

Pourkerman, M., Marriner, N., Morhange, C., Djamali, M., Amjadi, S., Lahijani, H., ... & Shah-Hoesseini, M. (2018). Tracking shoreline erosion of "at risk" coastal archaeology:

The example of ancient Siraf (Iran, Persian Gulf). Applied Geography, 101, 45-55.

Pourkerman, M., Marriner, N., Morhange, C., Djamali, M., Lahijani, H., Amjadi, S.,... & Naderi, M. (2020). Late Holocene relative sea-level fluctuations and coastal uplift in the Persian Gulf: implications for Bataneh (Najirum) archaeological site, Iran. Unpublished paper.

Pous, S., Carton, X. J., & Lazure, P. (2012). A process study of the tidal circulation in the Persian Gulf.

Purser, B. H., & Seibold, E. (1973). The principal environmental factors influencing Holocene sedimentation and diagenesis in the Persian Gulf. In The Persian Gulf (pp. 1-9). Springer, Berlin, Heidelberg.

Reynolds, R. M. (1993). Physical oceanography of the Gulf, Strait of Hormuz, and the Gulf of Oman—Results from the Mt Mitchell expedition. Marine Pollution Bulletin, 27, 35-59.

Ricks, T. M. (1970). Persian Gulf seafaring and East Africa: ninth-twelfth centuries. African Historical Studies, 339-357.

Sharland, P. R., Casey, D. M., Davies, R. B., Simmons, M. D., & Sutcliffe, O. E. (2004). Arabian plate sequence stratigraphy–revisions to SP2. GeoArabia, 9(1), 199-214.

Sheriff, A. (1987). Slaves, spices and ivory in Zanzibar: Integration of an East African commercial empire into the world economy, 1770–1873. Ohio University Press.

Southon, J., Kashgarian, M., Fontugne, M., Metivier, B., & Yim, W. W. (2002). Marine reservoir corrections for the Indian Ocean and Southeast Asia. Radiocarbon, 44(1), 167-180.

Spada, G., & Melini, D. (2019). SELEN4 (SELEN version 4.0): a Fortran program for solving the gravitationally and topographically self-consistent Sea Level Equation in Glacial Isostatic Adjustment modeling. Geoscientific Model Development, 12(12), 5055-5075.

Stiffe, A. W. (1895). Ancient Trading Centres of the Persian Gulf: I. Siráf. Geographical Journal, 166-173.

Tabari, 1987, The History of al-Tabari vol.1. State University of New York, Albany.

Thoppil, P. G., & Hogan, P. J. (2010). Persian Gulf response to a wintertime shamal wind event. Deep Sea Research Part I: Oceanographic Research Papers, 57(8), 946-955.

Vacchi, M., Ermolli, E.R., Morhange, C., Ruello, M.R., Di Donato, V., Di Vito, M.A., Giampaola, D., Carsana, V., Liuzza, V., Cinque, A. and Boetto, G. (2020). Millennial variability of rates of sea-level rise in the ancient harbour of Naples (Italy, western Mediterranean Sea). Quaternary Research, 93(1), 284-298.

Vosougi, M. B., Sefatgo, M. (2016). The historic atlas of ports and marine navigation in Iran. Ports and Maritime Organization [Farsi].

Whitehouse, D. (1983). Maritime trade in the Gulf: The 11th and 12th centuries. World Archaeology, 14(3), 328-334.

Whitehouse, D., & Williamson, A. (1973). Sasanian maritime trade. Iran, 11(1), 29-49.

Whitehouse, D., (1968), Excavations at Siraf: First Interim Report. Iran 6, 1–22.

Whitehouse, D., (1969), Excavations at Siraf: Second Interim Report. Iran 7, 39–62.

Whitehouse, D., (1970), Excavations at Siraf: Third Interim Report. Iran 8, 1–18.

Whitehouse, D., (1971), Excavations at Siraf: Fourth Interim Report. Iran 9, 1–17.

Whitehouse, D., (2009) Siraf, History, Topography and Environment. Oxford

Wilkinson, T. J. (1974). Agricultural decline in the Siraf region, Iran. Paléorient, 123-132.

Wood, W. W., Bailey, R. M., Hampton, B. A., Kraemer, T. F., Lu, Z., Clark, D. W. James, R.H. and Al Ramadan, K. (2012). Rapid late Pleistocene/Holocene uplift and coastal evolution of the southern Arabian (Persian) Gulf. Quaternary Research, 77(2), 215-220.

Ya¯qu¯ t, 1955–57, Mu'jam al-Buldan. Beirut.

CHAPTER FOUR:
Tracking Shoreline Erosion of "At Risk" Coastal Archaeology: The Example of Ancient Siraf (Iran, Persian Gulf)

Abstract

Successful heritage management requires a robust comprehension of the threats facing archaeological sites, at both current and future timescales. Siraf, on the Persian Gulf of Iran, is a site of national and international importance whose history stretches back to the Sassanid period (224–652 AD). In the present context of global change (drought and relative sea-level rise) and anthropogenic impacts (coastal artificialization and reduced sediment supply), the city's waterfront archaeology is undergoing significant erosion. Nonetheless, at present, the processes leading to the loss of Siraf's in situ archaeological remains are still poorly understood, including the rates, timing and drivers of coastal erosion. Here we use Landsat images to monitor shoreline changes along the Siraf coastline between 1973 and 2016. We spatially quantify the causes and impacts of surface changes along 244 transects. The results demonstrate that coastal erosion is responsible for widespread and archaeologically significant damage, with 48% of the studied transects showing erosion during the period 1973–2016. We elucidate significant temporal variations in the data and, most notably, demonstrate that continued drought since the early 2000s has impacted upon sediment supply to coastal areas, severely accentuating erosion. For instance, between 2003 and 2016, 70% of transects recorded shoreline retreat with worrying implications for the waterfront archaeology of Siraf. These quantitative results provide invaluable spatial information regarding the causes and impacts of erosion upon Siraf's waterfront heritage, in addition to furnishing a template for the protection of the city's internationally important cultural heritage.

Keywords: GIS, Remote sensing, Waterfront archaeology, Coasts, Heritage management

1. Introduction

Probing the rates, timing and drivers of erosion on and around archaeological sites is key to developing effective heritage management strategies (Ahmad, 2006) to ensure the long-term survival of threatened remains (Mourtzas & Marinos, 1994; Dawson, 2005; Dromgoole, 2006). Damage to archaeological sites can derive from a plethora of both natural (Stewart, 1999; Robinson et al., 2010) and anthropogenic (Wilkinson et al., 2006) factors, each of which may operate at different temporal and spatial timescales. In the current context of global change, archaeological sites in coastal areas are particularly vulnerable and at risk from erosion (Erlandson, 2008, 2012), essentially underpinned by three cumulative factors: (1) the dynamic geomorphological character of coastal areas; (2) relative sea-level rise (e.g. Brunel and Sabatier, 2009; Ford and Kench, 2015); and (3) climate and human-induced reductions in sediment supply to coastal areas (Syvitski et al., 2005; El Banna and Frihy, 2009; Anthony et al., 2014). Quantifying the drivers and rates of change of "at risk" coastal sites, using integrated geographical, geoarchaeological and geomorphological approaches, is therefore critical in developing informed approaches to the management and effective conservation of archaeological remains (Franco, 1996; Marriner & Morhange, 2005; Andreou et al., 2017).

Quantitative techniques, based on historical documents and satellite images, have been demonstrated to be powerful tools in quantifying shoreline changes at annual to decadal timescales (Pardo-Pascual et al., 2012; García-Rubio et al., 2015). For instance, Landsat sensor series (MSS, TM, ETM+ and OLI) have provided continuous and widely democratized data since 1972, and have become one of the most common data sources employed to map and monitor shoreline changes (Miller et al., 2011). Satellite imagery techniques have also been used in archaeological reconnaissance (Beck et al., 2007; Deroin et al., 2011; Lasaponara and Masini, 2011). The infrared and visible bands of the Landsat sensors are particularly useful in differentiating between land surface and water (Yamazaki et al., 2015), and can therefore aid in quantitatively probing the spatial and temporal dimensions of recent shoreline change. These approaches are extremely valuable for assessing longer-term patterns of change around archaeological sites in coastal areas.

1.1. Research aims and archaeological context

This study uses a series of Landsat satellite images from 1973 to 2016, and various statistical techniques (Net Shoreline Movement [NSM], End Point Rate [EPR], Last Median of Square [LMS]), to monitor 44 years of coastal erosion along the Siraf coastline. Our analysis helps to identify “at risk” archaeological zones, findings that were corroborated during recent field

surveys by the authors. The erosion of Siraf's archaeological remains has been highlighted by a number of recent publications (e.g. Khakzad et al., 2015a) but quantitative estimates to assess the spatial and temporal dimensions of these changes have been hitherto lacking. As an ancient port city, Siraf possesses extensive waterfront archaeology, where geomorphic processes are particularly active and capable of exacerbating this erosion potential. Coupled with global change and human impacts, the combined consequences of these factors mean that Siraf's archaeological remains are being subjected to high rates of decay and destruction. The deterioration of Siraf's archaeological remains is compounded by the fact that the site has yet to be registered on the list of national heritage sites of Iran, although it features on the UNESCO World Heritage Tentative List since 2007. Addressing these challenges is imperative to the effective present and future preservation of the site's archaeological heritage (Khakzad et al., 2015b).

In this chapter we probe the when, where and why of coastal erosion along the coast of Siraf and assess it within the context of the city's cultural heritage. The aims of the present section are:

(1) to quantitatively assess the erosion rates along Siraf's waterfront, between 1973-2016;

(2) to map these changes using different chronological windows, in order to understand the spatial dimensions and implications of this erosion in relation to the archaeological remains and other sensitive urban areas;

(3) to probe the causes of coastal change; and

(4) to propose maps of "at risk" waterfront remains for local, national and international planners, heritage managers and other stakeholders.

2. Study area

Siraf occupies a narrow coastal plain, around 0.5 to 1 km wide, delimited by the foothills of the Zagros Mountain range in the north and ephemeral watercourses to the east and west. Siraf is one of the most important ancient ports of the Persian Gulf (Fig. 20), with a documented history stretching back to the Sassanian period, when Shapur II established a coastal fort at the site in the 4th century AD. Archaeological understanding of Siraf is based largely on the work of Whitehouse and colleagues who extensively excavated the site during the 1960s and early 1970s. More recently, the waterfront archaeology of Siraf has been investigated by Khakzad et al. (2014a).

During the Sassanian period (224-652 AD), imported objects indicate that trade relations had developed between Siraf and the Arabian Sea region as far as the Makran and Sind coasts near the regions of

Karachi and Gujarat (Ricks, 1970; Whitehouse and Williamson, 1973; Whitehouse, 2009). By the 6th century AD, contacts extended west to at least Aden and south along the Indian coast and on to Sri Lanka (Whitehouse, 2009). Chinese ceramics are first attested before c. 750–775 AD (Whitehouse, 2009; Pashazanous et al., 2014).

There is abundant textual and archaeological evidence pertaining to the medieval period at Siraf. The site appears to have enjoyed its greatest period of prosperity during the 9th and 10th centuries AD. The large Congregational Mosque, constructed over the Sassanian fort, was completed in 825 AD (Whitehouse, 1980). Remains of the medieval city of Siraf are extensive, with several mosques, bazaars, merchants' houses, a fortification system, cisterns and aqueducts. Cemeteries, in the coastal foothills, overlooked the settlement and beyond these valleys lay an extensive network of roads and semi-arable land (Wilkinson, 1974; Whitehouse, 2009). The wealth and prosperity of medieval Siraf is described by numerous historians from this period, including Tabari (9th-10th centuries), al-Muqaddasi (10th century), al-Balkhi (10th century), al-Istakhri (10th scentury), Ibn Hawqal (10th century), al-Mas'udi (10th century) and Ya¯qu¯ t (12th-13th centuries). They portray a wide trade network spanning the Red Sea to the East African coast, India and the Far East. After the mid-11th century AD, the city gradually lost its importance and when Ya¯qu¯t visited Siraf in the early 13th century, he

describes a settlement of just a few residents (Ya¯qu¯ t, 1955-57).

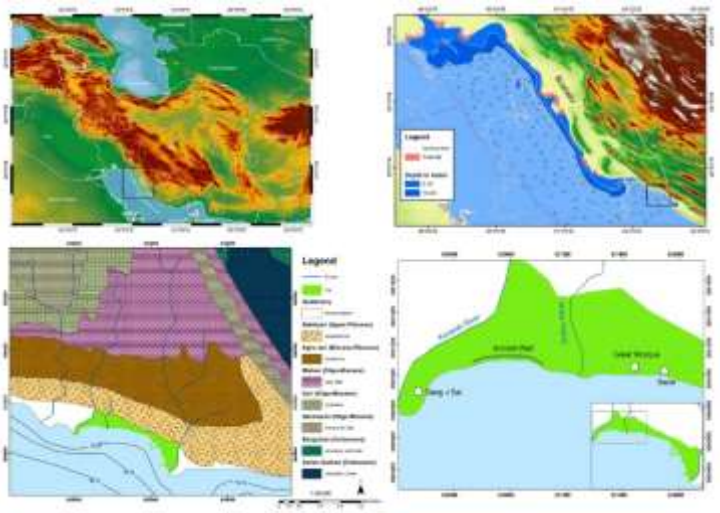

Figure 20: Location maps of Siraf in the Persian Gulf and local geomorphological context.

3. Methods

3.1. Data sources

To quantify shoreline changes along the Siraf coastline, we used multi-temporal Landsat data, Multispectral Scanner (MSS), Thematic Mapper (TM), Enhanced Thematic Mapper (ETM+) and Operational Land Imager (OLI), for the period 1973-2016. The Landsat satellites have overpass frequencies of 16 days with an equatorial crossing time at 10:00 am. The data properties are presented in Table 6. We downloaded Level

1T Landsat images from USGS EarthExplorer (http://earthexplorer.usgs.gov).

The Top of Atmospheric (TOA) was calculated from the DN (Digital Number) for every band (Equation 1).

$$L_{TOA} = M_L \times DN + A_L \quad (1)$$

The ML (gain) and AL (offset) values were given in the metadata files. TOA reflectance was calculated by normalizing LTOA to the band average solar irradiance (Equation 2):

$$\rho_{TOA} = \frac{\pi \cdot L_{TOA} \cdot d^2}{F0 \cdot \cos \theta_0} \quad (2)$$

Table 6: Data sources used in this paper (U.S. Geology Survey, 2014)

Sensor	Time (GTM +3:30)	Date of acquisition	Path/Row	Bands	resolution (m)	Wavelength (nm)
MMS	6:35:16	25-Jan-73		Band 4 - Green	60	0.5 - 0.6
				Band 5 - Red	60	0.6 - 0.7
				Band 6 - NIR 1	60	0.7 - 0.8
				Band 7 - NIR 2	60	0.8 - 1.1
TM	6:25:33	13-Oct-87	162/41	Band 1 - Blue	30	0.45 - 0.52
				Band 2 - Green	30	0.52 - 0.60
				Band 3 - Red	30	0.63 - 0.69
				Band 4 - NIR	30	0.76 - 0.90
				Band 5 - SWIR 1	30	1.55 - 1.75
				Band 6 - TIR	120	10.40 - 12.50

				Band 7 - SWIR 1	30	2.08 - 2.35
ETM+ (SLC on)	6:46:53	8-Apr-03	162/41	Band 1 - Blue	30	0.45 - 0.515
				Band 2 - Green	30	0.525 - 0.605
				Band 3 - Red	30	0.63 - 0.69
				Band 4 - NIR	30	0.75 - 0.90
				Band 5 - SWIR 1	30	1.55 - 1.75
				Band 6 - TIR	60	10.40 - 12.5
				Band 7 - SWIR 1	30	2.09 - 2.35
				Pan Band	15	0.52 - 0.90
OLI	6:58:04	15-Feb-16	162/41	Band 1 - Coastal aerosol	30	0.433–0.453
				Band 2 - Blue	30	0.450–0.515
				Band 3 - Green	30	0.525–0.600
				Band 4 - Red	30	0.630–0.680
				Band 5 - NIR	30	0.845–0.885
				Band 6 - SWIR 1	30	1.560–1.660
				Band 7 - SWIR 2	30	2.100–2.300
				Band 8 - Panchromatic	15	0.500–0.680
				Band 9 - Cirrus	30	1.360–1.390

Where d is the earth-sun distance, θ_0 the sun zenith angle and F0 solar irradiance for the band average. ρ_{TOA} denotes the sun reflectance observed by the sensor. In this study, we used simplified ρ_{TOA} for the atmospheric correction (Vanhellemont and Ruddick, 2014) (Equation 3).

$$\rho_{TOA} = \rho_r + \rho_a + t_0 t_v \rho_w \quad (3)$$

Where ρ_r and ρ_a are reflectance resulting from aerosols and Rayleigh scattering, t_0 is diffuse transmittance for the sun-sea and sea-sensor (t_v). t_0 and t_v paths are calculated by substituting θ with θ_0 and θ_v (Equation 4):

$$t = \exp[-(\frac{\tau_r}{2} + \tau_{oz})/\cos\theta \quad (4)$$

Where τ_r and τ_{oz} are the average bands of Rayleigh and Ozone optical thickness for a standard atmosphere.

Aerosol reflectance was estimated using a method outlined by Ruddic et al. (2000). The images were georeferenced using 1:100,000 topographic maps from the National Cartographic Center (NCC) with a Root Mean Square Error (RMSE) of between 0.01 to 0.05 pixels.

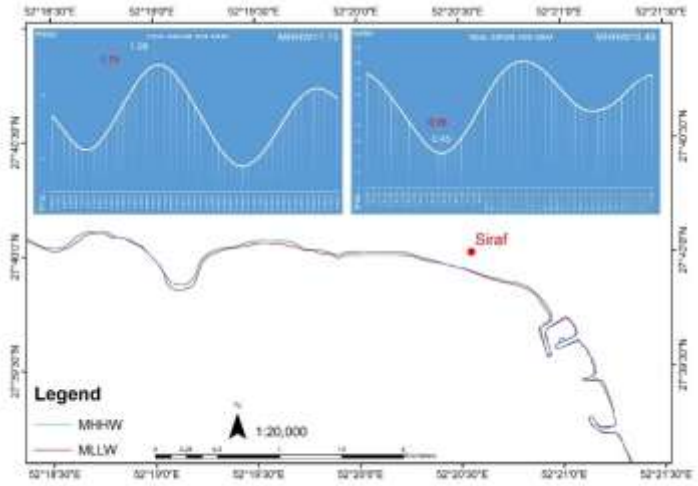

Figure 21: Tidal information for Bandar-e Taheri (Siraf), obtained from the NCC database (http://iranhydrography.ncc.org.ir).

1.1. Shoreline detection and digitization

The determination of reliable shoreline positions using RS techniques depends on various factors such as differences in the tidal range and meteorological conditions during image acquisition (Singh, 2002; Ryu et al., 2002; Boak and Turner, 2005). The tides in the study area are semidiurnal and Mean Higher High Water is 1.7 m. For the purposes of this investigation, we selected images acquired during calm sea conditions and in which the high-water line from the last high tide was clearly visible (Klemas, 2011). The tidal information for Siraf (Bandar-e Taheri) was obtained from the NCC database (http://iranhydrography.ncc.org.ir; Figure 21). The data were

available for the years 2006 to 2016 and provide useful information for the sea-level position during MHHW at Siraf on Landsat OLI images. We used these data as a baseline to choose other images according to the sea-level position on the variable beach morphology. This approach helps to dramatically reduce the tide-effected width during shoreline mapping.

NWDI is a suitable method to extract shoreline positions from MSS images because it has a limited wavelength, from 0.5 to 1.1 nm. The NIR band of the MSS images helps to delineate the water-saturated zone in the vicinity of the land-water boundary (Tulbure et al., 2016). AWEI were employed to detect shoreline positions from the TM, ETM+ and OLI, which supported wider spectral wavelength (Table 7).

Table 7: Land-water extraction indices

Index	Equation	Reference
Normalized Difference Water Index	NDWI = (Green – NIR) / (Green + NIR)	McFeeters, 1996
Automated Water Extraction Index	AWEI= 4 × (Green - SWIR 1) – (0.25 × NIR + 2.75 × SWIR2)	Feyisa et al., 2014

A threshold value was applied to the NWDI and AWEI images in order to differentiate between the surface water/non-surface water zone along the Siraf coastline (Figure 22). The selected pixels representing the shoreline position were converted into vector layers using ArcGIS ver. 10.3.

1.1. Littoral cells and transects

Field observations and existing information from coastal surveys undertaken by the hydrographic department of the NCC (2012) were used to define four coastal cells (zones 1 to 4; see Figure 22). The beaches of zones 1, 2 and 4 are gravel dominated whereas zone 3 essentially comprises sand. The littoral cells have been subdivided into perpendicular transects against the baseline. The baseline was defined as the 1973 shoreline. Using the Digital Shoreline Analysis System (DASA ver. 4.3), shoreline changes were assessed for 244 transects at 50-m intervals. There are 46 transects in zone 1, 64 in zone 2, 87 in zone 3 and 47 in zone 4.

1.2. Uncertainty and predictability

Accurately mapping shoreline positions has always been associated with significant uncertainties, because the shoreline position is constantly influenced by long-shore sediment movements and tides (Appeaning Addo et al., 2008). Typical inventory errors have been estimated by several studies. The shoreline position error was calculated using summation errors, such as satellite data resolution and scale, the topographic map SOI reference used for geo-referencing and digitizing error (Moore, 2000; Morton et al., 2004). A separate error was calculated for each shoreline. These error margins were incorporated into all transects.

1.3. Shoreline changes and prediction

Siraf shoreline changes were measured using NSM and EPR methods for the periods 1973-1987, 1987-2003, 2003-2016, 1987-2016 and 1973-2016. For each transect, the distance between the oldest and the most recent shoreline was calculated by NSM (Manca et al., 2013). The EPR was calculated by dividing shoreline change by time. The EPR unit is meters per year (Equation 5).

$$EPR = \frac{d_1 - d_0}{t_1 - t_0} \quad (5)$$

Where d is the distance in meters between the intersected shoreline-transect and the baseline, and t indicates time.

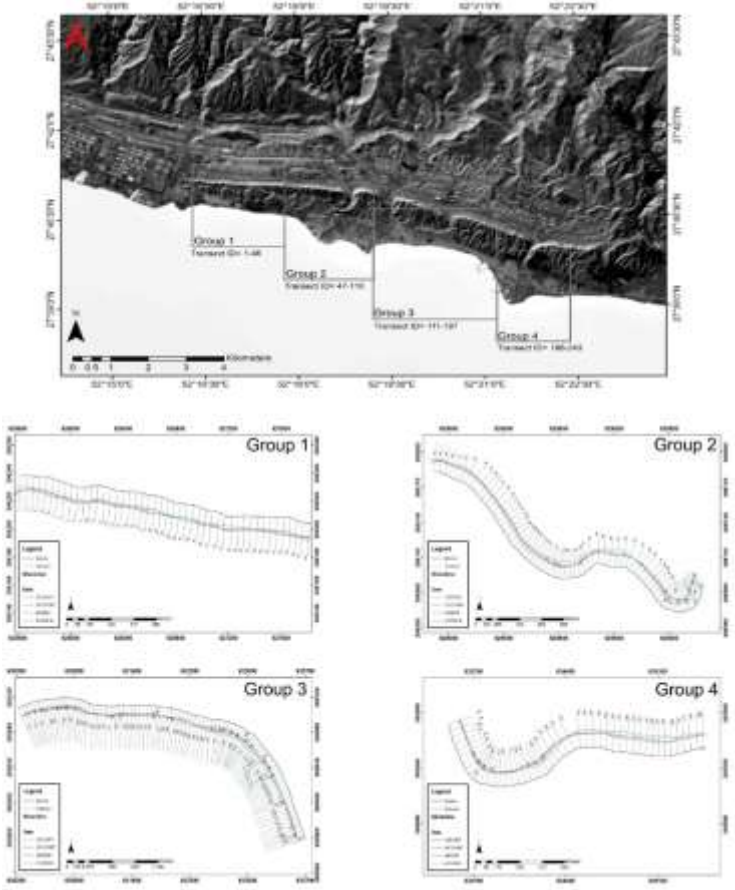

Figure 22: Position of the 244 transects used in this study. These have been grouped into four zones based on the local littoral cells.

The Last Median of Square (LMS) is a rate-of-change statistical method used to determine the rate of shoreline change by fitting least square regression lines to all shoreline intersections for a particular transect. Unlike

linear regressions that are based on the mean of the residuals, the LMS uses the median value of the squared residuals to give a best-fit line equation (Rousseeuw and Leroy, 2005). This method provides more reliable regression estimates and minimizes shoreline prediction errors.

4. Results and discussion

Our results manifest temporal and spatial variations in shoreline change rates at Siraf and highlight a number of pressing concerns with regards to the city's waterfront archaeology. For the total period 1973-2016, the study area shows a general trend towards moderate progradation with a mean shoreline advance rate of 0.24 m/year (Figures 23 & 24), and minimum and maximum values of -1.57 m/year and 7.14 m/year respectively. For the three intervening periods, we recorded an overall erosional trend between 1973-1987 (mean = -0.11 m/year), a progradational trend between 1987-2003 (mean = 1.1 m/year) and a renewed erosional phase between 2003-2016 (mean = -0.35 m/year; Figure 25). We focus notably on the period 2003-2016, which is most important in contextualizing the present predicament of Siraf's waterfront remains. As outlined above, during data processing the results were divided into four areas consistent with the local littoral cells, due to the significant spatial differences in both the EPR and NSM results. The EPR and NSM results are discussed below in

relation to each of these areas, before the overall trends are considered together as part of a wider discussion of the results.

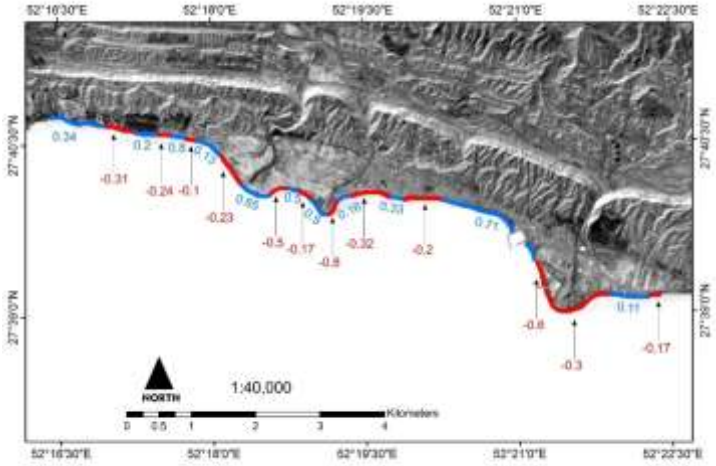

Figure 23: Map of average EPR erosion/accretion rates, in m/year, for the period 1973-2016.

4.1. Zone 1

Zone 1 has the lowest number of transects in our study (n=46). Total change from all geomorphic processes identified within zone 1 resulted in extremely moderate mean shoreline advance of 0.007 m/year for the total study period of 1973 to 2016. For the three intercalating time windows, we observed average erosion of -0.192 m/year for the period 1973-1986, accretion of 0.6 m/year for the period 1987-2003 and average erosion of -0.478 m/year between 2003-2016. For the period 2003-2016,

shoreline retreat was observed along 80 % of the transects in this zone (Figure 26). Spatially, erosion was distributed throughout the entire length of the zone, and appears to be linked to down-drift reductions in sediment supply from the two local watercourses in zone 2. The maximum rate of erosion was -2.03 m/year along transect 21.

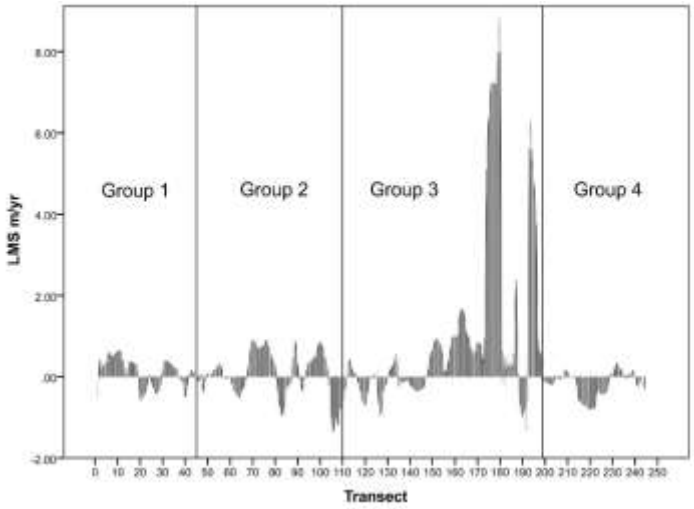

Figure 24: Histogram of LMS erosion/accretion rates, in m/year and by transect, for the period 1973-2016.

1.1. Zone 2

Zone 2 has a total of 64 transects. Overall, for the 44-year survey period, erosion in zone 2 was -0.06 m/year. We reconstructed average accretion of 0.078 m/year and 0.506 m/year for the periods 1973-1987 and 1987-2003 respectively, consistent with two fluvial systems in this zone that supply sediment. By contrast, the

most recent period, 2003-2016, was characterized by a switch to an erosional trend, with average erosion rates of -0.905 m/year. For this 13-year time window, erosion was particularly pronounced around the mouths of the two fluvial systems in this area, in addition to around the old city walls of Siraf. Between 2003 and 2016, 80 % of the transects recorded shoreline retreat with maximum rates of -3.19 m/year in transect 102.

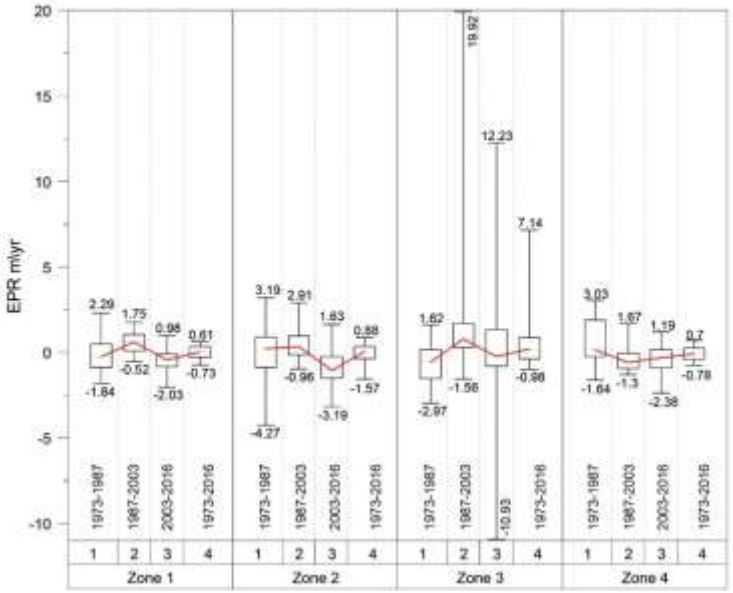

Figure 25: Boxplots of EPR shoreline changes by zone and for the different time periods (1: 1973-1987; 2: 1987-2003; 3: 2003-2016 and 4: 1987-2016) investigated in this study.

1.1. Zone 3

Zone 3 contains the highest number of transects in our study, with a total of 87. This area is significant because it contains a high density of archaeological vestiges, including, from west to east, Bang-I Sar, the ancient fort wall, the Great Mosque and the Bazar. The zone records overall accretion for the period 1973-2016 with an average rate of 0.766 m/year. Nonetheless, over the 44-year period, we observed significant temporal variations in the data. Between 1973-1986, 69 % of the transects in this area recorded erosion with a total average rate of -0.582 m/year and a maximum rate of -2.97 in transect 170 (Figures 25 & 26). By contrast, the period 1986-2003 was characterized by generalized progradation, notably around Siraf port. During this timeframe, we recorded strong average accretion of 2.539 m/year for the zone as a whole, with a maximum rate of 19.92 m/year at transect 179. These highly skewed data are the result of the construction of seawalls to create a coastal resort in 2008. Not only did these structures significantly artificialize zone 3 but they also affected longshore sediment transport to other littoral cells along the Siraf coastline. The structure acts as a sediment bypass and, by longshore processes, transports sediment to the fishing harbour of Siraf. For the period 2003-2016, the overall trend is accretional, with an average rate of 0.174 m/year. Nonetheless, 57 % of the transects show an erosional trend with significant implications for the

waterfront archaeology in this area (Figure 27). In particular, erosion rates >1 m/year were recorded at the foot of the sea-facing wall of Siraf's old city, which is disturbing and deteriorating important cultural deposits and structures, a finding that we corroborated during field surveys in late November 2016 (Figure 28). Our reconstructed change rates in zone 3 are consistent with data from Khakzad et al. (2014a), who describe, between 1973 and 2012, total coastal retreat of around 8 m on the southern flank of Siraf's old coastal mosque (52 20 06.42E; 27 40 02.49N). This rate is consistent with the value of 8.6 m (average -0.2 m/yr) that we obtained in the same area for the period 1973 to 2016.

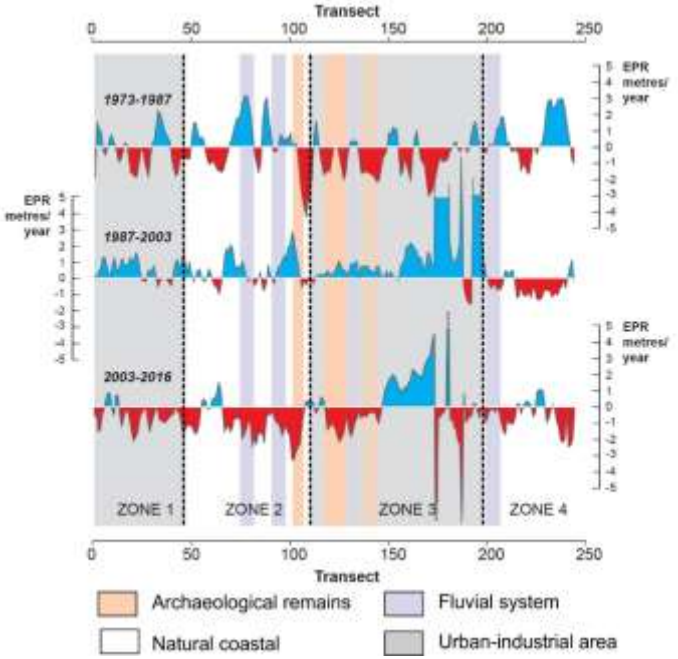

Figure 26: Histogram of EPR erosion/accretion rates, in m/year and by transect, for the period 1973-1987, 1986-2003 and 2003-2016. The archaeological areas/sites are denoted.

1.1. Zone 4

Zone 4 comprises 47 transects. This zone includes an ephemeral fluvial system. Total change from all geomorphic processes identified within zone 1 resulted in mean shoreline retreat of -0.08 m/year for the total study period of 1973 to 2016. Between 1973-1987, the dominant geomorphological regime was accretionary with an average rate of 0.614 m/year. By contrast, the periods 1987-2003 and 2003-2016 manifest the switch to

an erosional regime with average erosion rates of -0.427 m/year and -0.442 m/year. The strong erosional trend since 1987 appears to be linked to two factors: (1) sharp falls in sediment supply from the ephemeral fluvial system that exists in this area; and (2) construction of the fishing harbour of Siraf, that acts as a downdrift sediment trap and that blocks sediment transfer into zone 4. For the periods 1987-2003 and 2003-2016, 77 % and 70 % of the 46 transects in this zone manifest erosion trends.

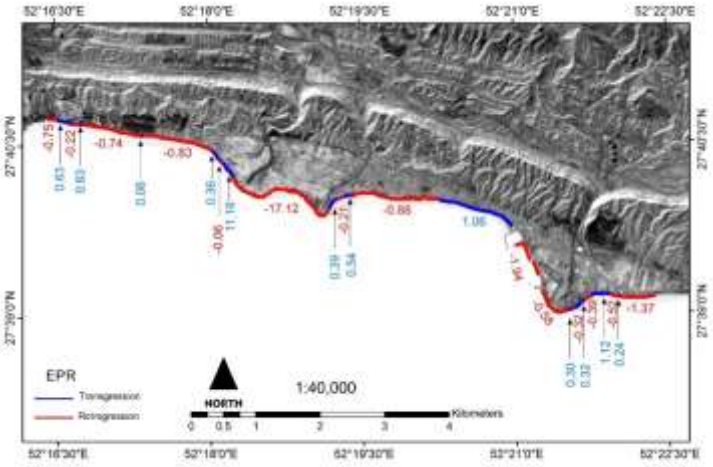

Figure 27: Map of average EPR erosion/accretion rates, in m/year, for the period 2003-2016.

1.1. Siraf's waterfront archaeology and the wider implications of coastal erosion

Understanding the geomorphological processes encountered in particular landscape contexts is

fundamental to developing effective heritage management strategies. In coastal environments in particular, the potential for the widespread and damaging erosion of archaeological remains is considerable. This is in part due to the increased erosion rates typically encountered in coastal areas, which has been excaberated by global change and anthropogenic impacts on sediment supply. At Siraf, continued drought since the early 2000s has severely affected sediment supply to coastal areas (Figures 10 and 11) leading to extensive erosion of the coastline during the past two decades. The area has recorded a stepwise decrease in total precipitation, with an annual average of 196.53 mm/year between 1973-1986, 187.97 mm/year between 1986-2003 and 174.24 mm/year between 2003-2014. This trend is mirrored by the regional water courses of Mand and Hilla which, although not in direct vicinity of Siraf, are representative of the fluvial systems in the Busher province. We note a threefold decrease in discharge rates between 1970-1986 and 2003-2011, with significant impacts on sediment delivery to the region's coasts. The city's waterfront archaeology is particularly exposed and at danger due to the highly erodible nature of its deposits (Figure 31). The erosion of Siraf's coastal archaeology is an ongoing legacy problem that must be urgently addressed by local, national and international stakeholders, including urban and coastal planners, heritage managers, archaeologists and geomorphologists. To effectively combat the

problem, we suggest continued and close monitoring of the ongoing erosion.

Figure 28: Photographs of the coastal erosion at the base of Siraf's old city walls (Group 3 transects).

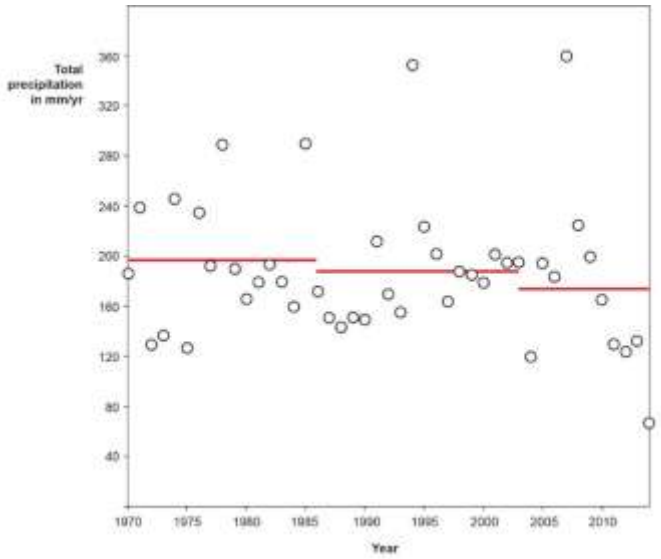

Figure 29: Annual total precipitation for the Siraf area (data from http://climate.geog.udel.edu/~climate/html_pages/Global2014/README.GlobalTsP2014.html). The red lines denote annual averages for the periods 1970-1986, 1986-2003 and 2003-2014.

5. Conclusions

Analyses of Landsat images have provided an effective methodology for monitoring the why, when and where of coastal change at Siraf. 70 % of the coastline is presently undergoing erosion with widespread implications for the city's important archaeological deposits and upstanding structural remains. Although further work is required to assess when this erosion takes place, we suggest that low-magnitude erosion plays an important role in destabilizing surface deposits, with the

most significant occurring during high-magnitude storm events. At present, the resolution of our present data does not allow us to effectively probe this aspect of the coastal erosion, and a local monitoring program would be advantageous.

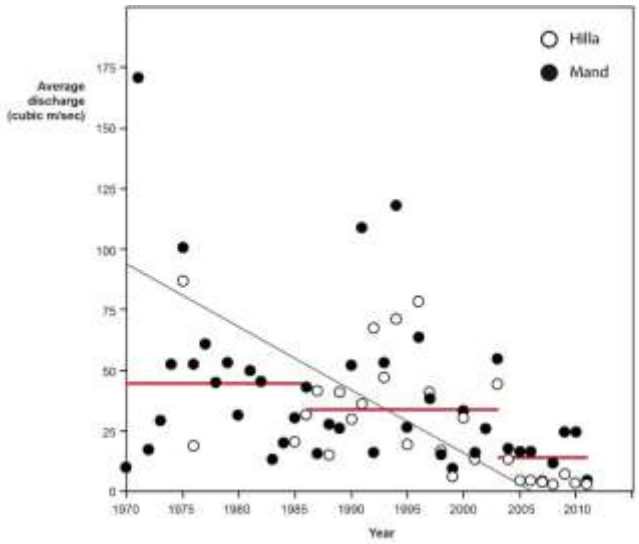

Figure 30: Average annual discharge of the rivers Mand and Hilla on the Persian Gulf (for the linear correlation, r = -0.44). The red lines denote annual averages for the periods 1970-1986, 1986-2003 and 2003-2011.

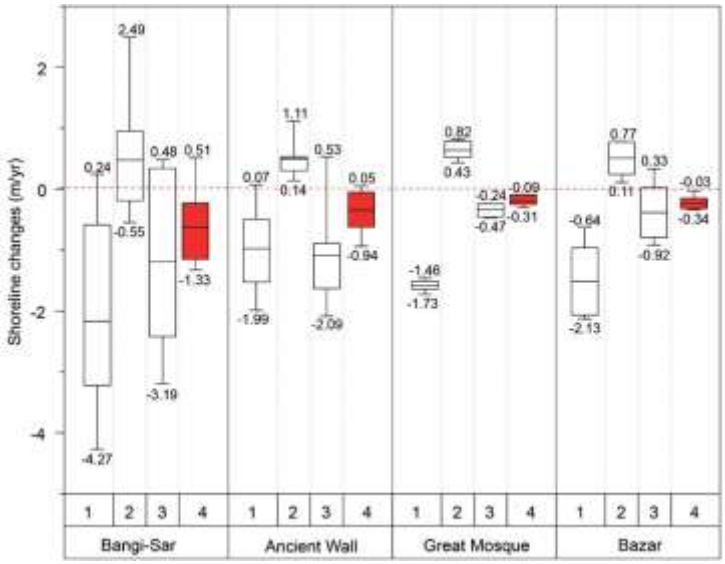

Figure 31: Box plots of shoreline changes rates at important archeological sites for the different time periods (1: 1973-1987; 2: 1987-2003; 3: 2003-2016 and 4: 1987-2016).

In sum, our research suggests that a well-defined management and protection plan is urgently required for Siraf. Our data and mapping of the erosion now provide a baseline of geographic information with which to develop an appropriate and targeted management plan, which must include national and international stakeholders. This research has emphasized the need for interdisciplinary approaches to the research and management Siraf's waterfront archaeology. There is an urgent need for appropriate mitigation strategies to be designed and implemented in order to combat this rapid coastal erosion,

which is threatening a site of national and international importance.

References

Ahmad, Y., 2006. The scope and definitions of heritage: from tangible to intangible. International Journal of Heritage Studies, 12, 292-300.

Andreou, G. M., Opitz, R., Manning, S. W., Fisher, K. D., Sewell, D. A., Georgiou, A., Urbana, T., 2017. Integrated methods for understanding and monitoring the loss of coastal archaeological sites: The case of Tochni-Lakkia, south-central Cyprus. Journal of Archaeological Science: Reports, 12, 197-208.

Anthony, E. J., Marriner, N., Morhange, C., 2014. Human influence and the changing geomorphology of Mediterranean deltas and coasts over the last 6000 years: from progradation to destruction phase? Earth-Science Reviews, 139, 336-361.

Appeaning Addo, K. A., Walkden, M., Mills, J. P., 2008. Detection, measurement and prediction of shoreline recession in Accra, Ghana. ISPRS Journal of Photogrammetry and Remote Sensing, 63, 543-558.

Beck, A., Philip, G., Abdulkarim, M., Donoghue, D., 2007. Evaluation of Corona and Ikonos high resolution satellite imagery for archaeological prospection in western Syria. Antiquity 81 (311), 161-175.

Brunel, C., Sabatier, F., 2009. Potential influence of sea-level rise in controlling shoreline position on the French Mediterranean Coast. Geomorphology, 107, 47-57.

Dawson, T. (Ed.), 2005. Coastal Archaeology and Erosion in Scotland. Historic Scotland, Edinburgh.

Deroin, J.-P., Téreygeol, F., Heckes, J., 2011. Evaluation of very high to medium resolution multispectral satellite imagery for geoarchaeology in arid regions — case study from Jabali, Yemen. J. Archaeol. Sci. 38 (1), 101-114.

Dromgoole, S. (Ed.), 2006. The protection of the underwater cultural heritage: national perspectives in light of the UNESCO convention 2001. Brill.

El Banna, M., Frihy, O.E., 2009. Human-induced changes in the geomorphology of the northeastern coast of the Nile delta, Egypt. Geomorphology 107, 72–78.

Erlandson, J.M., 2008. Racing a rising tide: global warming, rising seas, and the erosion of human history. J. Island Coast. Archaeol. 3 (2), 167–169.

Erlandson, J.M., 2012. As the world warms: rising seas, coastal archaeology and the erosion of maritime history. J. Coast. Conserv. 16, 137–142.

Ford, M. R., Kench, P. S., 2015. Multi-decadal shoreline changes in response to sea level rise in the Marshall Islands. Anthropocene, 11, 14-24.

Franco, L., 1996. Ancient Mediterranean harbours: a heritage to preserve. Ocean & coastal management, 30, 115-151.

García-Rubio, G., Huntley, D., Russell, P., 2015. Evaluating shoreline identification using optical satellite images. Marine Geology, 359, 96-105.

Khakzad, S., Trakadas, A., Harpster, M., Wittig, N., 2015a. Maritime aspects of Medieval Siraf, Iran: a pilot project for the investigation of coastal and underwater archaeological remains. Int. J. Naut. Archaeol. 44 (2), 258–276.

Khakzad, S., Pieters, M., Van Balen, K., 2015b. Coastal cultural heritage: a resource to be included in integrated coastal zone management. Ocean Coast. Manag. 2015, 1–19.

Lasaponara, R., Masini, N., 2011. Satellite remote sensing in archaeology: past, present and future perspectives. J. Archaeol. Sci. 38 (9), 1995-2002.

Manca, E., Pascucci, V., Deluca, M., Cossu, A., Andreucci, S., 2013. Shoreline evolution related to coastal development of a managed beach in Alghero, Sardinia, Italy. Ocean and Coastal Managemeny, 85, 65-76.

Marriner, N., Morhange, C., 2005. Under the city centre, the ancient harbour. Tyre and Sidon: heritages to preserve. Journal of Cultural Heritage, 6, 183-189.

Miller, H. M., Sexton, N. R., Koontz, L., Loomis, J., Koontz, S. R., Hermans, C., 2011. The Users, Uses, and Value of Landsat and Other Moderate-resolution Satellite Imagery in the United States - Executive Report. U.S. Geological Survey Open-File Report 2011-1031.

Moore, L. J., 2000. Shoreline mapping techniques. Journal of Coastal Research, 16, 111-124.

Morton, R. A., Miller, T. L., Moore, L. J., 2004. National assessment of shoreline change, part 1: historical shoreline changes and associated coastal land loss along the U.S. Gulf of Mexico. U.S. Geological Survey Open-file report 2004–1043.

Mourtzas, N. D., Marinos, P. G., 1994. Upper Holocene sea-level changes: Paleogeographic evolution and its impact on coastal archaeological sites and monuments. Environmental Geology, 23, 1-13.

Pardo-Pascual, J. E., Almonacid-Caballer, J., Ruiz, L. A., Palomar-Vázquez, J., 2012. Automatic extraction of shorelines from Landsat TM and ETM+ multi-temporal images with subpixel precision. Remote Sensing of Environment, 123, 1-11.

Pashazanous, H. R., Montazer Zohouri, M., Ahmadi, T., 2014. Sea trade between Iran and China in the Persian Gulf based on the excavations of Siraf city. Indian Journal of Economics and Development 2, 6-13.

Ricks, T. M., 1970. Persian Gulf Seafaring and East Africa: Ninth-Twelfth Centuries. African Historical Studies, 3, 339-57.

Robinson, M.H., Alexander, C.R., Jackson, C.W., McCabe, C.P., Crass, D., 2010. Threatened archaeological, historic, and cultural resources of the Georgia Coast: identification, prioritization and management using GIS technology. Geoarchaeology, 25, 312-326.

Rousseeuw, P.J. and Leroy, A.M., 2005. Robust regression and outlier detection, Vol. 589. John Wiley & Sons.

Stewart, D. J., 1999. Formation processes affecting submerged archaeological sites: an overview. Geoarchaeology, 14, 565-587.

Syvitski, J.P.M., Vörösmaty, C.J., Kettner, A.J., Green, P., 2005. Impacts of humans on the flux of terrestrial sediments to the global coastal ocean. Science 308, 376-380.

Tulbure, M.G., Broich, M., Stehman, S.V. and Kommareddy, A., 2016. Surface water extent dynamics from three decades of seasonally continuous Landsat time series at subcontinental scale in a semi-arid region. Remote Sensing of Environment, 178, 142-157.

Whitehouse, D., Williamson, A., 1973. Sasanian Maritime Trade. Iran 11, 29-49.

Whitehouse, D., 1980. Siraf III. The Congregational Mosque and other mosques from the ninth to the twelfth centuries. London.

Whitehouse, D., 2009. Siraf, History, Topography and Environment. Oxford.

Wilkinson, T. J., 1974. Agricultural decline in the Siraf region, Iran. Paléorient, 2, 123–32.

Wilkinson, K., Tyler, A., Davidson, D., Grieve, I., 2006. Quantifying the threat to archaeological sites from the erosion of cultivated soil. Antiquity 80, 658–670.

Yamazaki, D., Trigg, M. A., Ikeshima, D., 2015. Development of a global ~90m water body map using multi-temporal Landsat images. Remote Sensing of Environment, 171, 337-351.

Ya¯qu¯ t, 1955–57. Mu'jam al-Buldan. Beirut.

CHAPTER FIVE:
Conclusions

Conclusions

The RSL oscillations in the Persia Gulf are controlled by eustatic sea-level changes and crustal mobility via the Persian Gulf axial zone subsidence and localized uplift through the fault systems. For this reason the reconstructed RSL is not correlated with the ICE—6G (VM5a) model for the study sites. Although the model shows a continuous fall, the studied facies record three RSL oscillations. The duration between each oscillation was correlated with the modeled sea-level position and the important harbours displacements. An increasing water column in the central basin floor can lead to increasing crustal mobility in coastal areas. Meanwhile, the time interval between the lowstand and the ensuing highstand decreased.

From environmental point of view RSL oscillations, summer Shamal wind, the Persian Gulf surface current regimes and morphology of basin had significant impacts on navigation and port activities. The first important harbour shift was happened at zone I from Rishar to Apologus. It was concurrent with emerging first evidence of human trace at Siraf (44 BC – 452 AD). By the time RSL reached cal. 3 meter below current level at Siraf. It had negative impacts on the Rishar port operation due to its shallow coastal morphology. The evidence of economic prosperity in the northwest of the Persian Gulf continuous until 9th century when a dramatic economic

decline was happened. Meanwhile, the major settlement being founded in central part of the Persian Gulf (Priestman, 2005). The archaeological findings suggested that the Apologus prosperity continuous by the first recorded lowstand in the studied cores and emerging second anthropogenic horizon at Siraf (113 – 477 AD). During this event, RSL could be maintained by Shatt-Al-Arab delta subsidence and local uplifts (Uchupi et al., 1999).

During second lowstand (780 – 900 AD) the Shatt-al- Arab River channel had prograded into the sea over its palaeo-delta. It had negligible impacts on the pro-delta that was below low-tide level. A small and shallow tidal channel developed at the delta front. As a result, the navigable water column became too shallow during low-tide in the Shatt-al- Arab estuary. On the other hand, increase in summer Shamal winds around 650 AD was accelerated risk of navigations through Ras-e-Motaf and Shatt-al-Arab estuary during storm conditions. The danger of navigation through the northwest of the Persian Gulf is mentioned by ancient geographers such as Ibn Hawqal (1965) and Al-Istakhri (1870). By the time shift in important harbours from northwest (Apologus) to central (Siraf) part of the Persian Gulf were taken place.

Siraf and Najirum were suitable place for harbour activities because their close location to Ras-e-Motaf at zone III and II, respectively. By the second RSL

fall, Najirum recorded 3.7 m uplift. The uplift was under the influences of Darang salt pillow growth by the salt injection via Hormuz salt formation through N-S Dashti fault system. Coastal uplift was a key factor in reducing port accessibility and therefore activity. Therefore, the studied side had a low harbour potentiality during flourishing of Siraf. As the results, location of Najirum's harbour town is still unclear.

One of the reasons that Bataneh (Najirum) port failed was probably due to coastal uplift. The diapiric fold has exposed lithological units with evaporation minerals such as gypsum and gypsum marl. The concentration of deep rill erosion features in the upland areas shows their high sensitivity to water erosion. As well as, geomorphological features such as wadi and alluvial fans in Bataneh underscore high potential risk of flooding and debris flow. The runoff water that sourced from evaporation geological units was harnessing and directing to the city for extraction gypsum. The expansion of Siraf brought rapid urbanization of the city and local towns. This rapid expansion required new building materials. At this time, cooked gypsum was widely used as cement, plaster motifs and decorative objects. Therefore, gypsum very soon became a noteworthy commercial good. Several ancient gypsum mines existed around Siraf. Traditional mining required time and labor for the extraction and transfer of raw gypsum, as a result, gypsum became expensive. New gypsum extraction methods via

evaporation pools at Bataneh led to cheaper gypsum. The method took advantage of Bataneh's geomorphological characters and gypsum units present in the local geology.

The harbour history of Siraf was started with the decline of the port of Apologus around 750 AD. Siraf was surpassed by Bataneh because of relative coastal stability with low vertical movements and a steep coastal morphology. The city's fresh water was supplied by harnessing and storing rainfall via numerous wells and cisterns on the hills overlooking Siraf, and stocked in alluvial sediments overlooking the ancient settlement. A modified Qanat system was designed for collecting and transferring freshwater to the city. Access to freshwater was possible in form of shallow well for domestic and agricultural purposes. The city extended at least 300 m from the present shoreline (Khakzad et al., 2014). This suggests that falling RSL and positive coastal sediment budgets allowed the medieval city to extend seawards. The Persian Gulf surface current and summer Shamal wind led to flourishing harbour activates at Siraf (Fig 32).

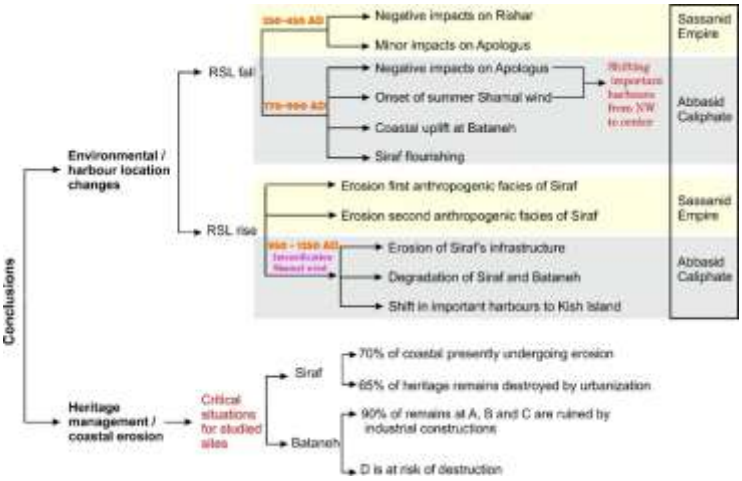

Figure 32: Summery of the results of this study

Rising RSL and increasing summer Shamal wind intensity accelerated erosion of Siraf's port. The foundations of medieval Siraf were sensitive to erosion. Erosion removed the lower compact sediments and it leading to the collapse of overlying infrastructure. Due to the absence of robust construction materials, coastal processes easily eroded gypsum between the plastered rubble. Therefore, the structures were easily degraded and the sediment fractions reworked by coastal processes and longshore currents. Furthermore, RSL rise significantly compromised the city's water resources. RSL rise, led to salt-water intrusion into wells. Access to fresh water in the city therefore became limited. In light of the environmental impacts on civil and trade infrastructure, Siraf's population gradually migrated away from the city.

The Bataneh was abandon simultaneously because of its economic dependence on Siraf (Fig 32).

The studied ancient sites are at risk of destruction due to the natural and anthropogenic processes. Costal erosion has significant impacts on Siraf waterfront ancient remains. On the other hand, South Pars offshore oil and gas field has led to the expansion of several petrochemical companies along the coastal. It leads to create new job opportunity and expanding cities and industrial structures over the ancient sites. The images are represented critical situation of the ancient remains in studies sites. Same trend is observed for the other visited heritage remains (Fig 33).

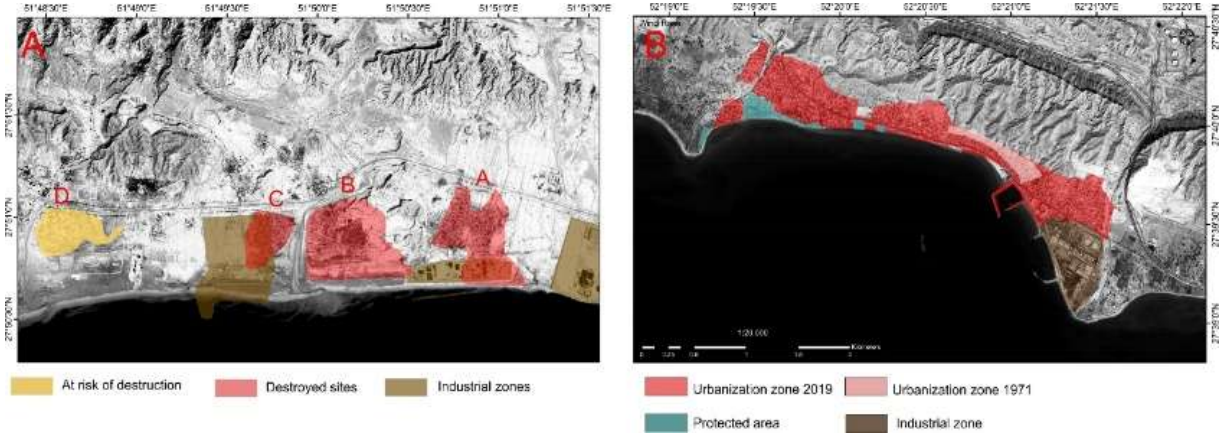

Figure 33: Destruction of ancient remains at Bataneh (A) and Siraf (B) by the industrial construction and urbanization since 1971

References

Al-Istakhri, (1870), M. J. de Goeje (trans. & ed.), Kitab Al-Masalik wa-al-Mamalik. Leiden.

Ibn Hawqal, (1965). J. H. Kramers (trans. & ed.), Kitab Surat al-Ard. Bibliotheca Georaphorum Arabicorum, Leiden.

Khakzad, S. and Trakadas, A. 2014, The world in a grain of sand: Siraf, in S. Sindbæk and A. Trakadas (eds), The World in the Viking Age, 108–110. Roskilde.

Priestman, S. (2005). Settlement & ceramics in Southern Iran: An analysis of the Sasanian & Islamic periods in the Williamson collection (Doctoral dissertation, Durham University).

Uchupi, E., Swift, S. A., & Ross, D. A. (1996). Gas venting and late Quaternary sedimentation in the Persian (Arabian) Gulf. Marine Geology, 129(3-4), 237-269.

Research prospective

Majid Pourkerman has participated in numerous field work projects which have been added to his experiences for marine and coastal studies. During work at the INIO-AS Majid Pourkerman worked at the internal office and organization (Maritime and Port Organization). The PhD project gave him the opportunity to develop scientific collaborations with researcher from institutions in Iran (University of Tehran and Institute of archaeology of Iran), France (Aix-Marseille and Besançon Universities) and Italy (Venice, Pisa and Urbino Universities) Germany (University of Bremen). During his PhD, Majid Pourkerman has increased his international network with European universities and UNESCO.

Majid Pourkerman has contributed to write ECR project on the Persian Gulf under title: "At the crossroads of civilisation: multidisciplinary archaeological and palaeoenvironmental perspectives on the making, rise and fall of complex societies in southern Iran and the Persian Gulf". At this project he will continuous his research on Coastal heritage management of Persian Gulf coastal archaeology.

As well as, he had submitted a Marie Curie proposal entitle "Evaluation of coastal erosion and flooding at UNESCO world heritage sites along the Mediterranean seaboard". The aim of the project is to

evaluate risk of coastal erosion and flooding at waterfront UNESCO heritage sites. This project will investigate 49 world heritage sites located in low-lying coastal areas of the Mediterranean, with cooperation of UNESCO WHSs.